Universiteit Utrecht

Department of Mathematics

*Mathematical Sciences*

# Homoclinic Orbits of Planar Maps: Asymptotics and Mel'nikov Functions

A thesis submitted for the degree of
*Master of Science*

*Author:*
Dirk van Kekem

*Project Supervisor:*
Prof. dr. Yu.A. Kuznetsov
*Second Examiner:*
Dr. H. Hanssmann

# Homoclinic Orbits of Planar Maps: Asymptotics and Mel'nikov Functions

Dirk van Kekem
3287815
Utrecht University

December 13, 2013

**Abstract**

Homoclinic orbits to saddle fixed points of planar diffeomorphisms generically imply complicated dynamics due to Smale Horseshoes. Such orbits can be computed only numerically, which is time-consuming. The aim of this project is to explore an alternative method to compute homoclinic orbits near degenerate fixed points of codimension 2 with a double multiplier 1. The method will be based on approximating the map near the bifurcation by the time-1-shift along orbits of a planar ODE and evaluating the Mel'nikov function along its homoclinic loop. Zeroes of this Mel'nikov function are intersections of the stable and unstable manifold and will approximate the homoclinic orbit. The main part of this project is devoted to the derivation of a prediction for both the homoclinic orbit and the homoclinic bifurcation curve in the case of the normal form of 1:1 resonance.

# 0

# Preface

Writing these sentences, I realize that my master's project is almost finished. I can look back on a good year in which I learned a lot on bifurcations, homoclinic orbits, the Mel'nikov function and programming in MATLAB. What is contained in this Master Thesis is only a fraction of the beautiful things I have seen in the past year — of course, the most important part. I invite you to go through my work and to see what I have seen. But let's first introduce the main subject and the process.

**Introduction to the subject** As one may, or may not, know, the stable and unstable manifolds of a hyperbolic saddle of a map can have very complex behaviour, including infinitely many intersections (see section 1.2). In some cases, such behaviour can also show up for non-hyperbolic saddles, for example, in the case of the normal form of 1:1 resonance. Arrowsmith et al. [1] have described the dynamics of a map with similar behaviour, the *Bogdanov map*. In this useful article they look at the development of invariant circles near a homoclinic tangle.

With MATCONT — a continuation and bifurcation toolbox for MATLAB — it is possible to compute the stable and unstable manifolds to the saddle of a chosen map, locate their intersection points and subsequently continue to find the whole region for which these intersections are present. This, however, requires a lot of (human) effort.

Some work to improve on this method, is already done by Chávez by starting the continuation of tangential homoclinic orbits near 1:1 resonances using a center manifold reduction and flow approximation [3]. His method is not completely satisfying, since he has to make an initial guess of an intersection point to start his method. One has to be lucky to choose a point which is good enough to get useful results out of the process. Moreover, the work of Chávez contains errors inherited from earlier publications and related to the prediction in the parameter space. In this project I investigate a way to obtain such initial points in a correct and efficient way. For that purpose

I make use of the so-called Mel'nikov function, which gives a prediction for the location of the intersection points of the stable and unstable manifolds of a certain map (see section 1.3) and thus providing us with a good initial guess to start the continuation with.

First of all, I test the Mel'nikov function on the McMillan map, which is well-known for having transversal intersections. The resulting prediction of the intersection points is superb for this map and very promising (see section 2.2).

To apply the Mel'nikov function to the normal form of 1:1 resonance, some more work has to be done, because the corresponding flow does not posses a Hamiltonian part, nor is the solution of the homoclinic orbit known explicitly. Its approximating ODE is already calculated by Kuznetsov [8]. Using more Picard iterations I have improved his result. These Picard iterations also provide the flow of this system, which turns out to be very close to the original map. The next step — and this is one of the main parts of my project — is to find beforehand an accurate expression for the homoclinic orbit of the ODE. For this, I make use of the method of center manifold reduction as given in [9]. This method relates the approximating ODE of the normal form of 1:1 resonance to the normal form of the Bogdanov-Takens bifurcation. The result is a good prediction of the homoclinic orbit and the homoclinic bifurcation curve for the 1:1 resonance case, which are needed to compute the Mel'nikov function. Since I have gone through all the calculations in that specific article independently, I give a summary of it and details of some of the derivations in Appendix A.

As a final step, I actually compute the Mel'nikov function for the described situation with small values of $\varepsilon$, the perturbation parameter. However, there are still open questions on this part, which can be investigated in further research. For example, by numerically computing the invariant manifolds of the saddle for values of parameters near the bifurcation point of 1:1 resonance I am not able to see transversal intersections of these manifolds and therefore I cannot really check if the outcome of the Mel'nikov function indeed gives a valuable result to start the continuation with. Secondly, the Mel'nikov function for this map does not show — as it does for the McMillan map — a kind of vertical translation when I modify only one parameter in order to obtain tangencies instead of intersections. Furthermore, one can wonder what the outcome of the Mel'nikov function means in this case. Having solved these problems, it remains to implement this method in numerical software, which gives the opportunity to continue directly from its results for a given system.

During this research I also obtained a transformation of a general system, which satisfies the Bogdanov-Takens conditions, to a specific form of the Bogdanov-Takens normal form. This transformation has not been performed explicitly anywhere in the literature. Its result is used further to derive a system which has a Hamiltonian part with a perturbation part added. This

specific form turns out to be particularly useful when it is related to the approximating ODE for the normal form of 1:1 resonance.

**Acknowledgements** I would like to thank all people who helped me with this project, in particular my supervisor Yuri Kuznetsov for his never ceasing support. Without his creative and inspiring ideas, I would not finish this project successfully. I am grateful to Hil Meijer for his support and the encouraging discussions we had. Also thanks to Bashir Al Hdaibat, who works on the same problems, for the discussions and double-checking my results. And I would like to thank Heinz Hanßmann for his critical final look at this thesis. Last but not least, I am deeply grateful to my parents, who gave me the possibility to study and for their support with my — for them — incomprehensible work.

# Contents

# 1

# Theory

## 1.1 Introduction to Dynamical Systems

Mathematics can be viewed in some sense as an idealistic branch of science: reality is represented in such a simplified form that mathematical analysis is possible, equations can be solved and something can be proven. There are many other sciences — as physics, biology, economics and even social science — where one uses mathematical models of a real phenomenon on the basis of data. With such simplifications one can trace back in the past or looking forward in the future how the real configuration will behave approximately by knowing its present state, assuming that its laws wouldn't change in time. Preferably, such a model of a real situation has known or even exact solutions. But, in this respect, reality and its models are far from ideal: results in accordance with practice almost never have such nice properties.

Therefore, it is necessary to make approximations or to look at only part of a system, that is, its local or global behaviour. To reduce further, one can look at the interesting parameters only and keep the other parameters fixed. This can give the opportunity to determine and analyse for each point of the system its possible states and evolution in time, under certain (initial) conditions and restricted to a suitable subarea. Loosely speaking, this describes the notion of a *dynamical system*: it consists of the set of all possible states, a certain range of time and specified laws, describing the behaviour in time and space.

Depending on the situation, time can be viewed in two ways, namely

1. as *continuous* with $t \in \mathbb{R}$. That is how we often perceive reality: as a fluently and permanently changing world. Systems with continuous time are most often defined by differential equations, depending on $n$ spatial variables and $m$ parameters,

$$\dot{x} = f(x, \alpha), \quad x \in \mathbb{R}^n, \quad \alpha \in \mathbb{R}^m. \tag{1.1}$$

2. as *discrete* with $t \in \mathbb{Z}$. Such a system changes step-by-step, each new time it is in a (possibly) new state. Such systems occur often in statistics or economics and can be viewed as taking measurements one time in a hour or year. In general a discrete-time dynamical system is a map $f$, sufficiently smooth in its $n$ coordinates and $m$ parameters,

$$x \mapsto f(x, \alpha), \quad x \in \mathbb{R}^n, \quad \alpha \in \mathbb{R}^m, \tag{1.2}$$

describing the behaviour of the system in time as a discrete sequence $\{f^t(x, \alpha), t \in \mathbb{Z}\} = \{\ldots, f^{-2}(x, \alpha), f^{-1}(x, \alpha), x, f(x, \alpha), f^2(x, \alpha), \ldots\}$, (assuming the invertibility of $f$).

In this thesis we restrict ourselves to systems with only two coordinates (i.e. planar maps) and two parameters — that is to say, there can be more parameters but they are kept fixed during the research.

Given a general system, its behaviour is determined by specifying an initial state and the values of the parameters. Once we know these, we can investigate how the system will evolve when time is running (either to the past or the future). Doing this, one will find *orbits* (trajectories of points, defined by the dynamics), *equilibria* or fixed points, *cycles* (periodic orbits), and other sets invariant under $f$. To make the behaviour clear, it is helpful to determine for each invariant set its stability, that is to say whether it is attracting or repelling nearby orbits. All interesting orbits of a dynamical system are combined in a *phase portrait*. In order to be able to predict accurate things after a long time, one might need to enlarge the area of consideration or to improve the model.

In many cases it is very interesting to know what the effect is of changing the values of (some of the) parameters. This can influence the behaviour not only in time but also on a local or global scale of the system. This phenomenon is described in the next section.

## 1.2 Bifurcations

Indeed, varying the parameters can cause a sudden change in the local or global behaviour of the system. Two equilibria, for example, can collide and disappear. Loosely speaking, such a change is called a bifurcation. In formal language one would say that a *bifurcation* is the appearance of a topologically nonequivalent phase portrait under variation of parameters, see [8]. Such a change of topology occurs as the parameters pass through *bifurcation (critical) values*. Topologically equivalent situations can be transformed into each other via a homeomorphism: a continuous, invertible map such that the inverse is also continuous.

Such a bifurcation can be described by specifying a phase object (e.g. equilibrium or cycle) and one or more *bifurcation conditions*, equations that

describe a smooth submanifold in the parameter space $\mathbb{R}^m$, at which the change in the dynamics takes place. The number of independent bifurcation conditions is called the *codimension* of the bifurcation, which — as it indicates — depends on the dimension of the parameter space. For each bifurcation that can happen in some system, one can make a *bifurcation diagram* by visualising the bifurcation conditions in the parameter space as smooth submanifolds — that is as points, curves, surfaces, etc. —, together with the characteristic phase portraits. If these submanifolds divide the parameter space in several regions, then the system should have topologically equivalent phase portraits at each point of a separate region. So, if the bifurcation diagram of a system is known, then it is easy to determine which behaviour and behaviour changes can happen at which point.

It might be difficult to draw the phase portrait or bifurcation diagram for a general system immediately by hand. For most of the standard bifurcations there is a simple system, called topological *normal form*, which exhibits that particular bifurcation at or near the origin with parameters equal to zero. If we can show that a generic system (1.1) or (1.2) is locally topologically equivalent to this normal form, then such a system will exhibit the same bifurcation with (topologically) the same local bifurcation diagram. Often, there are some conditions that need to be fulfilled before we can speak about a 'generic' system. We can distinguish them in *nondegeneracy* conditions, stating that the critical equilibrium is not too degenerate, and transversality conditions, which guarantee that this equilibrium is 'unfolded' in a generic way.

In the following we discuss three bifurcations that are relevant for this study, which mainly concerns the normal form of 1:1 resonance:

1. First of all, the Bogdanov-Takens bifurcation of codimension 2, since its normal form is closely related to the approximating flow of the normal form of 1:1 resonance.

2. Secondly, we shortly introduce the codimension 1 Neimark-Sacker bifurcation to make the conditions we meet in the case of 1:1 resonance more clear.

3. And then, as third one, we describe the important case: the codimension 2 bifurcation of 1:1 resonance, which is a bifurcation related to the Neimark-Sacker bifurcation.

For other possible bifurcations one can have a look at [8] for a list and a description of them.

### 1.2.1 Bogdanov-Takens bifurcation

Consider a continuous-time system (1.1) with $n = m = 2$, and suppose that it has at $(x, \alpha) = (0, 0)$ an equilibrium with two zero eigenvalues for which

the Jacobian matrix $A = f_x(0,0) \neq 0$. This is the so-called *Bogdanov-Takens condition*. The following consideration is preliminary to the derivation of the corresponding normal form, see [8].

At $\alpha = 0$ we can write the system as

$$\dot{x} = Ax + \hat{f}(x),$$

where $\hat{f}(x) = f(x,0) - Ax$, a smooth function of second order in $x$. The Jacobian $A$ is a matrix satisfying $\operatorname{tr} A = \det A = 0$. There exist two real, linearly independent vectors $q_{1,2} \in \mathbb{R}^2$, such that

$$Aq_1 = 0, \qquad Aq_2 = q_1.$$

Note that $q_1$ is an eigenvector of $A$, while the vector $q_2$ is called a *generalized eigenvector* corresponding to the eigenvalue 0. Similarly, let $p_{1,2} \in \mathbb{R}^2$ be the *adjoint eigenvectors* of the transposed matrix $A^T$, given by

$$A^T p_2 = 0, \qquad A^T p_1 = p_2.$$

Choose these eigenvectors such that they also satisfy

$$\begin{aligned} &\langle q_1, p_1 \rangle = \langle q_2, p_2 \rangle = 1, \\ &\langle q_2, p_1 \rangle = \langle q_1, p_2 \rangle = 0, \end{aligned}$$

using the standard inner product.

Take $q_{1,2}$ as the basis for the plane of the system, then each vector $x \in \mathbb{R}^2$ gets a unique representation

$$x = y_1 q_1 + y_2 q_2,$$

for real numbers $y_{1,2} = \langle p_{1,2}, x \rangle$. Rewrite system (1.1) in the new coordinates $(y_1, y_2)$ to obtain for small $\alpha$ the general form

$$\begin{cases} \dot{y}_1 = \langle p_1, f(y_1 q_1 + y_2 q_2, \alpha) \rangle, \\ \dot{y}_2 = \langle p_2, f(y_1 q_1 + y_2 q_2, \alpha) \rangle. \end{cases} \tag{1.3}$$

Notice that the matrix $A$ for this system at $\alpha = 0$ is given by

$$A = \begin{pmatrix} 0 & 1 \\ 0 & 0 \end{pmatrix},$$

which is the form of the zero Jordan block.

The Taylor expansion of the right-hand side of (1.3) with respect to $y$ at $y = 0$ reads

$$\begin{cases} \dot{y}_1 = a_{00} + a_{10} y_1 + a_{01} y_2 + a_{20} y_1^2 + a_{11} y_1 y_2 + a_{02} y_2^2 + \mathcal{O}(\|y\|^3), \\ \dot{y}_2 = b_{00} + b_{10} y_1 + b_{01} y_2 + b_{20} y_1^2 + b_{11} y_1 y_2 + b_{02} y_2^2 + \mathcal{O}(\|y\|^3), \end{cases} \tag{1.4}$$

with $a_{kl}, b_{kl}$ smooth functions in $\alpha$, satisfying $a_{00}(0) = a_{10}(0) = b_{00}(0) = b_{10}(0) = b_{01}(0) = 0$ and $a_{01}(0) = 1$. This system can be turned via certain smooth transformations into a much simpler form: the *Bogdanov-Takens* (BT) *normal form*. Actually, there are two popular forms: one of them, where the $y_1$-term survives in the $\dot{y}_2$-part, is also described by Kuznetsov [8]; the other, where the $y_2$-term survives, is not done explicitly anywhere. We discuss the last one first, since we will use it frequently in this project.

### Transformation to BT normal form

In this section we transform system (1.4) into a system which has a Hamiltonian part with a perturbation part proportional to $\varepsilon$ added. First, we bring a general system with unknown coefficients and satisfying certain conditions into the Bogdanov-Takens normal form with the $y_2$-term in the second equation.

**Lemma 1.** *Consider the smooth planar system*

$$\dot{\xi} = F(\nu, \xi) = F_0(\nu) + F_1(\nu, \xi) + F_2(\nu, \xi), \quad \xi \in \mathbb{R}^2, \quad \nu \in \mathbb{R}^2, \tag{1.5}$$

*with each function $F_k$ defined by*

$$F_0(\nu) = \begin{pmatrix} a_{00}(\nu) \\ b_{00}(\nu) \end{pmatrix},$$
$$F_1(\nu, \xi) = \begin{pmatrix} a_{10}(\nu)\xi_1 + a_{01}(\nu)\xi_2 \\ b_{10}(\nu)\xi_1 + b_{01}(\nu)\xi_2 \end{pmatrix},$$
$$F_2(\nu, \xi) = \begin{pmatrix} a_{20}(\nu)\xi_1^2 + a_{11}(\nu)\xi_1\xi_2 + a_{02}(\nu)\xi_2^2 \\ b_{20}(\nu)\xi_1^2 + b_{11}(\nu)\xi_1\xi_2 + b_{02}(\nu)\xi_2^2 \end{pmatrix}.$$

*The coefficients $a_{kl}(\nu), b_{kl}(\nu)$ are smooth functions of $\nu$ and satisfy*

$$a_{00}(0) = a_{10}(0) = b_{00}(0) = b_{10}(0) = b_{01}(0) = 0.$$

*Assume that the following conditions hold*

$$a_{01}(0) \neq 0, \tag{1.6a}$$
$$b_{20}(0) \neq 0, \tag{1.6b}$$
$$b_{11}(0) \neq 0, \tag{1.6c}$$
$$\text{the map } (\nu, \xi) \mapsto \left( F(\nu, \xi), \operatorname{tr}\left( \frac{\partial F(\nu, \xi)}{\partial \xi} \right), \det\left( \frac{\partial F(\nu, \xi)}{\partial \xi} \right) \right) \tag{1.6d}$$
*is regular at $(\nu, \xi) = (0, 0)$.*

*Then there are smooth invertible variable transformations, smoothly depending on the parameters, smooth invertible parameter changes and direction-preserving time reparametrisations, reducing (1.5) to the two-parameter* Bogdanov-Takens normal form

$$\begin{cases} \dot{\eta}_1 = \eta_2, \\ \dot{\eta}_2 = \beta_1 + \beta_2\eta_2 + \eta_1^2 + s\eta_1\eta_2 + \mathcal{O}(\|\eta\|^3), \end{cases} \tag{1.7}$$

*where* $s = \operatorname{sign}(a_{01}(0)b_{20}(0)b_{11}(0)) = \pm 1$.

*Proof.* The proof is subdivided into four steps.

**Step 1** First, introduce new variables $(u_1, u_2)$, using (1.5), as follows:

$$\begin{aligned} u_1 &= \xi_1, \\ u_2 &= \dot{\xi}_1 = a_{00} + a_{10}\xi_1 + a_{01}\xi_2 + a_{20}\xi_1^2 + a_{11}\xi_1\xi_2 + a_{02}\xi_2^2. \end{aligned}$$

This reduces (1.5) to a nonlinear oscillator, written as

$$\begin{cases} \dot{u}_1 = u_2, \\ \dot{u}_2 = f_{00}(\nu) + f_{10}(\nu)u_1 + f_{01}(\nu)u_2 \\ \qquad\quad + f_{20}(\nu)u_1^2 + f_{11}(\nu)u_1u_2 + f_{02}(\nu)u_2^2 + \mathcal{O}(\|u\|^3), \end{cases}$$

where the functions $f_{kl}$, smoothly depending on $\nu$, are defined by

$$\begin{aligned} f_{00} &= b_{00} + \tfrac{a_{00}}{a_{01}^3}\big(a_{00}a_{01}b_{02} - (a_{01}^2 + a_{00}a_{02})b_{01}\big); \\ f_{10} &= b_{10} + \tfrac{1}{a_{01}^3}\big(a_{00}a_{01}(a_{11}b_{01} + 2a_{10}b_{02}) - 2a_{00}a_{10}a_{02}b_{01} \\ &\quad - a_{01}^2(a_{10}b_{01} + a_{00}b_{11})\big); \\ f_{01} &= \tfrac{1}{a_{01}^3}\big(a_{01}^2b_{01} + 2a_{00}a_{02}b_{01} - 2a_{00}a_{01}b_{02}\big); \\ f_{20} &= b_{20} + \tfrac{1}{a_{01}^3}\big(a_{01}(a_{10}a_{11}b_{01} - a_{01}a_{20}b_{01} + a_{10}^2b_{02} - a_{10}a_{01}b_{11}) - a_{10}^2a_{02}b_{01}\big); \\ f_{11} &= \tfrac{1}{a_{01}^3}\big(2a_{10}a_{02}b_{01} + a_{01}(a_{01}b_{11} - 2a_{10}b_{02} - a_{11}b_{01})\big); \\ f_{02} &= \tfrac{1}{a_{01}^3}\big(a_{01}b_{02} - a_{02}b_{01}\big), \end{aligned}$$

using condition (1.6a). Note that we have at $\nu = 0$, $f_{00}(0) = f_{10}(0) = f_{01}(0) = 0$ and $f_{20}(0) = b_{20}(0), f_{11}(0) = \frac{b_{11}(0)}{a_{01}(0)}, f_{02}(0) = \frac{b_{02}(0)}{a_{01}^2(0)}$.

**Step 2** Next, change the time $t$ into the new time $\tau$, via

$$\mathrm{d}t = (1 + \vartheta(\nu)u_1)\mathrm{d}\tau, \tag{1.8}$$

where $\vartheta(\nu)$ is some smooth function of $\nu$ which we define later on. This time reparametrisation preserves the direction of time in the neighbourhood of the origin for small $\|\nu\|$. It yields the system

$$\begin{cases} \dot{u}_1 = \frac{\mathrm{d}}{\mathrm{d}\tau}u_1 = \frac{\mathrm{d}}{\mathrm{d}t}u_1\frac{\mathrm{d}t}{\mathrm{d}\tau} = u_2(1 + \vartheta u_1), \\ \dot{u}_2 = \frac{\mathrm{d}}{\mathrm{d}\tau}u_2 = \frac{\mathrm{d}}{\mathrm{d}t}u_2\frac{\mathrm{d}t}{\mathrm{d}\tau} = f_{00} + (f_{10} + \vartheta f_{00})u_1 + f_{01}u_2 \\ \qquad + (f_{20} + \vartheta f_{10})u_1^2 + (f_{11} + \vartheta f_{01})u_1u_2 + f_{02}u_2^2 + \mathcal{O}(\|u\|^3). \end{cases}$$

Since we want only the $u_2$-term in the expression for $\dot{u}_1$, we transform the system again like in step 1:

$$\begin{aligned} v_1 &= u_1, \\ v_2 &= \dot{u}_1 = u_2(1 + \vartheta u_1). \end{aligned}$$

In these new coordinates the system becomes

$$\begin{cases} \dot{v}_1 = v_2, \\ \dot{v}_2 = g_{00} + g_{10}v_1 + g_{01}v_2 + g_{20}v_1^2 + g_{11}v_1v_2 + g_{02}v_2^2 + \mathcal{O}(\|v\|^3), \end{cases} \tag{1.9}$$

with the functions $g_{kl}$, smoothly depending on $\nu$, defined by

$$\begin{aligned} g_{00}(\nu) &= f_{00}(\nu); \\ g_{10}(\nu) &= f_{10}(\nu) + 2\vartheta(\nu)f_{00}(\nu); \\ g_{01}(\nu) &= f_{01}(\nu); \\ g_{20}(\nu) &= f_{20}(\nu) + 2\vartheta(\nu)f_{10}(\nu); \\ g_{11}(\nu) &= f_{11}(\nu) + \vartheta(\nu)f_{01}(\nu); \\ g_{02}(\nu) &= f_{02}(\nu) + \vartheta(\nu). \end{aligned}$$

We are now ready to eliminate $g_{02}$, the term proportional to $v_2^2$, by defining $\vartheta$ as

$$\vartheta(\nu) = -f_{02}(\nu),$$

which makes the time reparametrisation (1.8) explicit. The other functions involving $\vartheta$ are now defined as

$$\begin{aligned} g_{10} &= f_{10} - 2f_{00}f_{02}; \\ g_{20} &= f_{20} - 2f_{10}f_{02}; \\ g_{11} &= f_{11} - f_{01}f_{02}. \end{aligned}$$

For completeness, we point out that $g_{00}(0) = g_{10}(0) = g_{01}(0) = 0$, $g_{20}(0) = f_{20}(0)$ and $g_{11}(0) = f_{11}(0)$.

**Step 3** Change the coordinates in the $v_1$-direction by the following parameter-dependent shift,

$$\begin{aligned} v_1 &= w_1 + \delta(\nu), \\ v_2 &= w_2. \end{aligned}$$

The system (1.9) then takes the form

$$\begin{cases} \dot{w}_1 = w_2, \\ \dot{w}_2 = g_{00} + g_{10}(w_1 + \delta) + g_{01}w_2 \\ \qquad + g_{20}(w_1 + \delta)^2 + g_{11}(w_1 + \delta)w_2 + \mathcal{O}(\|w\|^3) \\ \quad = \big(g_{00} + g_{10}\delta + g_{20}\delta^2 + \mathcal{O}(\delta^3)\big) + \big(g_{10} + 2g_{20}\delta + \mathcal{O}(\delta^2)\big)w_1 \\ \qquad + \big(g_{01} + g_{11}\delta + \mathcal{O}(\delta^2)\big)w_2 + \big(g_{20} + \mathcal{O}(\delta)\big)w_1^2 \\ \qquad + \big(g_{11} + \mathcal{O}(\delta)\big)w_1w_2 + \mathcal{O}(\|w\|^3). \end{cases} \tag{1.10}$$

In order to eliminate the term proportional to $w_1$, we have to find a suitable definition of $\delta(\nu)$ such that $h_{10}(\nu) := g_{10} + 2g_{20}\delta + \mathcal{O}(\delta^2)$ becomes equal to 0. To achieve this, we make the assumption that $g_{20}(0) = f_{20}(0) = b_{20}(0) \neq 0$, which is precisely condition (1.6b). The *Implicit Function Theorem* then guarantees the local existence of a smooth function $\delta(\nu)$, which is for small $\nu$ approximately equal to

$$\delta(\nu) \approx -\frac{g_{10}(\nu)}{2g_{20}(0)}.$$

With this definition of $\delta$ the system becomes

$$\begin{cases} \dot{w}_1 = w_2, \\ \dot{w}_2 = h_{00}(\nu) + h_{01}(\nu)w_2 + h_{20}(\nu)w_1^2 + h_{11}(\nu)w_1w_2 + \mathcal{O}(\|w\|^3), \end{cases} \tag{1.11}$$

with the functions $h_{kl}(\nu)$ smoothly defined in accordance with (1.10), as

$$\begin{aligned} h_{00}(\nu) &= g_{00}(\nu) - \tfrac{g_{10}^2(\nu)}{2g_{20}(0)} + \mathcal{O}(\delta^2); \\ h_{01}(\nu) &= g_{01}(\nu) - g_{11}(\nu)\tfrac{g_{10}(\nu)}{2g_{20}(0)} + \mathcal{O}(\delta^2); \\ h_{20}(\nu) &= g_{20}(\nu) + \mathcal{O}(\delta); \\ h_{11}(\nu) &= g_{11}(\nu) + \mathcal{O}(\delta). \end{aligned}$$

Note that we have $h_{00}(0) = h_{01}(0) = 0$, $h_{20}(0) = g_{20}(0)$ and $h_{11}(0) = g_{11}(0)$, as one can easily check.

**Step 4** In the last step we scale the coefficients of (1.11) to appropriate forms and set the surviving ones as new parameters. Beforehand, introduce the simpler notation $A(\nu) = h_{20}(\nu)$ and $B(\nu) = h_{11}(\nu)$ and assume that $b_11(0) \neq 0$, which is condition (1.6c). This and the conditions (1.6a) and (1.6b) guarantee that $A(0) = h_{20}(0) = g_{20}(0) = f_{20}(0) = \frac{b_{20}(0)}{a_{01}^2(0)} \neq 0$ and $B(0) = h_{11}(0) = g_{11}(0) = f_{11}(0) = b_{11}(0) \neq 0$.

First, we rescale the time $\tau$ — and call it $t$ again — by

$$t = \left|\frac{A(\nu)}{B(\nu)}\right| \tau.$$

This rescaling is now well-defined. Secondly, declare the new variables $\eta_1$ and $\eta_2$, by stating

$$\begin{aligned} \eta_1 &= \frac{B^2(\nu)}{A(\nu)} w_1, \\ \eta_2 &= \operatorname{sign}\left(\frac{A(\nu)}{B(\nu)}\right) \frac{B^3(\nu)}{A^2(\nu)} w_2. \end{aligned}$$

These three rescalings transform the system into the simple form

$$\begin{cases} \dot{\eta}_1 = \eta_2, \\ \dot{\eta}_2 = \beta_1(\nu) + \beta_2(\nu)\eta_2 + \eta_1^2 + s\eta_1\eta_2 + \mathcal{O}(\|\eta\|^3), \end{cases}$$

with

$$\begin{aligned} s &= \operatorname{sign}\left(\frac{A(0)}{B(0)}\right), \\ \beta_1(\nu) &= \frac{B^4(\nu)}{A^3(\nu)} h_{00}(\nu), \\ \beta_2(\nu) &= \frac{sB(\nu)}{A(\nu)} h_{01}(\nu). \end{aligned}$$

The coefficients $\beta_j$ both satisfy $\beta_1(0) = \beta_2(0) = 0$. In order to get a system depending only on the parameters $\beta$ instead of $\nu$, we have to assume that $\beta$ as function of $\nu$ is regular at $\nu = 0$:

$$\det\left(\frac{\partial\beta}{\partial\nu}\right)\Big|_{\nu=0} \neq 0.$$

This condition is equivalent to our fourth condition (1.6c), saying that the map

$$(\nu, \xi) \mapsto \left(F(\nu,\xi), \operatorname{tr}\left(\frac{\partial F(\nu,\xi)}{\partial\xi}\right), \det\left(\frac{\partial F(\nu,\xi)}{\partial\xi}\right)\right),$$

is regular at $(\nu, \xi) = (0, 0)$, which in turn implies that the determinant of the Jacobian matrix does not vanish.

Hence, we can define our system in terms of the parameters $\beta_{1,2}$ and $s$, and thus derive the desired form of the Bogdanov-Takens normal form

$$\begin{cases} \dot{\eta}_1 = \eta_2, \\ \dot{\eta}_2 = \beta_1 + \beta_2\eta_2 + \eta_1^2 + s\eta_1\eta_2 + \mathcal{O}(\|\eta\|^3), \end{cases} \tag{1.12}$$

where $s = \operatorname{sign}(A(0) \cdot B(0)) = \operatorname{sign}(a_{01}(0)b_{20}(0)b_{11}(0))$. □

### Derivation of a Hamiltonian normal form

Our next goal is to rescale system (1.12) such that it gets the form of a Hamiltonian part with some perturbation terms added. This transformation, done previously by Guckenheimer and Holmes [5], is the aim of the following lemma.

**Lemma 2.** *The smooth planar system, depending on two parameters,*

$$\begin{cases} \dot{\eta}_1 = \eta_2, \\ \dot{\eta}_2 = \beta_1 + \beta_2\eta_2 + \eta_1^2 \pm \eta_1\eta_2 + \mathcal{O}(\|\eta\|^3), \end{cases} \tag{1.13}$$

*can be transformed, using a singular rescaling, into the three parameter planar system*

$$\begin{cases} \dot{\zeta}_1 = \zeta_2, \\ \dot{\zeta}_2 = \gamma_1 + \varepsilon\gamma_2\zeta_2 + \zeta_1^2 \pm \varepsilon\zeta_1\zeta_2 + \mathcal{O}(\|\zeta\|^3). \end{cases}$$

*Proof.* Let $\varepsilon > 0$ be small. Then the transformation is performed by rescaling the time $t$ to $s = \varepsilon t$ and setting

$$\begin{aligned} \eta_1 &= \varepsilon^2\zeta_1; \\ \eta_2 &= \varepsilon^3\zeta_2; \\ \beta_1 &= \varepsilon^4\gamma_1; \\ \beta_2 &= \varepsilon^2\gamma_2. \end{aligned}$$

These changes brings (1.13) into a system with $(\eta_1, \eta_2)$-coordinates,

$$\begin{cases} \frac{\mathrm{d}}{\mathrm{d}s}\zeta_1 = \frac{\mathrm{d}}{\mathrm{d}t}\zeta_1\frac{\mathrm{d}t}{\mathrm{d}s} = \frac{1}{\varepsilon^2\cdot\varepsilon}\dot{\eta}_1 = \frac{1}{\varepsilon^2\cdot\varepsilon}\eta_2 = \frac{1}{\varepsilon^2\cdot\varepsilon}\varepsilon^3\zeta_2 = \zeta_2, \\ \frac{\mathrm{d}}{\mathrm{d}s}\zeta_2 = \frac{\mathrm{d}}{\mathrm{d}t}\zeta_2\frac{\mathrm{d}t}{\mathrm{d}s} = \frac{1}{\varepsilon^3\cdot\varepsilon}\dot{\eta}_2 \\ \qquad = \frac{1}{\varepsilon^4}\left(\varepsilon^4\gamma_1 + \varepsilon^2\gamma_2\cdot\varepsilon^3\zeta_2 + \varepsilon^4\zeta_1^2 \pm \varepsilon^2\eta_1\cdot\varepsilon^3\zeta_2 + \varepsilon^6\mathcal{O}(\|\zeta\|^3)\right) \\ \qquad = \gamma_1 + \varepsilon\gamma_2\zeta_2 + \zeta_1^2 \pm \varepsilon\zeta_1\zeta_2 + \varepsilon^2\mathcal{O}(\|\zeta\|^3). \end{cases}$$

The coefficients $\gamma_{1,2}$ and $\varepsilon$ are the new parameters. □

**Theorem 3.** *Consider a smooth planar system*

$$\dot{x} = f(x, \alpha), \quad x \in \mathbb{R}^2, \quad \alpha \in \mathbb{R}^2, \tag{1.14}$$

*with a double zero eigenvalue $\lambda_{1,2} = 0$ for $\alpha = 0$ at the equilibrium $x = 0$ and assume that $A(0) = f_x(0, 0) \neq 0$. Then system (1.14) can be transformed into system (1.4), with $a_{kl}, b_{kl}$ smooth functions in $\alpha$, satisfying $a_{00}(0) = a_{10}(0) = b_{00}(0) = b_{10}(0) = b_{01}(0) = 0$ and $a_{01}(0) = 1$.*

*Suppose that the following conditions hold:*

$$a_{01}(0) \neq 0, \tag{1.15a}$$

$$b_{20}(0) \neq 0, \tag{1.15b}$$

$$b_{11}(0) \neq 0, \tag{1.15c}$$

$$\text{the map } (x, \alpha) \mapsto \left(f(x, \alpha), \operatorname{tr}\left(\frac{\partial f(x, \alpha)}{\partial x}\right), \det\left(\frac{\partial f(x, \alpha)}{\partial x}\right)\right) \tag{1.15d}$$

*is regular at $(x, \alpha) = (0, 0)$.*

*Then (1.14) can be reduced via smooth invertible variable transformations, smoothly depending on the parameters, direction-preserving time reparametrisations, smooth invertible parameter changes and a singular rescaling to the system*

$$\begin{cases} \dot{u} = v, \\ \dot{v} = \gamma_1 + \varepsilon\gamma_2 v + u^2 + s\varepsilon uv + \varepsilon^2\mathcal{O}(\|u, v\|^3), \end{cases} \tag{1.16}$$

*with $s = \operatorname{sign}(a_{01}(0)b_{20}(0)b_{11}(0)) = \pm 1$.*

*Proof.* The proof is constituted by subsequently applying the lemmas 1 and 2. The new independent parameters are $\gamma_{1,2}$ and a small perturbation-parameter $\varepsilon$. The expression for $s$ is obtained by substituting the needed coefficients in the formula given in lemma 1. □

The right-hand-side of system (1.16) can be written in the form

$$\begin{pmatrix} \dot{u} \\ \dot{v} \end{pmatrix} = G_1(u,v) + \varepsilon G_2(u,v) + \varepsilon^2 \mathcal{O}(\|u,v\|^3), \quad \varepsilon \in \mathbb{R},$$

with $G_{1,2} : \mathbb{R}^2 \to \mathbb{R}^2$ defined by

$$G_1(u,v) = \begin{pmatrix} v \\ \gamma_1 + u^2 \end{pmatrix},$$
$$G_2(u,v) = \begin{pmatrix} 0 \\ \gamma_2 v \pm uv \end{pmatrix}.$$

If we now let $\varepsilon \to 0$,then only $G_1$ survives, which actually provides us with an integrable Hamiltonian system with Hamiltonian

$$H(u,v) = -\gamma_1 u + \tfrac{1}{2}v^2 - \tfrac{1}{3}u^3.$$

Its equations of motion form the system

$$\begin{cases} \dot{u} = \dfrac{\partial H}{\partial v} = v, \\ \dot{v} = -\dfrac{\partial H}{\partial u} = \gamma_1 + u^2. \end{cases} \tag{1.17}$$

Choosing $\gamma_1 = -4$ gives the phase portrait in figure 1.1. At the fixed points $(\pm\sqrt{-\gamma_1}, 0) = (\pm 2, 0)$ the Hamiltonian has the values $H(\pm 2, 0) = \pm 5\frac{1}{3}$. The left part of the level curve for this value is homoclinic to the saddle $(2,0)$, described by

$$(u_0(t), v_0(t)) = \left(2 - 6\,\mathrm{sech}^2(t), 12\,\mathrm{sech}^2(t)\tanh(t)\right). \tag{1.18}$$

This useful expression is used later on to obtain an approximation of the homoclinic orbit for the general system with $\varepsilon \neq 0$.

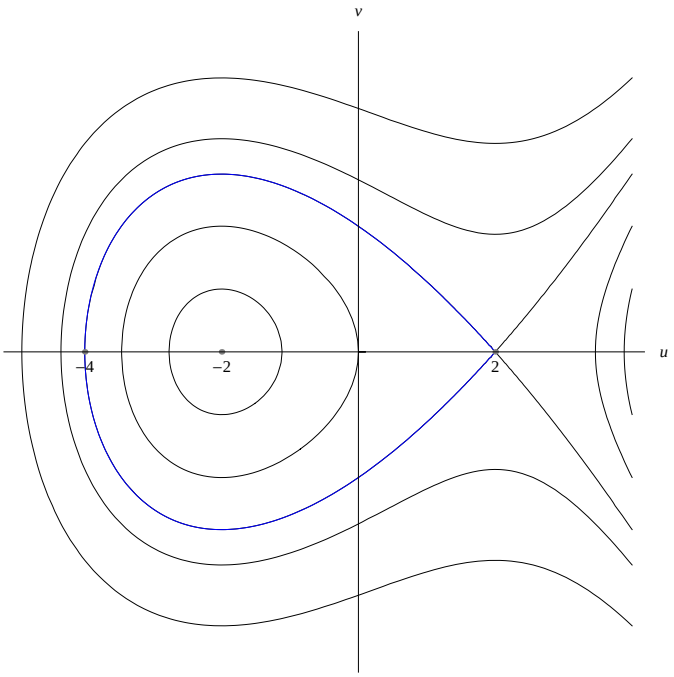


**Figure 1.1:** The phase portrait of (1.17) with $\gamma_1 = -4$. The blue level curve is the saddle connection with value $H(u,v) = 5\frac{1}{3}$ and is explicitly given by (1.18). The indicated points are the intersections of the level curves $H = \pm 5\frac{1}{3}$ with the $u$-axis.

### Transformation to BT normal form II

**Theorem 4.** *Consider a smooth planar system*

$$\dot{x} = f(x,\alpha), \quad x \in \mathbb{R}^2, \quad \alpha \in \mathbb{R}^2, \tag{1.19}$$

*with a double zero eigenvalue* $\lambda_{1,2} = 0$ *for* $\alpha = 0$ *at the equilibrium* $x = 0$ *and assume that* $A(0) = f_x(0,0) \neq 0$. *Then system* (1.19) *can be transformed into system* (1.4)*, with coefficients* $a_{kl}(\alpha), b_{kl}(\alpha)$ *smooth in* $\alpha$ *and satisfying* $a_{00}(0) = a_{10}(0) = b_{00}(0) = b_{10}(0) = b_{01}(0) = 0$ *and* $a_{01}(0) = 1$.

*Assume furthermore that the following conditions hold,*

$$a_{20}(0) + b_{11}(0) \neq 0, \tag{1.20a}$$

$$b_{20}(0) \neq 0, \tag{1.20b}$$

$$\text{the map } (x,\alpha) \mapsto \left( f(x,\alpha), \operatorname{tr}\left(\frac{\partial f(x,\alpha)}{\partial x}\right), \det\left(\frac{\partial f(x,\alpha)}{\partial x}\right)\right) \tag{1.20c}$$

*is regular at* $(x,\alpha) = (0,0)$.

*Then there are smooth invertible variable transformations, smoothly depending on its parameters, smooth invertible parameter changes and direction-*

*preserving time reparametrisations, reducing* (1.19) *to the two-parameter* Bogdanov-Takens normal form

$$\begin{cases} \dot{\eta}_1 = \eta_2, \\ \dot{\eta}_2 = \beta_1 + \beta_2\eta_1 + \eta_1^2 + s\eta_1\eta_2 + \mathcal{O}(\|\eta\|^3), \end{cases} \tag{1.21}$$

*where* $s = \operatorname{sign}\left(b_{20}(0)(a_{20}(0) + b_{11}(0))\right) = \pm 1$.

*Proof.* The first transformation of (1.19) into the form with the Taylor series (1.4) is already shown above. The further transformation to the Bogdanov-Takens normal form can be done in an almost similar way as we transformed the same system to the slightly different normal form (1.7). The transformation is obtained by repeating the procedure described for Lemma 1, while interchanging step 2 and 3 and taking some other suitable (and obvious) choices for $\delta(\alpha)$, $\vartheta(\alpha)$ and for the new variables. □

Observe that system (1.21) also has a Hamiltonian part. The solution to this Hamiltonian system is less known in the literature, however. For example, Guckenheimer & Holmes [5], Beyn [2] and Kuznetsov et al. [9] all use the formulation (1.7) of the Bogdanov-Takens normal form. We follow the same method as in the last paper to obtain an expression for the homoclinic orbit in the case of 1:1 resonance; see section 2.3.3 and Appendix A.

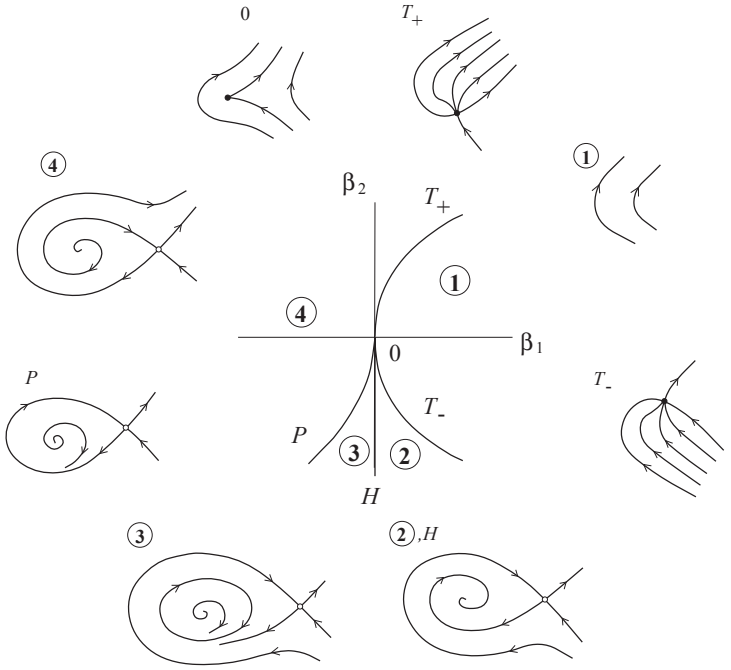


**Figure 1.2:** Bifurcation diagram for the Bogdanov-Takens normal form (1.21) with $s = -1$.

The bifurcation diagram of the normal form (1.21) for $s = -1$ and without the higher order terms, is shown in figure 1.2. The system has at most two equilibria at $\eta_2 = 0$ with $\eta_1$ a solution of $\beta_1 + \beta_2\eta_1 + \eta_1^2 = 0$. At the parabola $T$, given by $4\beta_1 = \beta_2^2$, the two equilibria collide into one non-hyperbolic equilibrium with eigenvalue zero. Indeed, at the left side of this line there are two equilibria, a saddle and a node, which collide at $T$ and thus leading to a *fold bifurcation*.

The line $H = \{(\beta_1, \beta_2) : \beta_1 = 0, \beta_2 < 0\}$ gives rise to equilibria with purely complex eigenvalues $\lambda_{1,2} = \pm i\omega$. This is a nondegenerate *Hopf bifurcation*: crossing the line from right to left yields a stable limit cycle.

The most important curve for our purposes is the one denoted by $P$, locally given by $\beta_1 = -\frac{6}{25}\beta_2^2 + \mathcal{O}(\beta_2^2)$ for $\beta_2 < 0$. This line corresponds to a saddle-homoclinic bifurcation, i.e. for small parameter values on this line we will find an orbit *homoclinic* to the saddle equilibrium, i.e. an orbit that is asymptotic to the same equilibrium as $t \to \infty$ and $t \to -\infty$. The appearance of the homoclinic orbit, which is a global change, can be checked by a blow-up of the normal form (1.21) and using a split function (see for example [8]). We will meet this curve again by looking at the normal form of 1:1 resonance, but in that case it will become a narrow region wherein homoclinic structures arise.

The case $s = +1$ can be studied similarly, by substituting $t \mapsto -t$ and $\eta_2 \mapsto -\eta_2$ into (1.21). Thus, the parametric portrait remains the same, except for the cycle, which becomes unstable near the Bogdanov-Takens bifurcation.

### 1.2.2 Neimark-Sacker bifurcation

Consider a discrete-time system (1.2), with $n = 2$, $m = 1$. The system undergoes a Neimark-Sacker bifurcation if, for sufficiently small $|\alpha|$, there exists for the fixed point $x = 0$ a pair of complex-conjugate eigenvalues (called *multipliers* in this case) crossing the unit circle: $\lambda_{1,2}(\alpha) = r(\alpha)e^{\pm i\varphi(\alpha)}$ with $r(0) = 1$ and $\varphi(0) = \vartheta_0$, satisfying $\mu_{1,2} = e^{\pm i\vartheta_0}, 0 < \vartheta_0 < \pi$ at $\alpha = 0$. Suppose that a transversality condition and a nondegeneracy condition holds. To wit:

$$r'(0) \neq 0, \tag{1.22a}$$

$$e^{ik\vartheta_0} \neq 1 \text{ for } k = 1, 2, 3, 4. \tag{1.22b}$$

Then, it can be proven that any such system exhibiting the Neimark-Sacker bifurcation can be transformed smoothly into the form

$$\begin{aligned}\begin{pmatrix} y_1 \\ y_2 \end{pmatrix} \mapsto (1+\beta) &\begin{pmatrix} \cos\vartheta(\beta) & -\sin\vartheta(\beta) \\ \sin\vartheta(\beta) & \cos\vartheta(\beta) \end{pmatrix} \begin{pmatrix} y_1 \\ y_2 \end{pmatrix} \\ + (y_1^2 + y_2^2) &\begin{pmatrix} \cos\vartheta(\beta) & -\sin\vartheta(\beta) \\ \sin\vartheta(\beta) & \cos\vartheta(\beta) \end{pmatrix} \begin{pmatrix} d(\beta) & -b(\beta) \\ b(\beta) & d(\beta) \end{pmatrix} \begin{pmatrix} y_1 \\ y_2 \end{pmatrix} + \mathcal{O}(\|y\|^4),\end{aligned} \tag{1.23}$$

where $\vartheta(0) = \vartheta_0$, see [8]. We can rewrite this system (1.23) in complex notation as

$$z \mapsto ze^{i\vartheta_0}(1 + d_1|z|^2) + \mathcal{O}(|z|^4),$$

where $d_1(\beta) = d(\beta) + ib(\beta) \in \mathbb{C}^1$. For a generic system to have Neimark-Sacker bifurcation we need the conditions in (1.22) and the extra nondegeneracy condition

$$d(0) = \text{Re } d_1(0) \neq 0.$$

If a generic discrete system satisfies the properties and conditions described above, then there is a neighbourhood of $x_0$ in which a unique closed invariant curve originates from the fixed point as $\alpha$ passes the bifurcation value 0. Depending on the sign of $d$ at zero, the closed invariant curve is either stable ($d(0) < 0$, *supercritical*, see figure 1.3) or unstable ($d(0) > 0$, *subcritical*).

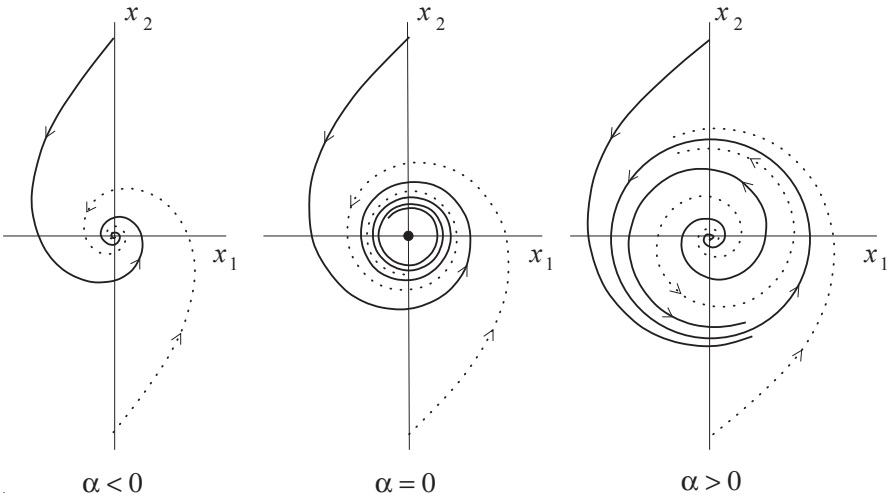


**Figure 1.3:** Phase portraits for the supercritical Neimark-Sacker bifurcation.

Note that the system (1.23) includes the higher order terms $\mathcal{O}(\|y\|^4)$. If we truncate at order three (leaving out all terms of order four and higher), we end up with a system which is in general *not* locally topologically equivalent. Therefore, we cannot simply remove these higher order terms in order to obtain a topological normal form for the Neimark-Sacker bifurcation, they do affect the bifurcation behaviour of the system. Nevertheless, some important features remain, such as the bifurcation of the locally unique invariant curve from the origin with the same direction and stability as in the system without the $\mathcal{O}(\|y\|^4)$-terms.

### 1.2.3 Resonance 1:1

Condition (1.22b) actually forms the connection with the codimension 2 bifurcation cases of 1:$k$ resonance, $k = 1, 2, 3, 4$. To have such a bifurcation for $k = 1, 2, 3, 4$, by definition this condition is violated. Indeed, in the case of 1:1 resonance there is a double eigenvalue

$$\lambda_{1,2}(\alpha_0) = e^{\pm ik\vartheta_0} = 1, \tag{1.24}$$

with $k = 1, \vartheta_0 = 0$. Such a codim 2 bifurcation can be located on the codim 1 curve of the Neimark-Sacker bifurcation (in a two-parameter-space) exactly at the point where (1.24) holds. (See for example figure 2.29 for the case of the normal form of 1:1 resonance.)

In a generic situation of 1:1 resonance, we consider a smooth map (1.2) with $n = m = 2$ which has at $\alpha_0 = 0$ a fixed point $x = 0$ (arrange this by a smooth translation) with a double unit multiplier $\lambda_{1,2} = 1$. Assume that the generalized and adjoint eigenvectors $q_{1,2}$ and $p_{1,2}$ of the Jacobian matrix $A = f_x(0, 0) \neq 0$ and its inverse $A^T$, respectively, satisfy

$$\begin{aligned} Aq_1 &= q_1, & Aq_2 &= q_1 + q_2, \\ A^T p_2 &= p_2, & A^T p_1 &= p_1 + p_2, \\ \langle q_1, p_1\rangle &= \langle q_2, p_2\rangle = 1, \\ \langle q_2, p_1\rangle &= \langle q_1, p_2\rangle = 0, \end{aligned}$$

using the standard inner product. Then we can use a similar reasoning as in the Bogdanov-Takens case (cf. section 1.2.1) to expand the right-hand-side of a generic map with the given properties as a Taylor series with respect to $y$ at $y = 0$, up to and including second order. We arrive then at the expansion

$$\begin{cases} y_1 \mapsto y_1 + y_2 + c_{00} + c_{10}y_1 + c_{01}y_2 \\ \qquad\quad + c_{20}y_1^2 + c_{11}y_1y_2 + c_{02}y_2^2 + \mathcal{O}(\|y\|^3), \\ y_2 \mapsto y_2 + d_{00} + d_{10}y_1 + d_{01}y_2 \\ \qquad\quad + d_{20}y_1^2 + d_{11}y_1y_2 + d_{02}y_2^2 + \mathcal{O}(\|y\|^3), \end{cases} \tag{1.25}$$

where the general coefficients $c_{kl}, d_{kl}$ smoothly depend on $\alpha$ and satisfy $c_{00}(0) = c_{10}(0) = c_{01}(0) = d_{00}(0) = d_{10}(0) = d_{01}(0) = 0$. These coefficients can be computed directly from the original map $f$ and the generalized and adjoint eigenvectors $q_{1,2}$ and $p_{1,2}$, by

$$\begin{aligned} c_{kl}(\alpha) &= \left.\frac{\partial^{k+l}}{\partial^k y_1 \partial^l y_2}\right|_{y=0} \langle p_1, f(y_1q_1 + y_2q_2, \alpha)\rangle, \\ d_{kl}(\alpha) &= \left.\frac{\partial^{k+l}}{\partial^k y_1 \partial^l y_2}\right|_{y=0} \langle p_2, f(y_1q_1 + y_2q_2, \alpha)\rangle. \end{aligned}$$

In this situation the Jacobian matrix $A$ gets the particular form

$$A = \begin{pmatrix} 1 & 1 \\ 0 & 1 \end{pmatrix},$$

a Jordan block of order 2.

One can prove (see [8]) that system (1.25) can be transformed under certain conditions into the normal form map.

**Theorem 5.** *Consider the expansion in* (1.25) *and suppose that the following conditions hold*

$$d_{20}(0) \neq 0; \tag{1.26a}$$

$$\det \left( \frac{\partial \nu}{\partial \alpha} \right) \Big|_{\alpha=0} \neq 0. \tag{1.26b}$$

*Then, for sufficiently small* $\|\alpha\|$*, there are smooth invertible transformations that transform* (1.25) *into the* normal form of 1:1 resonance*:*

$$N(\nu, \cdot) : \begin{pmatrix} \xi_1 \\ \xi_2 \end{pmatrix} \mapsto \begin{pmatrix} \xi_1 + \xi_2 \\ \xi_2 + \nu_1 + \nu_2 \xi_2 + B_1(\nu)\xi_1^2 + B_2(\nu)\xi_1\xi_2 \end{pmatrix} + \mathcal{O}(\|\xi\|^3), \tag{1.27}$$

*for smooth functions* $B_1(\nu)$ *and* $B_2(\nu)$ *and satisfy*

$$B_1(0) = a_0 := \tfrac{1}{2} d_{20}(0), \qquad B_2(0) = b_0 := c_{20}(0) + d_{11}(0).$$

□

The first condition is a nondegeneracy condition, while the second guarantees that, for small $\|\nu\|$, we may use $\nu$ as the new parameter via the Inverse Function Theorem, such that $\alpha(\nu = 0) = 0$.

We want to approximate the map (1.27) by the unit-time shift $\varphi^1$ of a flow $\varphi^t$ corresponding to a certain system of autonomous differential equations. For sufficiently small $\|\nu\|$ the following map represents the normal form (1.27):

$$N(\nu, \xi) = \varphi^1(\nu, \xi) + \mathcal{O}(\|\nu\|^2) + \mathcal{O}(\|\xi\|^2\|\nu\|) + \mathcal{O}(\|\xi\|^3).$$

The flow $\varphi^t(\nu, \cdot)$ here is obtained from the smooth planar system

$$\dot{\xi} = F(\nu, \xi) = F_0(\nu) + F_1(\nu, \xi) + F_2(\xi), \quad \xi \in \mathbb{R}^2, \quad \nu \in \mathbb{R}^2, \tag{1.28}$$

with each function $F_k$ defined by

$$F_0(\nu) = \begin{pmatrix} -\frac{1}{2}\nu_1 + \frac{1}{20}(-a_0 + 2b_0)\nu_1^2 + \frac{1}{3}\nu_1\nu_2 \\ \nu_1 + \frac{1}{60}(2a_0 - 5b_0)\nu_1^2 - \frac{1}{2}\nu_1\nu_2 \end{pmatrix},$$

$$F_1(\nu, \xi) = \begin{pmatrix} \xi_2 + \left(-\frac{1}{2}a_0 + \frac{1}{3}b_0\right)\nu_1\xi_1 + \left(\left(\frac{1}{5}a_0 - \frac{5}{12}b_0\right)\nu_1 - \frac{1}{2}\nu_2\right)\xi_2 \\ \left(\frac{2}{3}a_0 - \frac{1}{2}b_0\right)\nu_1\xi_1 + \left(\left(-\frac{1}{6}a_0 + \frac{1}{2}b_0\right)\nu_1 + \nu_2\right)\xi_2 \end{pmatrix},$$

$$F_2(\xi) = \begin{pmatrix} -\frac{1}{2}a_0\xi_1^2 + \left(\frac{2}{3}a_0 - \frac{1}{2}b_0\right)\xi_1\xi_2 + \left(-\frac{1}{6}a_0 + \frac{1}{3}b_0\right)\xi_2^2 \\ a_0\xi_1^2 + (-a_0 + b_0)\xi_1\xi_2 + \left(\frac{1}{6}a_0 - \frac{1}{2}b_0\right)\xi_2^2 \end{pmatrix}.$$

This system is obtained using Picard iterations to find the unknown coefficients up to the desired order (see section 1.4). We compute this flow up to the given order in section 2.3.2, which yields a unit-time shift that approximates the normal form well.

Under the additional nondegeneracy condition for the map (1.25),

$$c_{20}(0) + d_{11}(0) - d_{20}(0) \neq 0, \tag{1.29}$$

we can apply Theorem 4 to the approximating ODE (1.28) to show that it is locally topologically equivalent to the Bogdanov-Takens normal form (1.21) with $s = \operatorname{sign}\big(B_1(0)(B_2(0) - 2B_1(0))\big)$, see [8]. Moreover, if we change condition (1.29) into

$$c_{20}(0) + d_{11}(0) - \tfrac{1}{2}d_{20}(0) \neq 0, \tag{1.29$'$}$$

then — by Lemma 1 — system (1.28) is locally topologically equivalent to the other formulation of the Bogdanov-Takens normal form (1.7):

$$\begin{cases} \dot{\eta}_1 = \eta_2, \\ \dot{\eta}_2 = \beta_1 + \beta_2\eta_2 + \eta_1^2 + s\eta_1\eta_2 + \mathcal{O}(\|\eta\|^3), \end{cases}$$

with $s = \operatorname{sign}\big(B_1(0)(B_2(0) - B_1(0))\big)$. It follows that the behaviour of the flow $\varphi^t$ can be obtained from the Bogdanov-Takens theory, provided that the nondegeneracy and transversality conditions (1.6) or (1.20) are satisfied. These conditions are indeed satisfied for this system or they are described by the already posed conditions (1.26) and (1.29 or 1.29$'$). (Note that (1.26a) also gives the transversality of the Bogdanov-Takens bifurcation for free.)

### Bifurcation diagram

Following the reasoning before in the first case (the equivalence of the approximating ODE to the Bogdanov-Takens normal form (1.21)), a similar bifurcation diagram as figure 1.2 for the Bogdanov-Takens normal form with $s = -1$ can be drawn for the approximating flow $\varphi^1$ (for both $s = \pm 1$), if we take into account the correspondence between its variables $(\eta, \beta)$ and $(\xi, \nu)$. Because the Bogdanov-Takens normal form is an ODE, while the time-one-shift is a map, equilibria are changed into fixed points and limit cycles into closed invariant curves. We will meet the same bifurcation curves, but with the corresponding bifurcations for maps. For example the curve denoted by $H$ now gives a Neimark-Sacker bifurcation (also called Hopf-bifurcation for maps), generating a stable closed invariant curve, which disappears via a saddle-homoclinic bifurcation at $P$. The curve $T$, producing a saddle and

a stable fixed point, still corresponds to a fold bifurcation, but now in the case for maps.

However, the topological equivalence holds for the flow which only approximates the normal form. Therefore, the bifurcation diagram near the 1:1 resonance point is different from the diagram near a Bogdanov-Takens bifurcation. Although some features are still present, in the case of 1:1 resonance things become more difficult. A schematic bifurcation diagram for a generic map with 1:1 resonance is given in figure 1.4, with only some of the known bifurcations.

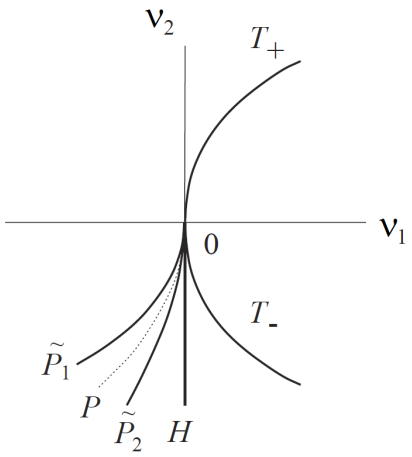


**Figure 1.4:** Bifurcation diagram of a generic planar map with 1:1 resonance.

The bifurcation curve $T$ again corresponds to a fold bifurcation: crossing $T$ from right to left leads to the appearance of two fixed points, a stable and an unstable one. The curve labelled $H$ denotes a Neimark-Sacker bifurcation. A closed invariant curve bifurcating from the stable fixed point exists for parameter values near $H$; it might be destroyed if we move away from $H$, due to complex behaviour in the generic situation.

The region enclosed by the curves $\tilde{P}_{1,2}$ is very interesting for the scope of this project. Did we have only one single curve $P$ for the Bogdanov-Takens case and even for the flow, in the generic situation of 1:1 resonance this curve has grown to a small region with the shape of a horn. The width of this 'horn' is somewhat exaggerated for clarity; in reality this region is exponentially narrow as can be seen in figure 2.18 where a real, computed version of this region is shown. What is going on in this region is explained below in more detail.

The four curves $T$, $H$, and $\tilde{P}_{1,2}$ meet each other tangentially at 0, the codimension 2 point of 1:1 resonance. We should warn the reader that both the flow $\varphi^1$ and the truncation of the normal form (1.27) do not provide

a topological normal form, since adding higher order terms alter the bifurcation diagram into a topologically nonequivalent one. However, both maps grant important information on the behaviour of systems close to the bifurcation point of 1:1 resonance.

### Homoclinic behaviour

The approximating flow $\varphi^1$ has a homoclinic orbit for parameter values exactly at the curve $P$, i.e. the stable and unstable manifolds of the saddle coincide. This coincidence disappears in the generic case of 1:1 resonance. In the region between the mentioned curves $\tilde{P}_{1,2}$ the stable and unstable manifold will intersect each other transversally. At the boundary curves $P_{1,2}$ these intersections disappear and we are left with only *homoclinic tangencies*: the manifolds are just tangent to each other. If we move away from $\tilde{P}_{1,2}$ at the outside of that region, then the stable and unstable manifold do not touch each other, so there are no intersections or tangencies at all.

The transversal intersections provide a homoclinic structure and thus infinitely many intersections. This can be seen from the fact that an intersection point, say $x_0$, belongs to both the stable and unstable manifold. An orbit starting at $x_0$ would therefore converge to the saddle $x_s$ in both directions. So, if we apply the map $f$ or $f^{-1}$ repeatedly to $x_0$, we find a sequence of points converging as $f^k(x_0) \to x_s$ as $k \to \pm\infty$. And again, each iteration $f^k(x_0)$ is an intersection point and belongs to both the stable and unstable manifold.

The resulting complex behaviour, called *Poincaré homoclinic structure*, is shown in case of the McMillan map in figure 1.5. One sees that both manifolds are oscillating faster and faster to gain the infinite intersections. The oscillations become bigger and more narrow for intersections near the saddle point $x_s$.

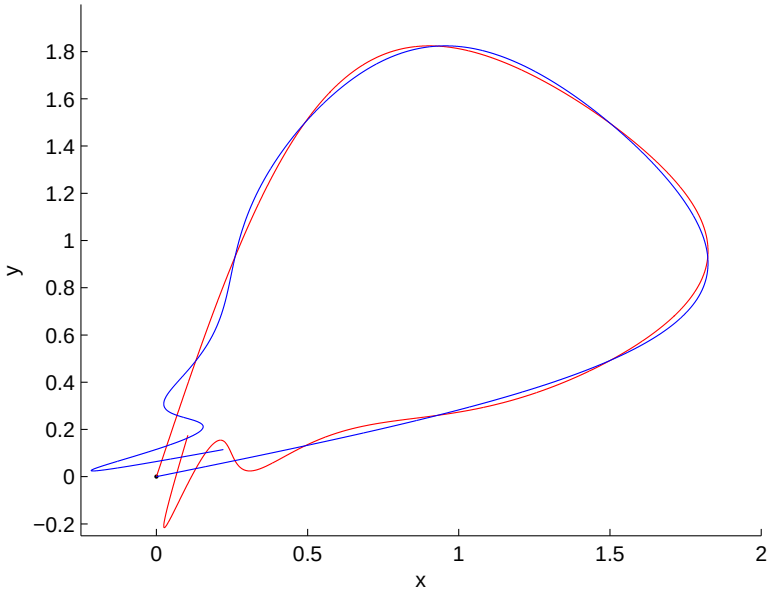


**Figure 1.5:** Transversal intersections of the stable and unstable manifolds in case of the McMillan map (2.1).

The homoclinic structure also results in infinitely many periodic points near the homoclinic orbit with arbitrarily high periods. This can be shown using the concept of a *Smale horseshoe*: consider for a sufficiently high number $N$, iterations $f^N(S)$ of a rectangle $S$ surrounding the stable manifold. The intersection of $S$ with $f^N(S)$ then forms several horseshoes. It is known from a theorem of Smale that the occurrence of each horseshoe implies a countable set of periodic orbits of arbitrarily long period, see [8].

## 1.3 Mel'nikov function

It is possible to compute the intersection points of the stable and unstable manifolds numerically, but there is also a way to approximate them up to first order in $\varepsilon$ using analytical methods. This is done by the so-called *Mel'nikov function*, which we describe in this section.

Consider a family of diffeomorphisms, given by

$$\Omega_\varepsilon : x \mapsto F(x) + \varepsilon G(x), \quad F, G : \mathbb{R}^2 \to \mathbb{R}^2, \quad x \in \mathbb{R}^2, \quad \varepsilon \in \mathbb{R}. \tag{1.30}$$

For $\varepsilon = 0$ this will give the unperturbed original map $F$, while for $\varepsilon \neq 0$ but small, an extra term comes into play. This extra term $\varepsilon G$ denotes the perturbation of the original map $F$.

Assume that the original map $F$ has a saddle at $x_s$ and that the stable and unstable manifolds for this point coincide with each other, at least at one side. For small perturbations the equilibrium remains a saddle point close to the original one, but the stable and unstable manifolds do not longer coincide. In fact, they might intersect each other infinitely often as is described in section 1.2.3.

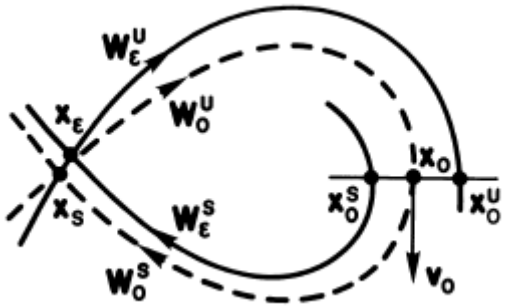


**Figure 1.6:** Perturbation of a loop ($W_0^{s,u}$, dashed) homoclinic to the saddle point $x_s$ for $\varepsilon = 0$. For small $\varepsilon \neq 0$ this saddle changes into $x_\varepsilon$ with $W_\varepsilon^{s,u}$ as local stable and unstable manifolds, respectively. The initial point $x_0$ is chosen freely along the homoclinic loop $W_0^s = W_0^u$.

Choose an initial point $x_0$ on the loop $W_0$ of the unperturbed map, with corresponding unit tangent vector $v_0$. Let $x_0^{s,u}(\varepsilon)$ denote the two intersection points of the perturbed, not explicitly known, stable resp. unstable manifolds $W_\varepsilon^{s,u}$ with the normal to $W_0$. The *Mel'nikov distance* $\Delta$ between these points — considered to be vectors from the origin — depends on the perturbation-parameter $\varepsilon$ and is given by

$$\begin{aligned} \Delta(\varepsilon) &= \Delta^u(\varepsilon) - \Delta^s(\varepsilon) := (x_0^u(\varepsilon) - x_0) \wedge v_0 - (x_0^s(\varepsilon) - x_0) \wedge v_0 \\ &= (x_0^u(\varepsilon) - x_0^s(\varepsilon)) \wedge v_0, \end{aligned} \tag{1.31}$$

where $\wedge$ denotes a 'wedge'-product, defined by $(x_1, x_2) \wedge (y_1, y_2) := x_1 y_2 - x_2 y_1$. We can expand this distance in $\varepsilon$ as follows:

$$\Delta(\varepsilon) = \varepsilon(M + \mathcal{O}(\varepsilon)),$$

where $M$ denotes the *Mel'nikov function*. If we take the derivative of the expression for $\Delta$ with respect to $\varepsilon$ at $\varepsilon = 0$, we obtain the value of $M$. When $M$ is equal to zero, the corresponding initial $x_0^{u,s}(\varepsilon)$ is approximately an intersection point of the two manifolds.

We can add a $t$-component to $\Delta, M$ and $x_0$, which denotes our free choice of the initial point $x_0$ along the homoclinic loop, if there is an explicit expression of it in $t$. Define for $k \geq 0$ the $k$-th iterate of the initial point $x_0^s(\varepsilon)$ on the stable manifold $W_\varepsilon^s$ by $x_k^s := \Omega_\varepsilon^k(x_0^s(\varepsilon))$ and similarly for $k \leq 0$ the $k$-th iterate of the initial point $x_0^u(\varepsilon)$ on the unstable manifold $W_\varepsilon^u$ by $x_k^u := \Omega_\varepsilon^k(x_0^u(\varepsilon))$. Note that for $\varepsilon = 0$ these definitions are complement to each other, so that we can define $x_k$ by

$$x_k := \begin{cases} x_k^s(0), & \text{if } k \geq 0; \\ x_k^u(0), & \text{if } k \leq 0; \end{cases}$$

in particular, $x_0 = x_0^s(0) = x_0^u(0)$. Furthermore, let $v_k := (D(F^k)x_0)v_0$ be an 'iterate' of the initial tangent vector $v_0$ to $x_0$ for $k \in \mathbb{Z}$.

The rate of change of the distance between the two manifolds can be computed via the formula in the following proposition, see also [4]:

**Proposition 6.** *Assume that $F$ is an orientation-preserving mapping. The derivative of the distance between the stable and unstable manifolds of the family of diffeomorphisms* (1.30) *is given by the* Mel'nikov function

$$M = \Delta'(0) := \frac{\mathrm{d}}{\mathrm{d}\varepsilon}\bigg|_{\varepsilon=0} \Delta(\varepsilon) = \sum_{k=-\infty}^{\infty} |DF^k(x_k)|^{-1} G(x_{k-1}) \wedge v_k, \quad (1.32)$$

*where $|\cdot|$ denotes the determinant of a square matrix.*

*Proof.* According to equation (1.31), we want to find $\Delta'(0) = \frac{\mathrm{d}}{\mathrm{d}\varepsilon}\big|_{\varepsilon=0} (x_0^u(\varepsilon) - x_0^s(\varepsilon)) \wedge v_0$. We show only the stable part $\frac{\mathrm{d}}{\mathrm{d}\varepsilon}\big|_{\varepsilon=0} x_0^s(\varepsilon) \wedge v_0 = y_0 \wedge v_0$, where we define in general $y_k$ for $k \geq 0$ as the derivative of $x_0^s(\varepsilon)$ at $\varepsilon = 0$. The unstable part goes in a similar way.

In order to derive an expression for $y_0 \wedge v_0$, we first look at a formula for general $k \geq 0$. By definition of $x_k$, it holds that $x_{k+1}^s = \Omega_\varepsilon(x_k^s(\varepsilon)) = F(x_k^s(\varepsilon)) + \varepsilon G(x_k^s(\varepsilon))$. This gives for $y_{k+1}$,

$$y_{k+1} = \frac{\mathrm{d}}{\mathrm{d}\varepsilon}\bigg|_{\varepsilon=0} x_{k+1}^s(\varepsilon) = DF(x_k)y_k + G(x_k).$$

Wedging this by $v_{k+1}$ gives then

$$y_{k+1} \wedge v_{k+1} = (DF(x_k)y_k) \wedge v_{k+1} + G(x_k) \wedge v_{k+1}$$

$$\begin{aligned} &= (DF(x_k)y_k) \wedge (DF(x_k)v_k) + G(x_k) \wedge v_{k+1} \\ &= |DF(x_k)|(y_k \wedge v_k) + G(x_k) \wedge v_{k+1}, \end{aligned} \tag{1.33}$$

which is valid for $k \geq 0$. For $k = 0$ this yields, after rearranging,

$$y_0 \wedge v_0 = |DF(x_0^s)|^{-1}(y_1 \wedge v_1 - G(x_0) \wedge v_1),$$

which is our first induction step to derive the general formula

$$y_0 \wedge v_0 = \frac{y_{k+1} \wedge v_{k+1}}{|DF^k(x_k)|} - \sum_{j=0}^{k} \frac{G(x_j) \wedge v_{j+1}}{|DF^j(x_j)|}. \tag{1.34}$$

Assume that the last equation is also valid for all integers up to $m = k$, then for $m = k + 1$, using (1.33), it holds that

$$|DF^k(x_k)|^{-1}(y_{k+1} \wedge v_{k+1}) = \frac{y_{k+2} \wedge v_{k+2} - G(x_{k+1}) \wedge v_{k+2}}{|DF^k(x_k)||DF(x_{k+1})|}.$$

Substituting this expression into (1.34) yields then,

$$\begin{aligned} y_0 \wedge v_0 &= \frac{y_{k+2} \wedge v_{k+2} - G(x_{k+1}) \wedge v_{k+2}}{|DF^k(x_k)||DF(x_{k+1})|} - \sum_{j=0}^{k} \frac{G(x_j) \wedge v_{j+1}}{|DF^j(x_j)|} \\ &= \frac{y_{k+2} \wedge v_{k+2}}{|DF^k(x_{k+1})|} - \sum_{j=0}^{k+1} \frac{G(x_j) \wedge v_{j+1}}{|DF^j(x_j)|}. \end{aligned}$$

Hence, (1.34) is valid for each integer $k \geq 0$.

The next task is to take the limit $k \to \infty$. We may assume for simplicity that $|DF(x)|$ is constant — with some adjustments, the proof still holds for nonconstant $|DF(x)|$. Let $\lambda_{1,2}$ be the eigenvalues of $DF$ at $x_s$, corresponding to the contracting and expanding directions, and assume that $F$ is orientation-preserving. Since the point $x_s$ is a saddle, we then have two eigenvalues satisfying $0 < \lambda_1 < 1 < \lambda_2$. This gives the following restrictions on each term in (1.34) as $k \to \infty$: $v_k \to 0$ in the order $\lambda_2^k$; $|DF^k(x_k)| = (\lambda_1\lambda_2)^k$ and $y_k$ is bounded. Hence, in the limit the term $|DF^k(x_k)|^{-1}(y_{k+1} \wedge v_{k+1})$ vanishes, resulting in the following expression for the stable part:

$$\left.\frac{\mathrm{d}}{\mathrm{d}\varepsilon}\right|_{\varepsilon=0} x_0^s(\varepsilon) \wedge v_0 = y_0 \wedge v_0 = -\sum_{j=0}^{\infty} |DF^j(x_j)|^{-1} G(x_j) \wedge v_{j+1}. \tag{1.35}$$

The unstable part gives similarly,

$$\left.\frac{\mathrm{d}}{\mathrm{d}\varepsilon}\right|_{\varepsilon=0} x_0^u(\varepsilon) \wedge v_0 = \sum_{j=-\infty}^{-1} |DF^j(x_j^u)|^{-1} G(x_j^u) \wedge v_{j+1}. \tag{1.36}$$

Combining the formulas (1.35) and (1.36) then gives the desired result (1.32) for $M = \Delta'(0)$. □

The Mel'nikov function (1.32) can be simplified when $F$ is an area-preserving mapping. In that case it holds that $|DF^k(x)| = 1$, so that the formula for the distance reduces to

$$M = \Delta'(0) := \sum_{k=-\infty}^{\infty} G(x_{k-1}) \wedge v_k. \tag{1.37}$$

In other cases the function $F$ can be complicated and therefore it might be difficult to compute its determinant. In such cases the determinant of $F^k$ can be approximated and computed in another way. Consider the determinant $|DF^k(x_k)|$ for arbitrary positive $k > 0$. (The case $k < 0$ is treated similarly, but gets an extra power -1.) First, we approximate for each $k$

$$F^l(x_k) \approx x_{k+l}.$$

Using the chain-rule for $DF^k$, then gives

$$\begin{aligned} DF^k(x_k) &= D(F \circ F^{k-1})(x_k) = DF(F^{k-1}(x_k))DF^{k-1}(x_k) \\ &\approx DF(x_{2k-1})DF^{k-1}(x_k). \end{aligned}$$

Obviously, the determinant for $k = 0$ is just 1, while $k = 1$ gives only the term $DF(x_1)$. By induction we thus obtain the following

$$DF^k(x_k) \approx DF(x_{2k-1})DF^{k-1}(x_k) = \prod_{j=0}^{k-1} DF(x_{k+j}).$$

The determinant of the last expression can be taken inside or outside,

$$|DF^k(x_k)| = \left| \prod_{j=0}^{k-1} DF(x_{k+j}) \right| = \prod_{j=0}^{k-1} |DF(x_{k+j})|,$$

using the rule that the determinant of the product of two equal-sized square matrices is equal to the product of the determinants of both separate matrices.

## 1.4 Picard iterations

Suppose we want to unravel the behaviour and bifurcations of a general map (1.2). When we analyse such a system it is not guaranteed that one would find all the information to construct a bifurcation diagram. To overcome this problem, at least partly, we approximate the map in question by shifts along the orbits of an approximating system of autonomous ordinary differential equations. Although maps and approximating ODE's have different properties, we can use the information provided in this way to say

more about the bifurcation structure of a map. For example, global bifurcations of closed invariant curves occur in a map near the homo- and heteroclinic bifurcations of the approximating ODE.

The approximating ODE for a map can be obtained by means of Picard iterations, see [8]. Start with the Taylor expansion of the map around the fixed point $x_0 = 0$,

$$x \mapsto f(x) = Ax + f^{(2)}(x) + f^{(3)}(x) + \dots, \quad x \in \mathbb{R}^n, \tag{1.38}$$

with $A = f_x(x_0)$ and $f^{(k)}(x)$ a smooth homogeneous polynomial vector-valued function of order $k$. Next, consider the Taylor expansion of approximating system

$$\dot{x} = F(x) = \Lambda x + F^{(2)}(x) + F^{(3)}(x) + \dots, \quad x \in \mathbb{R}^n, \tag{1.39}$$

with an equilibrium at $x_0 = 0$, $\Lambda$ a matrix and the functions $F^{(k)}(x)$ have the same properties as the $f^{(k)}(x)$. If the unit-time shift along the orbits of (1.39) coincides with the Taylor expansion of the map (1.38) up to and including terms of order $k$, i.e. it satisfies,

$$f(x) = \varphi^1(x) + \mathcal{O}(\|x\|^{k+1}),$$

then the map (1.38) is said to be *approximated up to order* $k$ by system (1.39).

To obtain the Taylor series of the unit-time shift, we use *Picard iterations* as follows: start with the initial solution of the linear equation $\dot{x} = \Lambda x$,

$$x^{(1)}(t) = e^{\Lambda t}x.$$

The next iterates $k > 1$ are given in terms of the $F^{(k)}$ as follows,

$$x^{(k)}(t) = e^{\Lambda t}x + \int_0^t e^{\Lambda(t-\tau)} \left( F^{(2)}(x^{(k-1)}(\tau)) + \dots + F^{(k)}(x^{(k-1)}(\tau)) \right) \mathrm{d}\tau,$$

for $k \geq 2$. If $k$ increases, then the approximation becomes better: each new iterate $l$ only affects terms of order $l$ and higher. For $t = 1$ and a chosen $k > 0$ we obtain the right $k$-th order Taylor expansion of $\varphi^1(x)$ up to including terms of order $k$:

$$\varphi^1(x) = x^{(k)}(x) = e^{\Lambda}x + g^{(2)}(x) + \dots + g^{(k)}(x) + \mathcal{O}(\|x\|^{k+1}),$$

where each function $g^{(j)}$ is a smooth homogeneous polynomial of order $j$. Since this unit time shift needs to approximate the map as good as possible, we can recover the ODE (1.39) by equating each of its terms as

$$e^{\Lambda} = A, \qquad g^{(j)}(x) = f^{(j)}(x), \quad j > 1.$$

Solving these equations — which is not always possible — gives an expression for the unit-time shift $\varphi^1(x)$ and for the system (1.39).

# 2

# Applications and results

At this point, it is time to put the previous theoretical part into practice. This chapter is devoted to the preparation for and the computation of the Mel'nikov function. Two different maps will be studied, namely the McMillan map and the normal form of 1:1 resonance, which have homoclinic structures in a certain region of the parameter space. We investigate the behaviour of these maps by numerical computation of, for example, its stable and unstable manifolds, homoclinic orbits and continuations. For this purpose we make extensively use of the software MatCont, see [6, 7]. After that, we do the preparing computations for the application of the Mel'nikov function. Our ultimate goal, at the end, is to apply the Mel'nikov function to each map.

## 2.1 Numerical computation of homoclinic orbits

Let's first shortly explain how homoclinic orbits are actually computed numerically. Via the definition of a homoclinic orbit, we can view such an orbit (homoclinic to $x_0$) as the solution of the infinite boundary value problem,

$$\begin{cases} \Gamma(\xi_{\mathbb{Z}}, \alpha_0) = 0, \\ \lim\limits_{n \to \pm\infty} \xi_n = x_0, \end{cases}$$

where $\Gamma$ is the operator

$$\begin{aligned} \Gamma : S^N_{\mathbb{Z}} \times \mathbb{R}^p &\to S^N_{\mathbb{Z}} \\ (x_{\mathbb{Z}}, \alpha) &\mapsto (x_{n+1} - f(x_n, \alpha))_{n \in \mathbb{Z}}, \end{aligned}$$

defined on the Banach space (with supremum-norm),

$$S^N_J := \left\{ x_J \in (\mathbb{R}^N)^J : \sup_{n \in J} \|x_n\| < \infty \right\},$$

for any norm $\|\cdot\|$ on $\mathbb{R}^N$ and $J = [N_-, N_+] \cap \mathbb{Z}$ for $N_+, N_- \in \mathbb{Z} \cup \{\pm\infty\}$ with $N_- < 0 < N_+$. But in numerical calculations we do not want to deal with infinitely long sets and hence, infinitely long computations, so we truncate the problem and replace $\Gamma$ by its finite version $\hat{\Gamma}$, defined as,

$$\begin{aligned}\hat{\Gamma} : S_J^N \times \mathbb{R}^p &\to S_J^N \\ (x_J, \alpha) &\mapsto \left( (x_{n+1} - f(x_n, \alpha))_{n \in \hat{J}}, b(x_{N_-}, x_{N_+}, \alpha) \right),\end{aligned}$$

where $b : \mathbb{R}^{2N} \times \mathbb{R}^p \to \mathbb{R}^N$ is a boundary condition and $\hat{J} = [N_-, N_+ - 1] \cap \mathbb{Z}$ for $N_+ < \infty$.

Suppose $\xi_{\mathbb{Z}} \in S_{\mathbb{Z}}^N$ is a transversal orbit, homoclinic to the saddle $x_0 \in \mathbb{R}^N$ of a given system (1.2) at parameter values $\alpha_0$. For sufficiently large $-N_-, N_+$ and under certain assumptions, there exist a unique zero $\xi_{0,J} \in S_J^N$ of $\hat{\Gamma}(\cdot, \alpha_0)$, which lies close to $\xi_{\mathbb{Z}}|_J$. Moreover, one can show (see [3]) that the following estimate holds,

$$\sup_{n \in J} \|\xi_{\mathbb{Z}}|_J - \xi_{0,J}\| \leq C \left( \|\xi_{N_-} - x_0\|^s + \|\xi_{N_+} - x_0\|^s \right),$$

for $C > 0$, while $s = 1$ or $2$, if $b$ is a periodic or a projection boundary condition, respectively.

Tangential[1] homoclinic orbits can be approximated by turning points of $\hat{\Gamma}$, that is to say, as zeroes of the operator $\Theta$:

$$\begin{aligned}\Theta : S_J^N \times S_J^N \times \mathbb{R}^p &\to S_J^N \times S_J^N \times \mathbb{R} \\ (x_J, u_J, \alpha) &\mapsto \begin{pmatrix} \hat{\Gamma}(x_J, \alpha) \\ \hat{\Gamma}_{x_J}(x_J, \alpha) u_J \\ \sum_{i=N_-}^{N_+} \|u_i\|^2 - 1 \end{pmatrix},\end{aligned}$$

where $\|\cdot\|$ denotes the Euclidean norm on $\mathbb{R}^N$.

## 2.2 McMillan map

The first system of study is the McMillan map, for which the method of the Mel'nikov function is known to work, see [4]. So, this is a good test case to see how the procedure works, how to set it up (although the McMillan map is much easier to handle than the normal form of 1:1 resonance) and how to interpret the outcome of the Mel'nikov function.

[1] The orbit $\xi_{\mathbb{Z}}$ is called *tangential*, if the homogeneous difference equation $u_{n+1} = f_x(\xi_n, \alpha_0) u_n$, $n \in \mathbb{Z}$ has only one independent bounded solution $u$.

### 2.2.1 Properties

The *McMillan map* is given by

$$\begin{pmatrix} x \\ y \end{pmatrix} \mapsto \begin{pmatrix} y \\ -x + 2\mu \frac{y}{1+y^2} + \varepsilon(\beta x + \gamma y) \end{pmatrix}, \tag{2.1}$$

with parameters $\mu > 1$, $\beta$, $\gamma$, and $\varepsilon$ a small perturbation coefficient. The fixed points of (2.1) are $a_0 = (0, 0)$ and

$$a_{1,2} = \pm \left( \sqrt{\frac{2\mu}{2 - \varepsilon(\beta+\gamma)} - 1}, \sqrt{\frac{2\mu}{2 - \varepsilon(\beta+\gamma)} - 1} \right).$$

The first, $a_0$, is a hyperbolic fixed point (saddle) for certain values of the parameters, as can be seen from the eigenvalues of the Jacobian matrix at $a_0$:

$$\begin{pmatrix} 0 & 1 \\ \varepsilon\beta - 1 & \frac{2\mu y_s}{1+y_s^2} - \frac{4\mu y_s}{(1+y_s^2)^2} + \varepsilon\gamma \end{pmatrix} = \begin{pmatrix} 0 & 1 \\ \varepsilon\beta - 1 & 2\mu + \varepsilon\gamma \end{pmatrix},$$

which are given by

$$\lambda_\pm = \tfrac{1}{2}(2\mu + \varepsilon\gamma) \pm \tfrac{1}{2}\sqrt{(2\mu + \varepsilon\gamma)^2 + 4(\varepsilon\beta - 1)}.$$

In the following numeric calculations, we use these useful values of the parameters to start with:

$$(\mu, \varepsilon, \beta, \gamma) = (2, 0.05, 0.1, 1.9), \tag{2.2}$$

The corresponding eigenvalues of $a_0$ are

$$\lambda_- = 0.259413, \quad \lambda_+ = 3.83559,$$

showing that, for these parameter values, $a_0$ is indeed a hyperbolic saddle.

### 2.2.2 Hamiltonian

The unperturbed McMillan map — obtained by taking $\varepsilon = 0$ — is an area-preserving and invertible map with invariant curves satisfying

$$x^2y^2 + x^2 + y^2 - 2\mu xy = C, \tag{2.3}$$

where $C$ is a constant depending on the initial condition. In particular, if $C = 0$, we obtain the lemniscate in figure 2.1. This indicates that the stable and unstable manifold exactly coincide if there is no perturbation. We can find exact solutions for the $x$- and $y$-coordinates of this homoclinic orbit by treating (2.3) as a Hamiltonian. Consider therefore the continuous

system derived from the same equation (multiplied by $\frac{1}{2}$) for $C = 0$ with Hamiltonian

$$H(x, y) = \frac{x^2}{2} + \frac{y^2}{2} - \mu xy + \frac{x^2 y^2}{2}.$$

The corresponding equations of motion read,

$$\begin{aligned} \dot{x} &= \frac{\partial H}{\partial y} = y - \mu x + x^2 y, \\ \dot{y} &= -\frac{\partial H}{\partial x} = -x + \mu y - x y^2. \end{aligned} \tag{2.4}$$

From these equations we can eliminate $y$, to obtain for $H = 0$ the differential equation,

$$\dot{x}^2 = x^2(\mu^2 - 1 - x^2),$$

which has the positive solution,[2]

$$x(t) = \sqrt{\mu^2 - 1}\,\operatorname{sech}\left(\sqrt{\mu^2 - 1} \cdot t - t_0\right), \tag{2.5}$$

with $t_0$ an initial choice on the homoclinic orbit. Substituting the solution for $x$ in the second equation of (2.4) yields a similar solution for $y$,

$$y(t) = \sqrt{\mu^2 - 1}\,\operatorname{sech}\left(\sqrt{\mu^2 - 1} \cdot t + \operatorname{arccosh}\mu - t_0\right). \tag{2.6}$$

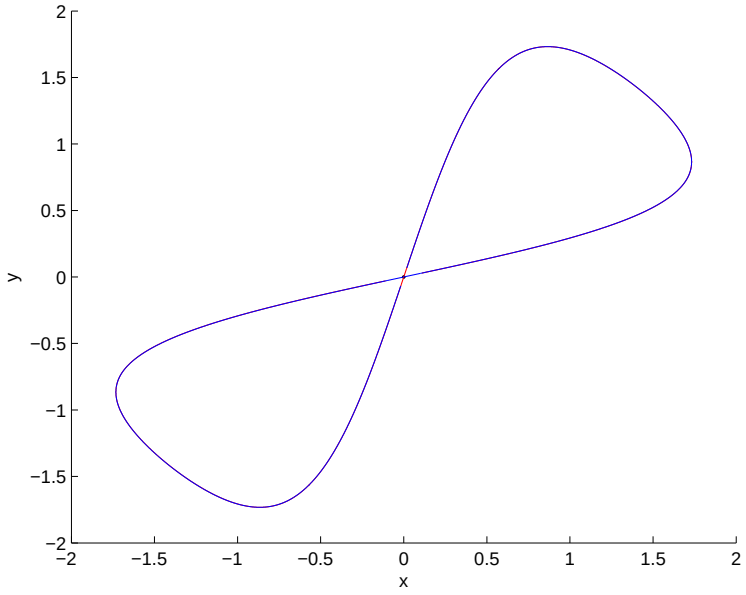


**Figure 2.1:** The original, unperturbed *McMillan map* (2.1) with parameter values $\mu = 2$ and $\varepsilon = 0$. Note that the stable and unstable manifolds exactly coincide, as it should be.

[2]Here, we make use of the hyperbolic function $\operatorname{sech} x = (\cosh x)^{-1}$.

Since the McMillan map itself is a discrete map, we have to switch back from a continuous Hamiltonian system to the discrete system. This is done by substituting for $t$ a certain time step $k\tau$ (where $\tau$ denotes the stepsize), such that for each integer $k$ we obtain a solution on the homoclinic orbit of the unperturbed McMillan map. The fact that $x_{k+1} = y_k$ holds (by the first component of the map), implies $\tau = \operatorname{arccosh}\mu \sinh(\operatorname{arccosh}\mu)^{-1}$. Substituting this result in (2.5) and (2.6), we have found the following parametrisation for the (homoclinic) orbit of the unperturbed McMillan map:

$$\begin{cases} x_k(t_0) = \sqrt{\mu^2 - 1}\,\operatorname{sech}(t_0 - k\operatorname{arccosh}\mu), \\ y_k(t_0) = \sqrt{\mu^2 - 1}\,\operatorname{sech}(t_0 - (k+1)\operatorname{arccosh}\mu), \end{cases} \tag{2.7}$$

where $t_0$ is a choice of the initial point on the homoclinic orbit, defining $(x_0, y_0)$.

### 2.2.3 Homoclinic structures and continuations

The equilibrium point $(0, 0)$ is a saddle with coinciding stable and unstable manifolds, i.e. a homoclinic orbit, as demonstrated in figure 2.1. For small perturbations the equilibrium remains a saddle point, but the stable and unstable manifolds may not longer coincide: they come apart from each other and eventually intersect each other. The numerical values in (2.2) result in such stable and unstable manifolds of the McMillan map with transversal intersections, as displayed in the figures 2.2 and 2.3.

We vary only $\beta$ and keep the other parameters fixed to obtain stable and unstable manifolds that do not intersect each other transversally anymore, but only show homoclinic tangencies, (Fig. 2.4). We would like to know for which values of $\beta$ and corresponding fixed point $x$ such a homoclinic structure exist. This is provided by a process called *continuation* (see [6]); the result is shown in figure 2.5.

Thereafter, we continue the curve of limit points in the two parameters $\mu$ and $\beta$ in order to find all possible combinations of parameter values $\mu$ and $\beta$ (while the others are fixed) for which the homoclinic structure, like figure 2.2, would exist. This continuation yields a 'crater-like' shape, visualised in figure 2.6. One would expect that this crater reaches to the point $(\beta, \mu) = (0, 1)$, because for $\mu \leq 1$ there is no homoclinic loop present for the unperturbed McMillan map. Moreover, for these parameter values the eigenvalues for the saddle (in the unperturbed case $\varepsilon = 0$) become both equal to 1, which means that it is not longer hyperbolic. If we take $\mu$ smaller than 1, then the eigenvalues become complex. Numerically, however, we do not reach the point $(0, 1)$, but it is possible to get closer to it, as we discuss in the next section.

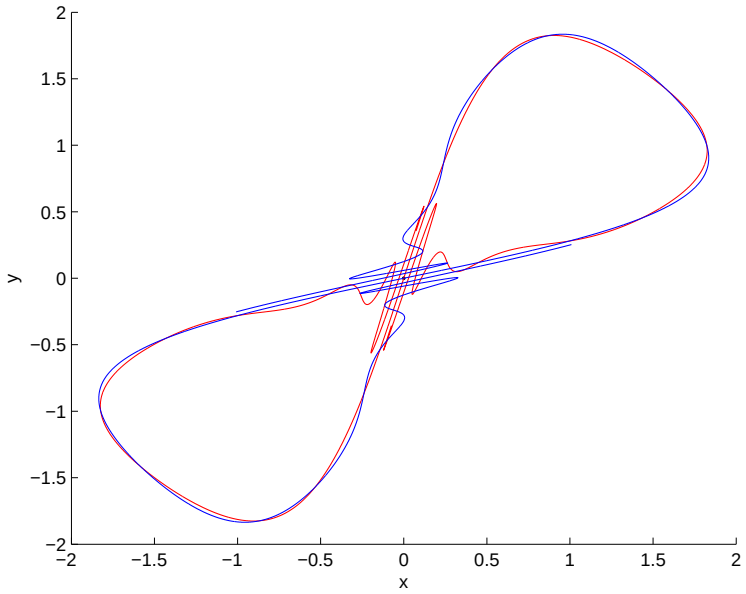


**Figure 2.2:** Transversal intersections and tangencies of the stable (blue) and unstable (red) manifolds of the saddle point $(0, 0)$ of the *McMillan map* (2.1) with parameter values as in (2.2).

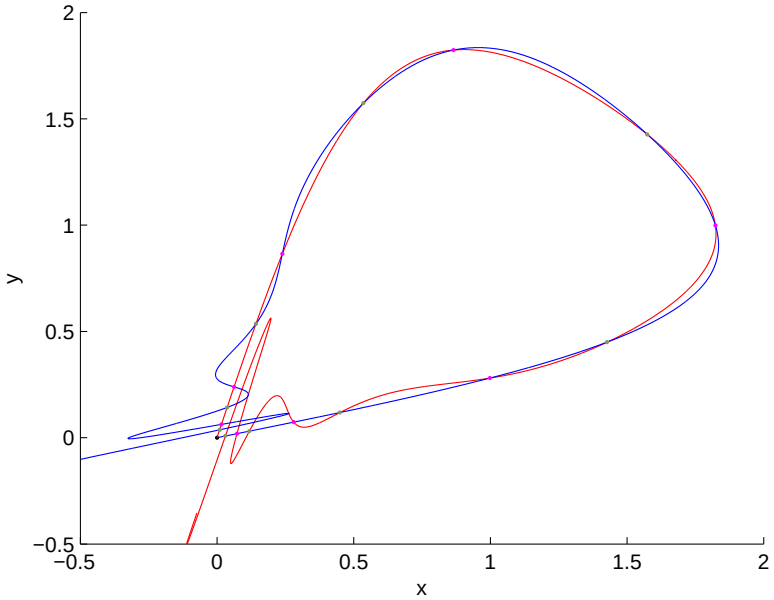


**Figure 2.3:** Close-up of the first quadrant of figure 2.2. Also shown is the location of the intersection points of the two manifolds in pink and green (8 and 9 points, respectively).

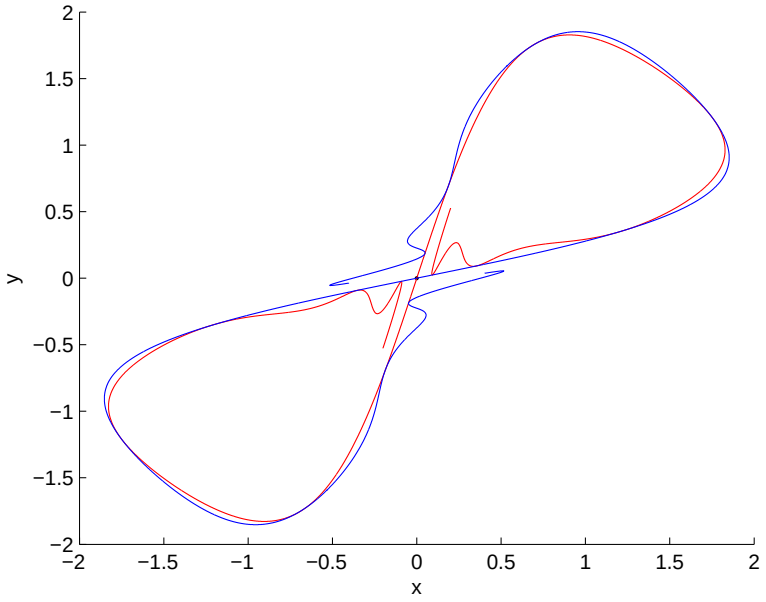


**Figure 2.4:** Homoclinic tangencies of the stable (blue) and unstable (red) manifolds of the saddle point $(0, 0)$ of the *McMillan map* (2.1) with parameter values as in (2.2), but with $\beta = 0.2593$.

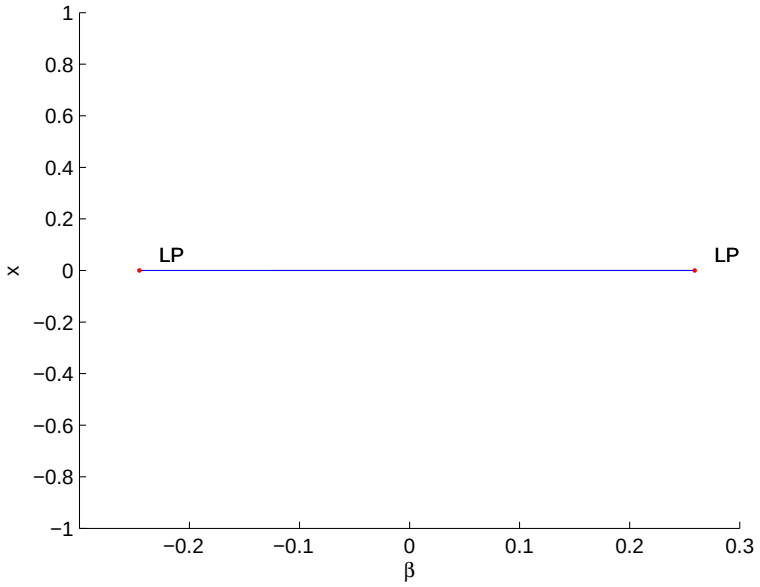


**Figure 2.5:** Continuation in $\beta$ of the homoclinic orbit for the *McMillan map* (2.1) with starting parameters given in (2.2).The points marked "LP", indicate the values for which the stable and unstable manifold are just tangent to each other.

### 2.2.4 Extension of the number of intersections

The continuation in two parameters, as mentioned above, is done with only nine of the located intersection points. This is not sufficient to come close to the point $(0, 1)$ of the parameter space. Therefore, we want to improve on this by taking more intersection points into account in the continuation, giving us the possibility to come closer to $(0, 1)$. The procedure to get more intersection points can be applied to the McMillan map as well as to other maps and it goes as follows:

1. Compute the eigenvalues of the Jacobian matrix of the map at the saddle $(x_s, y_s)$, which yields one eigenvalue, $\lambda_s$, inside the unit circle and the other one, $\lambda_u$, outside.

2. The last, numerically obtained, intersection point (i.e. the point closest to the saddle point) is close enough to the saddle, to use linearity of the orbit. So, take this intersection-point and multiply it with the appropriate eigenvalue (in the direction of the saddle point). This will produce another 'intersection' point, which lies closer to the saddle.

3. Repeat step 2 several times, each time taking the newly obtained intersection point and multiplying it with an extra factor $\lambda_{u,s}$. You will get a sequence of points moving towards the saddle fixed point along the homoclinic orbit.

4. The same can be done with the last, closest to the saddle, point, on the other side of the manifold.

We repeated step 2 in the procedure for the McMillan map 15 times at both sides, so that we gain 30 extra 'intersection' points. In total, we have now 39 points to do both continuations, in one and in two parameters, again. The continuation of the homoclinic orbit in one parameter doesn't change qualitatively from the original one (see Fig. 2.5), since $x = 0$ remains the fixed point and the limit points should not alter when more points are taken into consideration. Therefore, we don't show a figure of this continuation with the computed intersection points included. The continuation in two parameters gives now the picture in figure 2.7. Compare this with the original figure 2.6: originally, the tip of the horn lies at $(\beta, \mu) = (6.2709 \cdot 10^{-3}, 1.2418)$, while in the extension we reach the point $(\beta, \mu) = (2.6298 \cdot 10^{-9}, 1.0048)$. This is indeed much closer to the point $(0, 1)$.

### 2.2.5 Mel'nikov applied to McMillan

We are almost ready for the application of the Mel'nikov theory to the McMillan map. The functions $F$ and $G$ for the *McMillan map* are given by:

$$F\begin{pmatrix} x \\ y \end{pmatrix} = \begin{pmatrix} y \\ -x + 2\mu\frac{y}{1+y^2} \end{pmatrix},$$

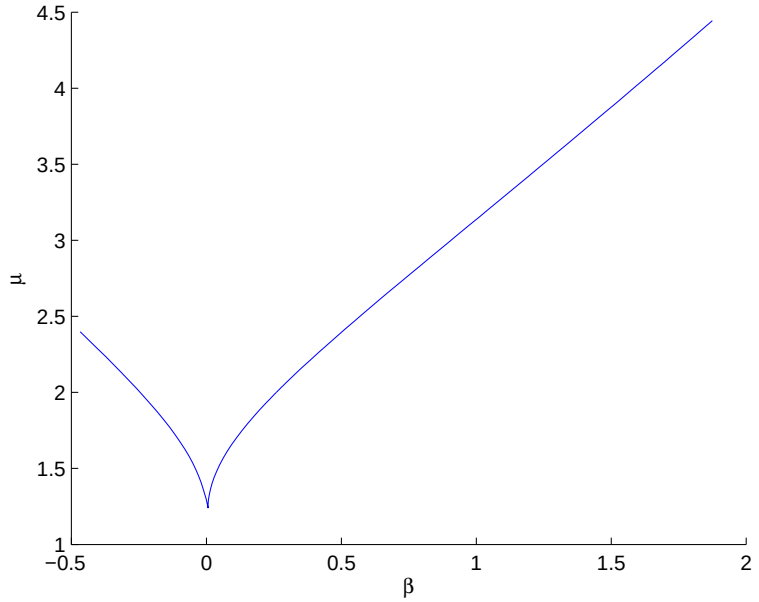


**Figure 2.6:** Branch of homoclinic tangencies of the *McMillan map* (2.1), with parameter-values (2.2).

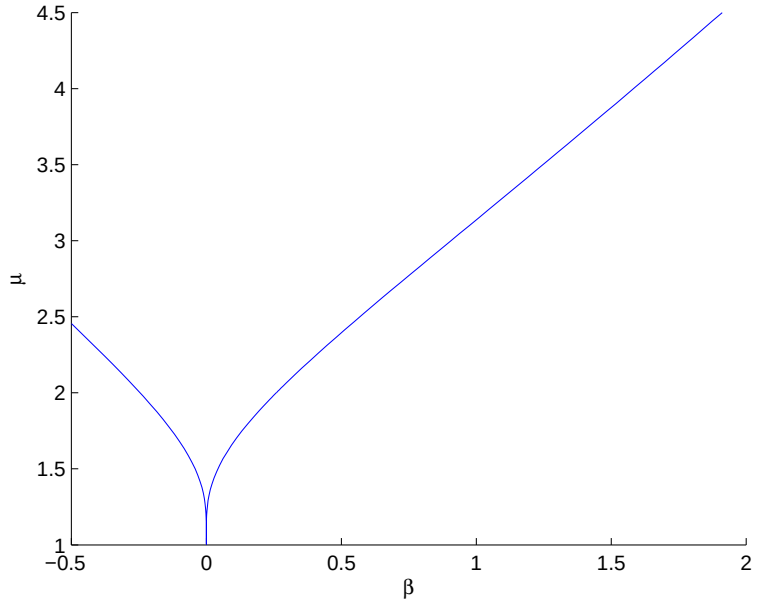


**Figure 2.7:** Extension of the branch in figure 2.6 of homoclinic tangencies of the *McMillan map* (2.1), with parameter-values (2.2).

$$G\begin{pmatrix} x \\ y \end{pmatrix} = \begin{pmatrix} 0 \\ \beta x + \gamma y \end{pmatrix}.$$

Since $F$ is an area-preserving map, we are allowed to use the simplified form of the Mel'nikov function (1.37).

To calculate the tangent vector $v_k$, we use the invariant curve (2.3) to get $u_k = (\mu x_k - y_k - x_k^2 y_k, x_k - \mu y_k + x_k y_k^2)$. The tangent vectors $v_k$ are then for each $k \in \mathbb{Z}$ given by

$$v_k = \frac{u_k}{\|u_0\|},$$

where we normalize such that $v_0$ is a unit tangent vector. Using these expressions for the tangent vectors $v_k$ at the point $(x_k, y_k)$ and the explicit formulae (2.7) for $x_k$ and $y_k$, we are able to compute the Mel'nikov function immediately. Notice that each $x_n, y_n$, and therefore also $u_n$ and $v_n$, still has a (suppressed) $t$-component, which denotes the chosen initial point along the homoclinic orbit.

In the computation of the Mel'nikov function, we let $t$ run along the curve of the McMillan map from -4 till 5.5 with stepsize 0.01. At each time $t$ we compute Mel'nikov's function again. We do not compute this infinite sum completely, but truncate it at a certain number of terms. Here, we compute up to and including $k = \pm 10$, because adding more terms does not have much effect, compared with the result of order 1: the terms for $k = 10$ are already of order $10^{-4}$ up to $10^{-10}$ (depending on $t$ in our range).

The application of the Mel'nikov function gives useful results if the parameters $\mu$ and $\beta$ are chosen above the crater in figure 2.7, and close to $(0, 1)$. This results in graphs as figures 2.8 and 2.10 (each time $\varepsilon = 0.05$ and $\gamma = 1.9$ are fixed). The intersection points of these graphs with the $t$-axis indeed correspond to the intersection points for the McMillan map. In order to compare the predicted values by the Mel'nikov function with the actual values of these intersection points, we show the first on a plot of the unperturbed McMillan map ($\varepsilon = 0$) together with the numerical obtained intersection points on the stable and unstable manifolds for $\varepsilon = \pm 0.05$, (Fig. 2.9).

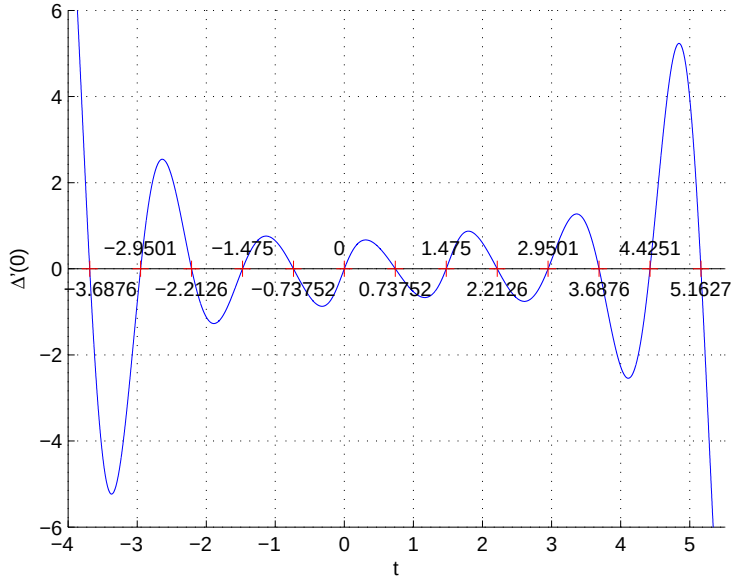


**Figure 2.8:** The approximated *Mel'nikov function* (1.37) for the McMillan map with $\mu = 2.3, \beta = 0$, while $k$ runs from -10 to 10.

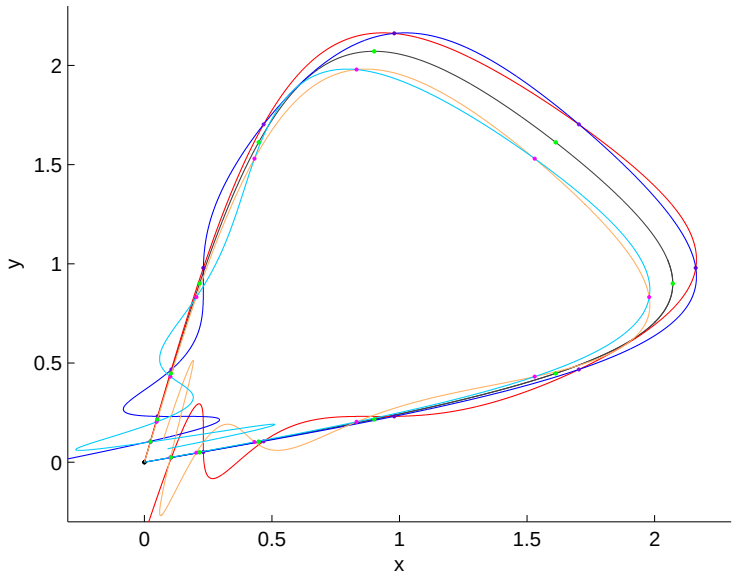


**Figure 2.9:** Plot of the unperturbed *McMillan map* for $\mu = 2.3$ in gray with the zeroes of the Mel'nikov function located thereon in green using (2.7). The stable and unstable manifolds of the McMillan map with $\beta = 0$ and $\varepsilon = \pm 0.05$ (shown in blue and red for positive, and in light-blue and orange for negative $\varepsilon$), intersect each other at the magenta and purple points, resp.

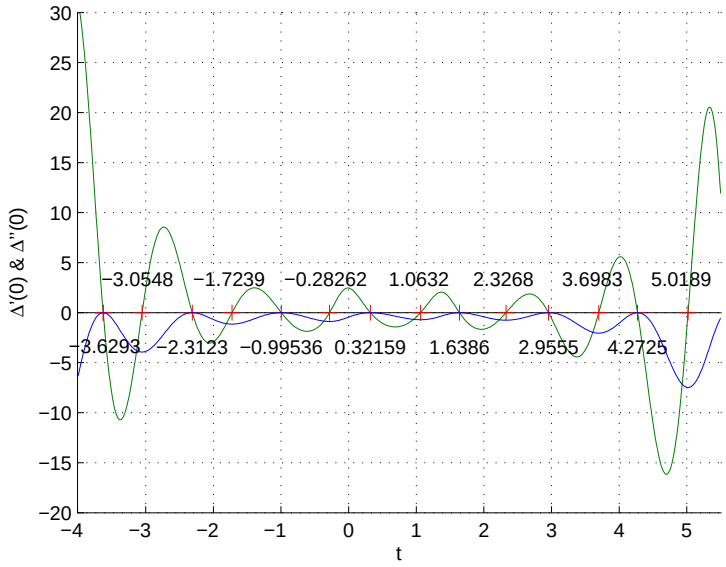


**Figure 2.10:** The approximated *Mel'nikov function* (1.37) in blue and its derivative with respect to $t$ in green for the McMillan map with $\mu = 2.0, \beta = 0.251571$, while $k$ runs from -10 to 10.

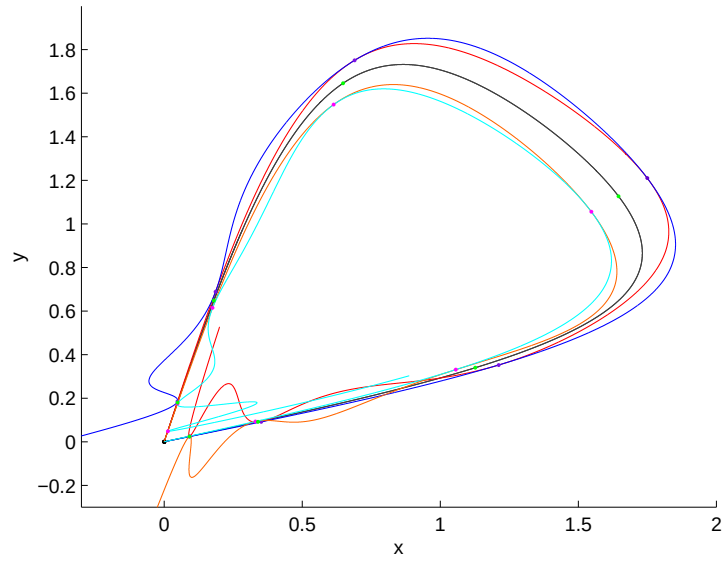


**Figure 2.11:** Plot of the unperturbed *McMillan map* for $\mu = 2.0$ in gray with the tangent points of the Mel'nikov function for $\beta = 0.251571$ located thereon in green using (2.7). The stable and unstable manifolds of the McMillan map for $\varepsilon = \pm 0.05$ (shown in blue and red for positive, and in light-blue and orange for negative $\varepsilon$), are tangent to each other for $\beta = 0.2591$.

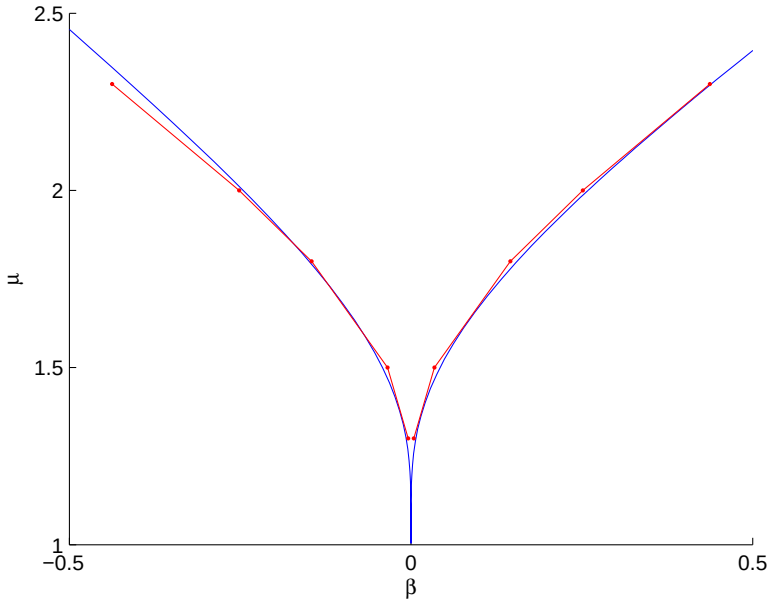


**Figure 2.12:** Close-up of figure 2.7, showing the branch of homoclinic tangencies of the *McMillan map* in the $(\beta, \mu)$-plane with $\varepsilon = 0.05$ and $\gamma = 1.9$ fixed. The connected red dots display an approximated crater at which one would expect homoclinic tangencies according to the Mel'nikov theory.

We investigate for which parameter values the Mel'nikov function predicts that the manifolds would not longer intersect each other, but only show homoclinic tangencies. In figure 2.12 the connected red points show the approximate boundary of the region for which the homoclinic structure is present, according to the Mel'nikov theory. As one can see, the boundary of the crater predicted by the Mel'nikov theory (which is entirely symmetric) doesn't exactly coincide with the one we found by numerical continuation. That is precisely the reason why we need to include in the tangent case the McMillan map with a different value for $\beta$ in figure 2.11, in order to have in both cases — predicted and numerical — tangencies.

| Numerically obtained | | Mel'nikov prediction | |
|---|---|---|---|
| $x$ | $y$ | $x$ | $y$ |
| 0.016330 | 0.062619 | 0.016438 | 0.061333 |
| 0.037245 | 0.142650 | 0.037694 | 0.140463 |
| 0.062619 | 0.239198 | 0.061333 | 0.227974 |
| 0.142650 | 0.535715 | 0.140463 | 0.513287 |
| 0.239198 | 0.865431 | 0.227974 | 0.805513 |
| 0.535715 | 1.573972 | 0.513287 | 1.484553 |
| 0.865430 | 1.823505 | 0.805513 | 1.726144 |
| 1.573972 | 1.427012 | 1.484553 | 1.340145 |
| 1.823505 | 0.998540 | 1.726144 | 0.929490 |
| 1.427012 | 0.449359 | 1.340145 | 0.432685 |
| 0.998541 | 0.280471 | 0.929490 | 0.268520 |
| 0.449359 | 0.118279 | 0.432685 | 0.117669 |
| 0.280471 | 0.073166 | 0.268520 | 0.072355 |
| 0.118279 | 0.030713 | 0.117669 | 0.031563 |
| 0.073166 | 0.018987 | 0.072355 | 0.019395 |

**Table 2.1:** The numerical computed intersection points for the McMillan map with values (2.2) compared with the ones predicted by the Mel'nikov theory.

In table 2.1 we list the coordinates of the intersection points we found at $(\mu, \beta) = (2, 0.1)$ using both methods. For small values of $x$ and $y$, the intersection points in both ways are close together (about 2% deviation); if we go further away from the origin, they diverge more (about 7% deviation). (See also figure 2.9). This behaviour is not very surprising, since the perturbation causes already a little expansion of the shape of the map: adding a perturbation blows up or shrinks down the graph a little, depending on the sign. Taking this phenomenon into account we may conclude that the location of the intersection points (on the unperturbed McMillan map) is very well predicted by the Mel'nikov function.

## 2.3 Normal form of 1:1 resonance (second order)

The most important system in this study is obviously the normal form of 1:1 resonance. When we speak in the following about the normal form of 1:1 resonance, we mean the form given in (1.27), truncated at second order. This version is studied extensively in this section, while we compare it shortly to a third order version in the next section.

### 2.3.1 Homoclinic structure

The second order *normal form of 1:1 resonance* has the following form

$$N_\nu : \begin{pmatrix} x \\ y \end{pmatrix} \mapsto \begin{pmatrix} x + y \\ y + \nu_1 + \nu_2 y + a_0 x^2 + b_0 xy \end{pmatrix}, \tag{2.8}$$

with parameters $\nu_1, \nu_2$ and $a_0, b_0$ fixed. In the following, we set the coefficients $a_0$ and $b_0$ equal to one. The two fixed points of the map are then given by

$$(x_{0,1}, y_{0,1}) = \left(\pm\sqrt{-\nu_1}, 0\right),$$

for $\nu_1 \leq 0$. The eigenvalues of the Jacobian matrix at the fixed point $(x_0, y_0) = (\sqrt{-\nu_1}, 0)$,

$$\begin{pmatrix} 1 & 1 \\ 2x_0 + y_0 & 1 + \nu_2 + b_0 x_0 \end{pmatrix} = \begin{pmatrix} 1 & 1 \\ 2\sqrt{-\nu_1} & 1 + \nu_2 + \sqrt{-\nu_1} \end{pmatrix},$$

are given by

$$\lambda_\pm = \tfrac{1}{2}\left(2 + \sqrt{-\nu_1} + \nu_2 \pm \sqrt{8\sqrt{-\nu_1} + \left(\sqrt{-\nu_1} + \nu_2\right)^2}\right).$$

So, for $\nu_1 < 0$, we can easily choose a value $\nu_2 > -2$ (and vice versa), making the positive fixed point a hyperbolic saddle.

As described in section 1.2.3, the normal form of 1:1 resonance shows a homoclinic structure for well-chosen parameter values within a small region of the parameter space. In the following couple of figures we present the visual results of the numerical computations. The first, figure 2.13, shows the stable and unstable manifolds of the positive saddle with transversal intersections. Fixing the value of $\nu_2$ and with the help of 15 intersection points, we continue the parameter $\nu_1$ to obtain the range of $\nu_1$ and corresponding values of $x_0$ for which a homoclinic structure is present, (Fig. 2.14). If we substitute the values of $\nu_1$ and $x_0 = \sqrt{-\nu_1}$ of the thus obtained limit points into the normal form, we get back homoclinic tangencies of the stable and unstable manifold. One situation for which this tangency occurs, is depicted

in figure 2.15. Continuation in both parameters supplies the 'horn'-like region of parameter values $\nu_{1,2}$ near 0 for which the homoclinic structure is present, (Fig. 2.16).

Again, to get more accurate results — that is, results closer to the origin —, we perform the method described in section 2.2.4 to obtain more 'intersection' points. For our initial parameter values, $(\nu_1, \nu_2) = (-0.3, -0.326)$, we have a saddle point at $x_0 = 0.547723$ with eigenvalues $\lambda_s = 0.0583712$, $\lambda_u = 2.16335$. We repeated step 2 of the procedure 25 times at both sides, so that we gain 50 extra 'intersection' points. In total, we have now 65 points to do both continuations again. The continuation in $\nu_1$ gives — as it should be — a result similar to the one in figure 2.14. The result of the continuation in two parameters is depicted in figure 2.17. One can compare with figure 2.16 that the resulting region comes indeed closer to the origin than without the extra intersection points. To be precise in the first case (Fig. 2.16) the tip of the horn lies at $(\nu_1, \nu_2) = (-0.1006, -0.2097)$, while in the extended case (Fig. 2.17) we reach the point $(\nu_1, \nu_2) = (-0.0068847, -0.0583)$.

The bifurcation diagram near the *Resonance 1:1* point, i.e. near the origin, is shown in figure 2.18. In this diagram the 'horn', bounding the region of homoclinic structures, is shown in red and labelled $T$. Note that these curves, together with the *Neimark-Sacker* curve, are or would become tangent to the *Fold*-line at the origin.

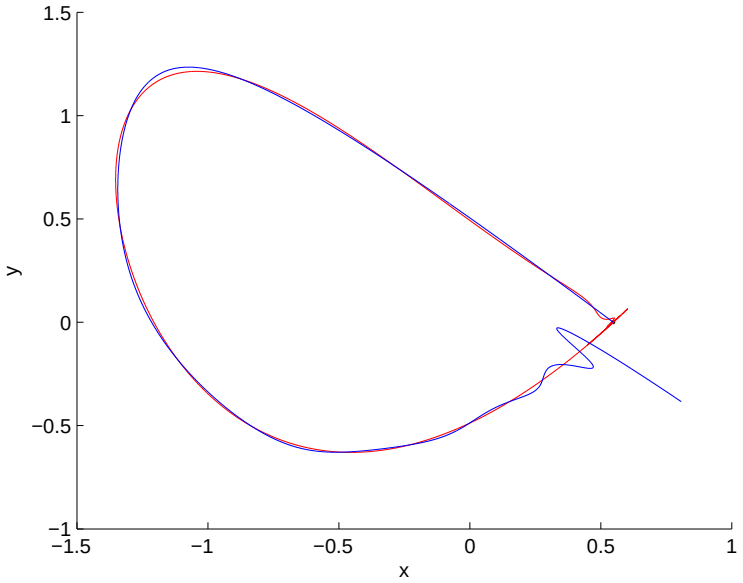


**Figure 2.13:** Transversal intersections of the stable (blue) and unstable (red) manifolds of the saddle point $(x_0, 0)$ of the *normal form for 1:1 resonance* (2.8) for parameter values $(\nu_1, \nu_2) = (-0.3, -0.326)$.

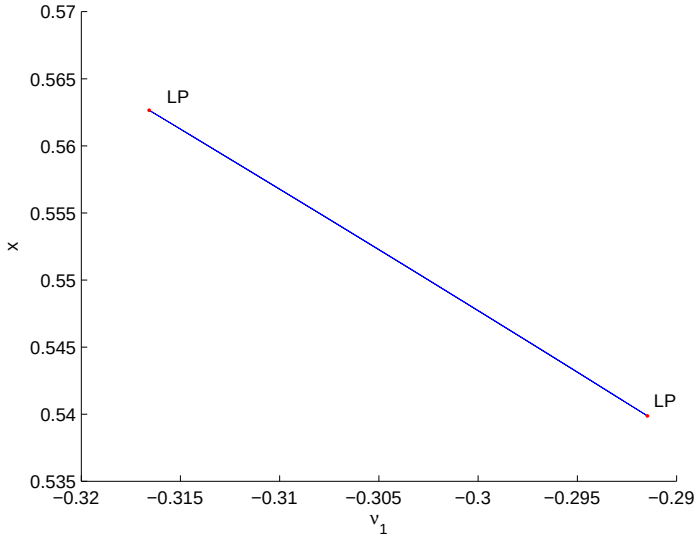


**Figure 2.14:** Continuation in $\nu_1$ of the homoclinic orbits for the *normal form of 1:1 resonance* (2.8). The starting parameters are $(\nu_1, \nu_2) = (-0.3, -0.326)$. The points marked "LP", indicate the values for which homoclinic tangencies occur.

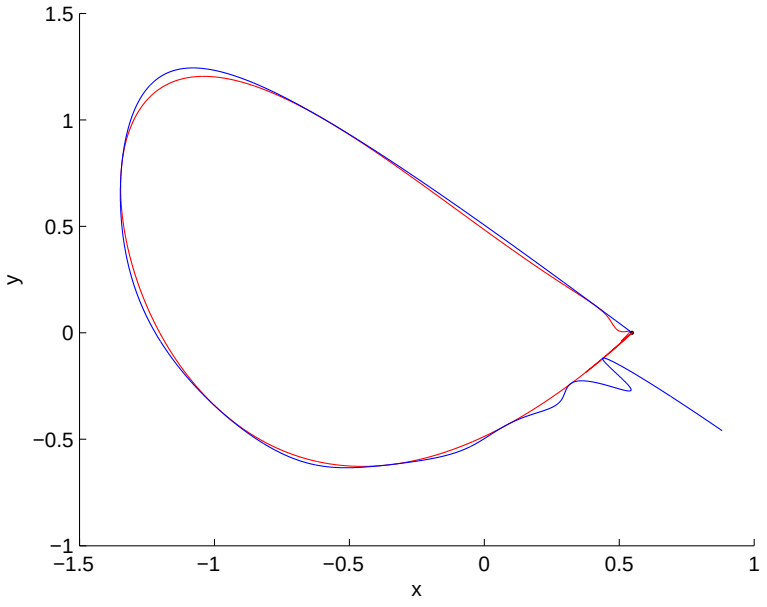


**Figure 2.15:** Homoclinic tangencies of the stable (blue) and unstable (red) manifolds of the saddle point $(x_0, 0)$ of the *normal form of 1:1 resonance* (2.8) at the parameter values $(\nu_1, \nu_2) = (-0.3, -0.3293211317)$.

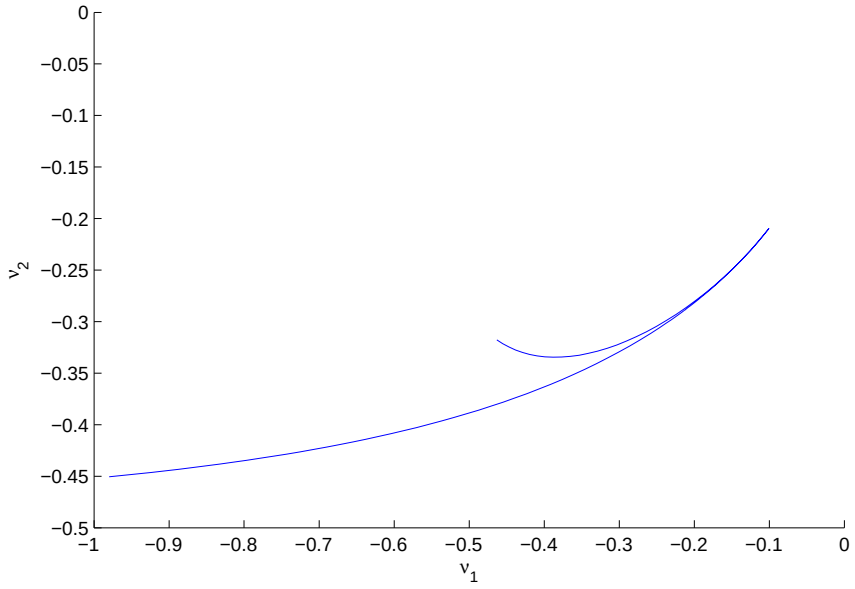


**Figure 2.16:** Branch of homoclinic tangencies of the *normal form of 1:1 resonance* (2.8). The continuation is done with respect to $\nu_1$ and $\nu_2$.

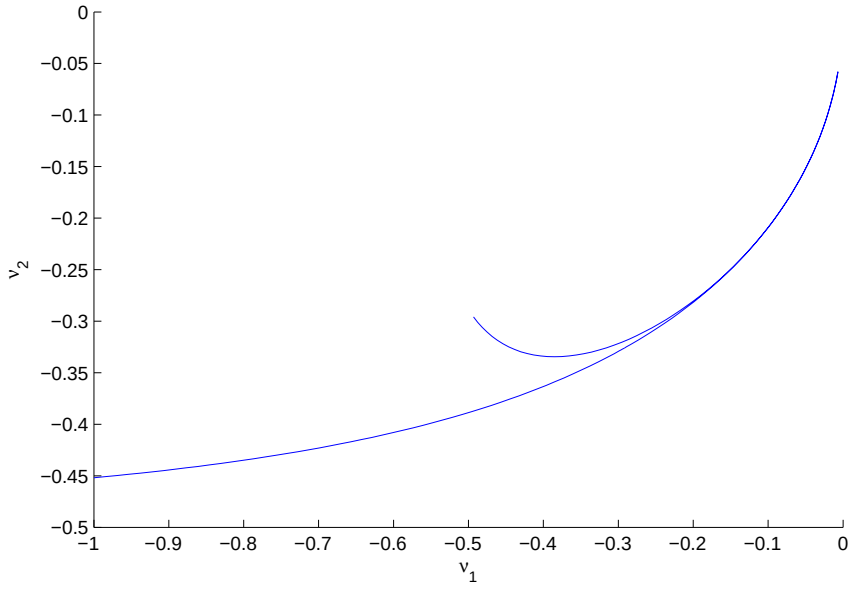


**Figure 2.17:** Branch of homoclinic tangencies of the *normal form of 1:1 resonance* (2.8) with the computed extra extension points included. Note that the tip of the 'horn' is closer to the origin than in figure 2.16. The two sides of the region become very close to each other near the origin, so that it is hard to distinguish them from each other.

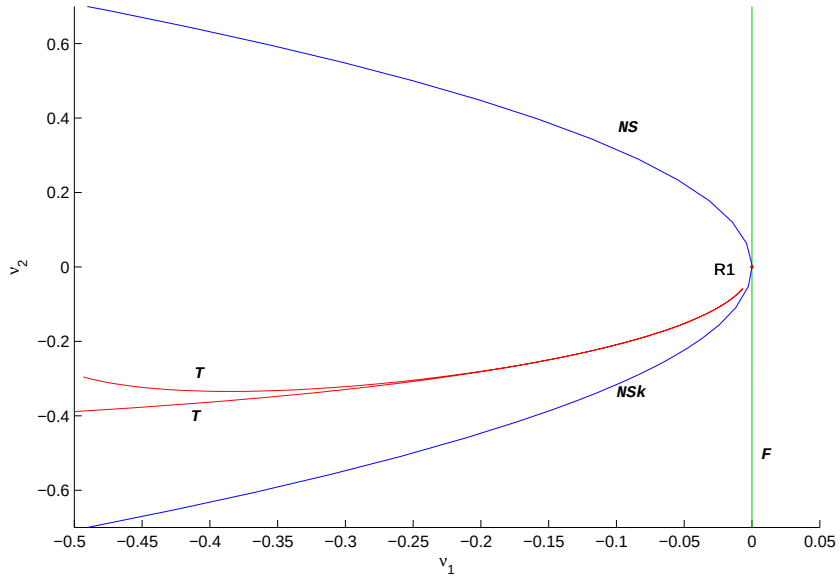


**Figure 2.18:** Bifurcation diagram of the *normal form of 1:1 resonance* (2.8) near the *Resonance 1:1* point at the origin. The green line is the path of *Fold* points ($F$); the upper part ($NS$) of the blue curve corresponds to the *Neutral Saddle* line, while the other one ($NSk$) is the *Neimark-Sacker* curve. The red curves, bounding the region of homoclinic structures, are labeled by $T$.

### 2.3.2 Approximation of the flow

Our purpose is to compute and predict the intersection points of the stable and unstable manifolds for the normal form via the Mel'nikov function, described in section 1.3. In order to be able to do so, we need to approximate the normal form (2.8) by the unit-time shift $\varphi_\nu^1$, which originates from the flow $\varphi_\nu^t$ of an approximating system of autonomous differential equations. The unit-time shift will allow us to write the normal form in the shape of a 'normal' (i.e. unperturbed) part plus a perturbation term. Moreover, the corresponding ODE possesses, as we will see, a homoclinic orbit, which can be derived explicitly.

The approximating ODE for the normal form of 1:1 resonance is derived using the method of the so-called *Picard iteration* in section 1.4. Start with a function $F^{(2)}(x)$ with unknown coefficients. The outcome should then be, at least up to second order, equal to the normal form. Equate these two formula's to recover the expressions of the unknown coefficients. After performing two Picard iterations, we obtain for sufficiently small $\nu$ the following smooth planar system:

$$\dot{\xi} = F(\nu, \xi) = F_0(\nu) + F_1(\nu, \xi) + F_2(\xi), \quad \xi \in \mathbb{R}^2, \quad \nu \in \mathbb{R}^2, \tag{2.9}$$

with each function $F_k$ defined by

$$F_0(\nu) = \begin{pmatrix} -\frac{1}{2}\nu_1 + \frac{1}{20}(-a_0 + 2b_0)\nu_1^2 + \frac{1}{3}\nu_1\nu_2 \\ \nu_1 + \frac{1}{60}(2a_0 - 5b_0)\nu_1^2 - \frac{1}{2}\nu_1\nu_2 \end{pmatrix},$$

$$F_1(\nu,\xi) = \begin{pmatrix} \xi_2 + \left(-\frac{1}{2}a_0 + \frac{1}{3}b_0\right)\nu_1\xi_1 + \left(\left(\frac{1}{5}a_0 - \frac{5}{12}b_0\right)\nu_1 - \frac{1}{2}\nu_2\right)\xi_2 \\ \left(\frac{2}{3}a_0 - \frac{1}{2}b_0\right)\nu_1\xi_1 + \left(\left(-\frac{1}{6}a_0 + \frac{1}{2}b_0\right)\nu_1 + \nu_2\right)\xi_2 \end{pmatrix},$$

$$F_2(\xi) = \begin{pmatrix} -\frac{1}{2}a_0\xi_1^2 + \left(\frac{2}{3}a_0 - \frac{1}{2}b_0\right)\xi_1\xi_2 + \left(-\frac{1}{6}a_0 + \frac{1}{3}b_0\right)\xi_2^2 \\ a_0\xi_1^2 + (-a_0 + b_0)\xi_1\xi_2 + \left(\frac{1}{6}a_0 - \frac{1}{2}b_0\right)\xi_2^2 \end{pmatrix}.$$

This system is locally topologically equivalent to the Bogdanov-Takens normal form (1.21) and, hence, it has the property that there exist a homoclinic orbit for suitably chosen parameter values, see [8]. These homoclinic orbits fit nicely to the manifolds of the normal form map, as is demonstrated in figures 2.19 and 2.20.

Let $\varphi^t(\nu,\cdot)$ denote the flow of the smooth planar system (2.9), then for $t = 1$ and sufficiently small $\nu$ the flow forms a map representing the normal form,

$$N(\nu,\xi) = \varphi^1(\nu,\xi) + \mathcal{O}(\|\nu\|^2) + \mathcal{O}(\|\xi\|^2\|\nu\|) + \mathcal{O}(\|\xi\|^3). \tag{2.10}$$

To obtain the flow $\varphi^t(\nu,\cdot)$ we need to integrate the ODE (2.9), using again the method of *Picard iterations*. The matrix $\Lambda$ for the first-order terms reads,

$$\Lambda = \begin{pmatrix} 0 & 1 \\ 0 & 0 \end{pmatrix},$$

obtained by the linear part of the system. In our case, we have the function $F$ defined up to $k = 2$, only, so we have in equation (1.39), $F^{(k)}(x) = 0$ for all $k \geq 3$.

Unfortunately, our system doesn't have the property that it is zero at $\xi = 0$. Therefore we need a trick, which is presented by Kuznetsov (see [8]): construct for small $\nu \neq 0$ the four-dimensional flow

$$X \mapsto \phi^1(\nu,\xi) = \begin{pmatrix} \varphi^1(\nu,\xi) \\ \nu \end{pmatrix}, \quad X = \begin{pmatrix} \xi \\ \nu \end{pmatrix} \in \mathbb{R}^4.$$

Suppose, this flow is generated by a four-dimensional system

$$\dot{X} = Y(X) = JX + Y_2(X) + Y_3(X) + \ldots,$$

with

$$J = \begin{pmatrix} 0 & 1 & -\frac{1}{2} & 0 \\ 0 & 0 & 1 & 0 \\ 0 & 0 & 0 & 0 \\ 0 & 0 & 0 & 0 \end{pmatrix}, \qquad Y_k(X) = \begin{pmatrix} Z_k(X) \\ 0 \end{pmatrix},$$

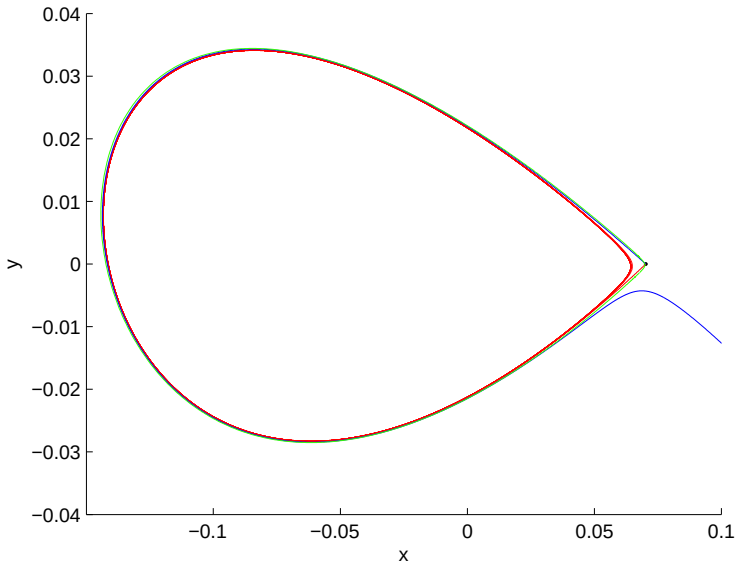


**Figure 2.19:** The stable (blue) and unstable (red) manifolds of the *normal form of 1:1 resonance* at the equilibrium point for parameter values $(\nu_1, \nu_2) = (-0.0049357243, -0.05)$. The green curve is the homoclinic orbit of the approximating ODE (2.9) for the same parameter values.

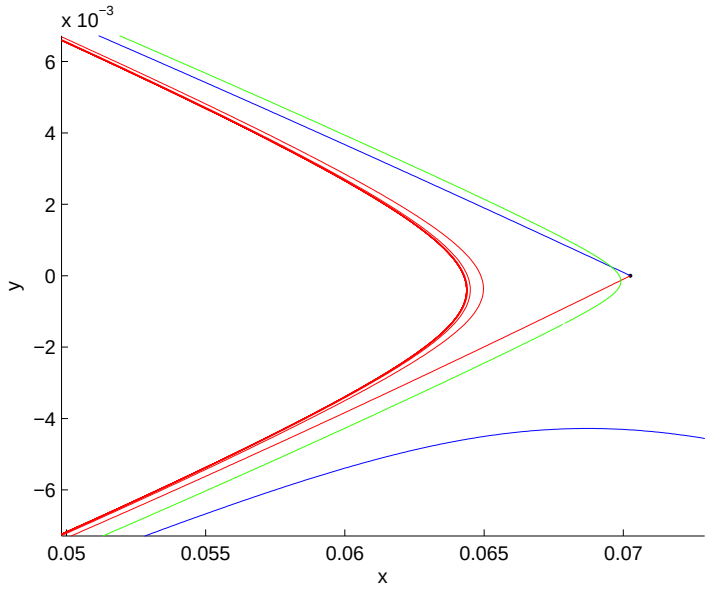


**Figure 2.20:** Close-up of figure 2.19 near the saddle.

where $Z_k(X)$ is a homogeneous polynomial function from $\mathbb{R}^4$ to $\mathbb{R}^2$ of order $k$. $Z_2$ is given by the sum of all second-order terms in $\nu$ and $\xi$ of (2.9), namely $Z_2(X) = F_0(\nu) + F_1(\nu,\xi) + F_2(\xi) - (\xi_2 - \frac{1}{2}\nu_1, \nu_1)^T$. For $k \geq 3$ we have again that $Z_k(X) = 0$ and therefore also $Y_k(X) = 0$, since there are no third order terms in $F$. So, the Picard iterations have to be done only with $Y_2$.

The first Picard iteration gives $X^{(1)}(t) = e^{Jt}X$. The second iterate yields (for $t = 1$),

$$X^{(2)}(1) = \begin{pmatrix} \xi_1 + \xi_2 \\ \nu_1 + (1+\nu_2)\xi_2 + a_0\xi_1^2 + b_0\xi_1\xi_2 \\ \nu_1 \\ \nu_2 \end{pmatrix}.$$

Indeed, the upper part of $X^{(2)}(1)$ is precisely the normal form. This is not very surprising, because system (2.9) is constructed in such a way that it will give back the normal form after performing two iteration steps. In the third step we use the full $X^{(2)}(t)$ for general $t$, so that the integrand reads $e^{J(1-\tau)}Y_2(X^{(2)}(\tau))$. Integrating gives a big expression with many terms of order higher than 2, however. Therefore, we first throw away all these unnecessary components, consisting of all the cubic terms in $\xi$ and all quadratic terms in $\nu$ except the ones without $\xi$. This leaves us, for $t = 1$, with a result of the following form:

$$X^{(3)}(1) = \begin{pmatrix} \varphi_3^1(\nu,\xi) \\ \nu \end{pmatrix} = \begin{pmatrix} \xi_1 + \xi_2 + f_{20}\xi_1^2 + f_{11}\xi_1\xi_2 + f_{02}\xi_2^2 \\ \nu_1 + (1+\nu_2)\xi_2 + g_{20}\xi_1^2 + g_{11}\xi_1\xi_2 + g_{02}\xi_2^2 \\ \nu_1 \\ \nu_2 \end{pmatrix}, \quad (2.11)$$

where each coefficient $f_{jk}, g_{jk}$ is determined by

$$\begin{aligned}
f_{20} &= \tfrac{1}{144}a_0(-2a_0 + b_0)\nu_1 - \tfrac{1}{12}\nu_2, \\
f_{11} &= \left(-\tfrac{1}{420}a_0^2 - \tfrac{1}{180}a_0b_0 + \tfrac{1}{90}b_0^2\right)\nu_1 + \tfrac{1}{6}(a_0 - b_0)\nu_2, \\
f_{02} &= \tfrac{1}{5040}\left(10a_0^2 - 17a_0b_0 + 21b_0^2\right)\nu_1 + \tfrac{1}{120}(3a_0 + 10b_0)\nu_2, \\
g_{20} &= a_0 - \tfrac{1}{120}\left(14a_0^2 - 15a_0b_0 + 10b_0^2\right)\nu_1 + \tfrac{a_0}{2}\nu_2, \\
g_{11} &= b_0 - \tfrac{1}{120}\left(2a_0^2 + 13a_0b_0\right)\nu_1 + \left(-\tfrac{5}{6}a_0 + b_0\right)\nu_2, \\
g_{02} &= -\tfrac{1}{5040}\left(50a_0^2 - 21a_0b_0 + 280b_0^2\right)\nu_1 - \tfrac{1}{6}(a_0 + 2b_0)\nu_2.
\end{aligned}$$

These computations give an approximation of the flow, considered as the map $\varphi_3^1(\nu,\xi)$. This is taken to be the unperturbed map $F$ in computing the Mel'nikov function. The normal form is considered as our 'full' perturbed map, so we can compute the perturbation part by taking the difference between the full map and the unperturbed part (see (2.10)). This yields

$$\varepsilon G(\xi) = N(\nu,\xi) - \varphi_3^1(\nu,\xi) = \begin{pmatrix} -f_{20}\xi_1^2 - f_{11}\xi_1\xi_2 - f_{02}\xi_2^2 \\ (a_0 - g_{20})\xi_1^2 + (b_0 - g_{11})\xi_1\xi_2 - g_{02}\xi_2^2 \end{pmatrix}, \quad (2.12)$$

which is in terms of the coefficients $f_{kl}$ and $g_{kl}$ of $\varphi_3^1(\nu,\xi)$.

### 2.3.3 Prediction of a homoclinic orbit

In order to obtain an explicit expression for the homoclinic orbit of the ODE (2.9), we can relate this system to another system for which we know the homoclinic orbit explicitly and the parameter values at which the homoclinic orbit shows up. One example is the case of the truncation of the Bogdanov-Takens normal form (1.7), that we can use in our case. There are two ways to transfer the expression of the homoclinic orbit from one to the other: one way is following the smooth transformations from system (2.9) to the Bogdanov-Takens normal form (see Lemma 1 and 2) in the reverse order. The other way is using the direct method as presented in [9]. Since the last one is much easier, we use it here. This method is explained in more detail in Appendix A; here we list only the relevant results.

Suppose, the truncated Bogdanov-Takens normal form (1.7) has the homoclinic orbit, approximated up to fourth order in $\varepsilon$,

$$\left(\frac{\varepsilon^2}{a}\left(u_0(\varepsilon t)+\varepsilon u_1(\varepsilon t)+\varepsilon^2 u_2(\varepsilon t)\right), \frac{\varepsilon^3}{a}\left(v_0(\varepsilon t)+\varepsilon v_1(\varepsilon t)\right)\right), \tag{2.13}$$

where $u_0$ and $v_0 = \dot{u}_0$ are the homoclinic solutions to (1.17) — the Hamiltonian part of the rescaled Bogdanov-Takens normal form — with $\gamma_1 = -4$,

$$(u_0(t), v_0(t)) = \left(2 - 6\,\mathrm{sech}^2(t), 12\,\mathrm{sech}^2(t)\tanh(t)\right),$$

while $u_1, v_1$ and $u_2$ are given by (see Appendix A.2 for the derivation)

$$\begin{aligned}
u_1(t) &= -\frac{72b}{7a}\frac{\sinh t}{\cosh^3 t}\log(\cosh t),\\
v_1(t) &= \frac{72b}{7a}\frac{\log(\cosh t)(1-2\sinh^2 t)+\sinh^2 t}{\cosh^4 t},\\
u_2(t) &= -\frac{216b^2}{49a^2}\frac{\log^2(\cosh t)}{\cosh^4 t}(\cosh 2t-2) - \frac{216b^2}{49a^2}\frac{\log(\cosh t)}{\cosh^4 t}(1-\cosh 2t),\\
&\quad - \frac{18b^2}{49a^2}\frac{6t\sinh 2t - 7\cosh 2t + 8}{\cosh^4 t}.
\end{aligned}$$

The homoclinic orbit is supposed to appear at parameter values

$$\begin{aligned}
\beta_1 &= -\frac{4}{a}\varepsilon^4 + \mathcal{O}(\varepsilon^5),\\
\beta_2 &= \frac{b}{a}\tau_0\varepsilon^2 + \frac{b}{a}\tau_2\varepsilon^4 + \mathcal{O}(\varepsilon^5),
\end{aligned} \tag{2.14}$$

where

$$\tau_0 = \frac{10}{7}, \qquad \tau_2 = \frac{288b^2}{2401a^2}.$$

We can transfer these known results of the homoclinic orbit and homoclinic bifurcation curve in the Bogdanov-Takens case to our initial problem

of the 1:1 resonance, by specifying the relations between the coordinates and parameters of both systems. Applying (A.5) to (2.13) provides an expression of the following form for the approximation of the homoclinic orbit in case of the normal form of 1:1 resonance up to order four in $\varepsilon$:

$$\begin{aligned}\xi_0(t,\varepsilon) = \varepsilon^2\left(\frac{b}{a}\tau_0 H_{0001} + \frac{1}{a}u_0(\varepsilon t)q_1\right) + \varepsilon^3\left(\frac{1}{a}v_0(\varepsilon t)q_2 + \frac{1}{a}u_1(\varepsilon t)q_1\right) \\ + \varepsilon^4\left(-\frac{4}{a}H_{0010} + \frac{b}{a}H_{0001}\tau_2 + \frac{1}{a}u_2(\varepsilon t)q_1 + \frac{1}{a}v_1(\varepsilon t)q_2 + \right. \\ \left. + \frac{1}{2a^2}H_{2000}u_0^2(\varepsilon t) + \frac{b}{a^2}\tau_0 H_{1001}u_0(\varepsilon t) + \frac{b^2}{2a^2}\tau_0^2 H_{0002}\right).\end{aligned} \tag{2.15}$$

The same is done for the parameters, by applying (A.6) to (2.14), which results in a formula for $\nu$ of order four in $\varepsilon$:

$$\nu(\varepsilon) = \frac{b}{a}\tau_0 K_{01}\varepsilon^2 + \left(-\frac{4}{a}K_{10} + \frac{b}{a}\tau_2 K_{01} + \frac{b^2}{2a^2}\tau_0^2 K_{02}\right)\varepsilon^4. \tag{2.16}$$

In section A.4.1 of the appendix we show in detail how the unknown coefficients of these two formulae are obtained. In the following we only display the results of the coefficients needed for this computation.

First of all, to compute these coefficients, we use the following Taylor expansion of the approximating system $F(\nu,\xi)$ in (2.9),

$$F(\nu,\xi) = A\xi + \tfrac{1}{2}B(\xi,\xi) + A_1(\xi,\nu) + J_1\nu + \tfrac{1}{2}J_2(\nu,\nu),$$

where $A, A_1, B, J_1, J_2$ are explicitly given by

$$\begin{aligned}
A &= F_\xi(\nu_0,\xi_0) \overset{(\nu_0,\xi_0)=(0,0)}{=} \begin{pmatrix}0 & 1\\ 0 & 0\end{pmatrix}, \qquad J_1 = F_\nu(\nu_0,\xi_0) = \begin{pmatrix}-\frac{1}{2} & 0\\ 1 & 0\end{pmatrix},\\
A_1(\xi,\nu) &= \begin{pmatrix}\left(-\frac{1}{2}a_0 + \frac{1}{3}b_0\right)\nu_1\xi_1 + \left(\left(\frac{1}{5}a_0 - \frac{5}{12}b_0\right)\nu_1 - \frac{1}{2}\nu_2\right)\xi_2\\ \left(\frac{2}{3}a_0 - \frac{1}{2}b_0\right)\nu_1\xi_1 + \left(\left(-\frac{1}{6}a_0 + \frac{1}{2}b_0\right)\nu_1 + \nu_2\right)\xi_2\end{pmatrix},\\
B(\xi,\eta) &= 2\begin{pmatrix}-\frac{1}{2}a_0\xi_1\eta_1 + \left(\frac{2}{3}a_0 - \frac{1}{2}b_0\right)(\xi_1\eta_2 + \xi_2\eta_1) + \left(-\frac{1}{6}a_0 + \frac{1}{3}b_0\right)\xi_2\eta_2\\ a_0\xi_1\eta_1 + (-a_0 + b_0)(\xi_1\eta_2 + \xi_2\eta_1) + \left(\frac{1}{6}a_0 - \frac{1}{2}b_0\right)\xi_2\eta_2\end{pmatrix}\\
J_2(\mu,\nu) &= \begin{pmatrix}\frac{1}{10}(-a_0 + 2b_0)\mu^2 + \frac{2}{3}\mu\nu\\ \frac{1}{30}(2a_0 - 5b_0)\mu^2 - \mu\nu\end{pmatrix}.
\end{aligned}$$

Furthermore, let $q_{1,2}$ and $p_{1,2}$ be the real, linearly independent eigenvectors of $A$ and $A^T$, respectively, satisfying $Aq_1 = 0$, $Aq_2 = q_1$ and $A^T p_2 = 0$, $A^T p_1 = p_2$. In our case we find $q_1 = (1,0)^T = p_1$, $q_2 = (0,1)^T = p_2$.

The constants $a$ and $b$ are then given by

$$a = \tfrac{1}{2}p_1^T B(q_1,q_1) = a_0, \tag{2.17}$$

$$b = p_1^T B(q_1,q_1) + p_2^T B(q_1,q_2) = b_0 - 2a_0. \tag{2.18}$$

If we define $A^{INV}$ as the operator such that $x = A^{INV}y$ by solving the non-singular bordered system

$$\begin{pmatrix} A & p_2 \\ q_1^T & 0 \end{pmatrix} \begin{pmatrix} x \\ s \end{pmatrix} = \begin{pmatrix} y \\ 0 \end{pmatrix},$$

then we find the term $H_{1100}$ by

$$\begin{aligned} H_{2000} &= A^{INV}\left(2aq_2 - B(q_1, q_1)\right) = (0, a_0)^T, \\ H_{1100} &= A^{INV}\left(bq_2 + H_{2000} - B(q_1, q_2)\right) = (0, -\tfrac{2}{3}a_0 + \tfrac{1}{2}b_0)^T. \end{aligned} \tag{2.19}$$

With these preliminary computations, we are able to solve (A.27) for $\hat{H}_{01}$ and $\hat{K}_1$:

$$\begin{aligned} \hat{H}_{01} &= [H_{0010}, H_{0001}] = \begin{pmatrix} -\frac{b_0}{4a_0} & 0 \\ \frac{1}{2} & 0 \end{pmatrix}, \\ K_1 &= [K_{10}, K_{01}] = \begin{pmatrix} 1 & 0 \\ \frac{1}{2}a_0 - \frac{5}{4}b_0 + \frac{b_0^2}{4a_0} & 1 \end{pmatrix}. \end{aligned}$$

The mixed component $H_{1001}$ is supplied by the formula

$$H_{1001} = -A^{INV}\left(B(q_1, H_{0001}) + A_1(q_1, K_{01})\right) = 0,$$

which uses previous results. Finally, the remaining quadratic coefficients $K_{02}$ and $H_{0002}$ are computed by

$$\begin{aligned} K_{02} &= -\left(p_2^T z\right) K_{10} = 0, \\ H_{0002} &= -A^{INV}(z + J_1 K_{02}) = 0, \end{aligned} \tag{2.20}$$

where

$$z = B(H_{0001}, H_{0001}) + 2A_1(H_{0001}, K_{01}) + J_2(K_{01}, K_{01}),$$

which is equal to 0, since both $H_{0001}$ and $J_2$ are equal to 0.

At this point we have gathered all necessary ingredients to know (2.15) completely, which provides us with the following approximation for the homoclinic orbit in the approximating ODE (2.9),

$$\xi_0(t, \varepsilon) = \left(\pi_2(t, \varepsilon)\varepsilon^2 + \pi_3(t, \varepsilon)\varepsilon^3 + \pi_4(t, \varepsilon)\varepsilon^4, \rho_3(t, \varepsilon)\varepsilon^3 + \rho_4(t, \varepsilon)\varepsilon^4\right), \tag{2.21}$$

where each component is given by,

$$\begin{aligned} \pi_2(t, \varepsilon) &= \frac{1}{a_0}\left(2 - 6\,\mathrm{sech}^2(\varepsilon t)\right) \\ \pi_3(t, \varepsilon) &= \frac{72(2a_0 - b_0)}{7a_0^2} \frac{\log(\cosh(\varepsilon t))\sinh(\varepsilon t)}{\cosh^3(\varepsilon t)} \end{aligned}$$

$$\begin{aligned}
\pi_4(t,\varepsilon) &= \frac{b_0}{a_0^2} - \frac{216(2a_0-b_0)^2}{49a_0^2}\frac{\log^2(\cosh(\varepsilon t))}{\cosh^4(\varepsilon t)}(\cosh(2\varepsilon t)-2) \\
&\quad - \frac{216(2a_0-b_0)^2}{49a_0^2}\frac{\log(\cosh(\varepsilon t))}{\cosh^4(\varepsilon t)}(1-\cosh(2\varepsilon t)) \\
&\quad - \frac{18(2a_0-b_0)^2}{49a_0^2}\frac{6\varepsilon t\sinh(2\varepsilon t)-7\cosh(2\varepsilon t)+8}{\cosh^4(\varepsilon t)} \\
\rho_3(t,\varepsilon) &= \frac{12}{a_0}\tanh(\varepsilon t)\operatorname{sech}^2(\varepsilon t) \\
\rho_4(t,\varepsilon) &= -\frac{2}{a_0} + \frac{1}{2a_0}\left(2-6\operatorname{sech}^2(\varepsilon t)\right)^2 + \\
&\quad + \frac{72(2a_0-b_0)}{7a_0^2}\frac{\log(\cosh(\varepsilon t))(1-2\sinh^2(\varepsilon t))+\sinh(\varepsilon t)^2}{\cosh^4(\varepsilon t)}
\end{aligned}$$

The homoclinic orbit is expected to show up at the homoclinic bifurcation curve, that is where the parameter values satisfy (2.16),

$$\begin{aligned}
\nu(\varepsilon) &= \left(-\frac{4}{a_0}\varepsilon^4, \frac{10(b_0-2a_0)}{7a_0}\varepsilon^2 + \left(\frac{288(b_0-2a_0)^3}{2401a_0^3} - \frac{2a_0^2-5a_0b_0+b_0^2}{a_0^2}\right)\varepsilon^4\right) \\
&= \left(-4\varepsilon^4, -\frac{10}{7}\varepsilon^2 + \frac{4514}{2401}\varepsilon^4\right),
\end{aligned} \tag{2.22}$$

where in the second equality we set $a_0 = b_0 = 1$. We can rewrite this formula in order to obtain the following simple expression of $\nu_2$ as a function of $\nu_1$:

$$\nu_2 = -\frac{5}{7}\sqrt{-\nu_1} - \frac{2257}{4802}\nu_1. \tag{2.23}$$

In figure 2.21 and 2.22 we compare the predicted homoclinic orbit (2.21) with the numerically obtained homoclinic orbit at almost the same parameter values. This is because the predicted curve of parameter values (2.22) deviates a bit from the numerical, real values for which a homoclinic orbit is present, as can be seen in figure 2.23. So, to get numerically a homoclinic orbit, we need to change the predicted parameter values a bit; we only change the value of $\nu_2$ because that leaves the location of the saddle untouched. As one can see, for small values of $\varepsilon$ this prediction is quite good. There is only a small displacement in the $x$-direction. This is caused by the term $\varepsilon^4\frac{b_0}{a_0^2}$.

The predicted curve of parameters in equation (2.22) is compared in figure 2.23 with the regions we detected by continuation for the normal form and for the approximating ODE. As one can see the predicted curve differs quite a lot from the real values, so we need to stay close to the origin.

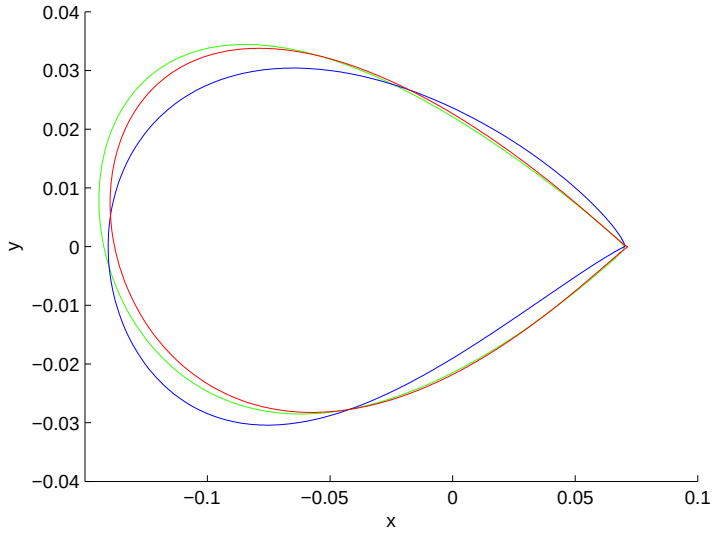


**Figure 2.21:** Three homoclinic orbits: the green one is numerically obtained from the approximating ODE (2.9) at parameter values $(\nu_1, \nu_2) = (-0.0049357243, -0.05)$; the red one is the predicted homoclinic orbit (2.21) but with $\nu_2 = -0.0478621$, using (2.23); for the blue orbit we use only the quadratic and cubic terms in $\varepsilon$ of (2.21) at the same parameter values as the red one.

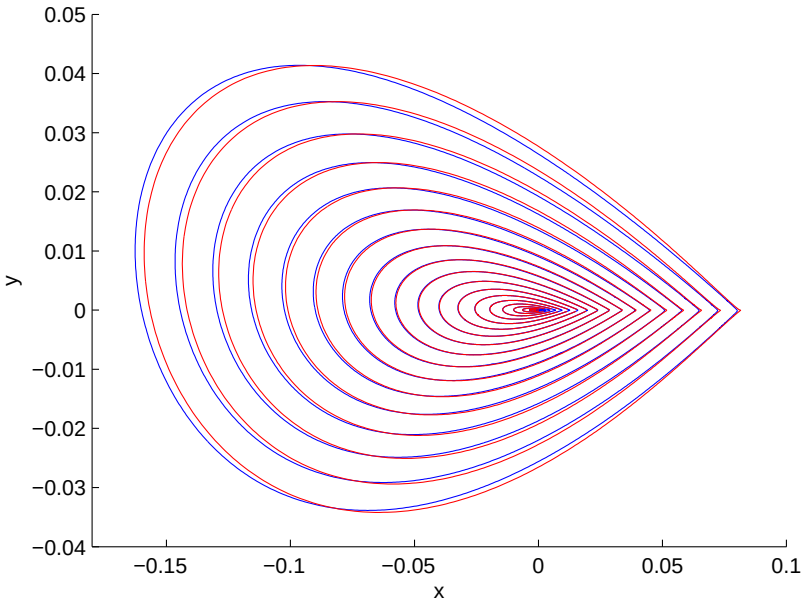


**Figure 2.22:** The predicted (2.21) (red) and numerical (blue) homoclinic orbits for the ODE (2.9) compared for parameter values (2.22) with $\varepsilon$ running from 0 to 0.2 with steps of 0.01.

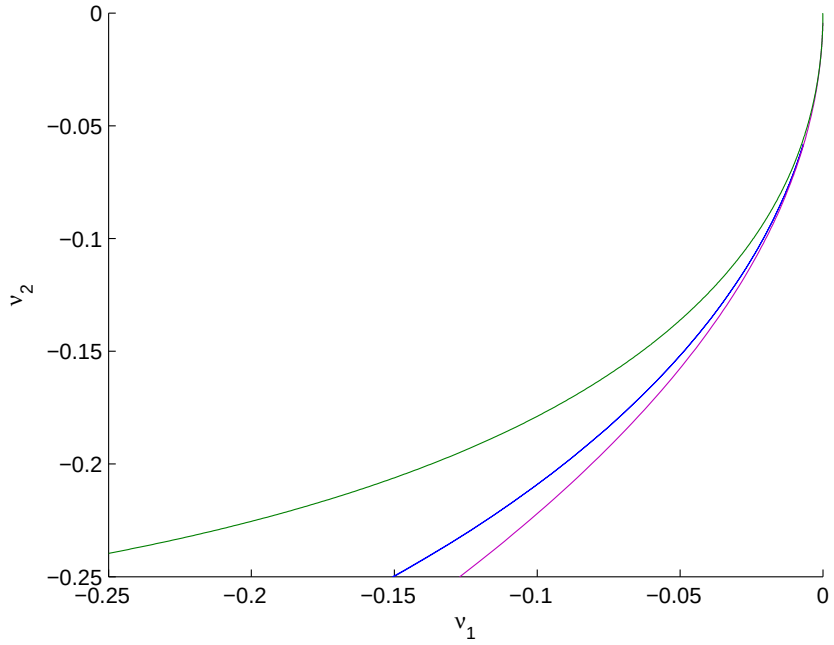


**Figure 2.23:** Comparison of the different regions for which a homoclinic orbit can be expected. The blue 'horn' (the two lines are very close to each other in this region) is obtained from the continuation in two parameters for the second order normal form (2.8) (as figure 2.17). The purple curve is the homoclinic bifurcation curve for the approximating ODE (2.9). The green line is the prediction (2.22).

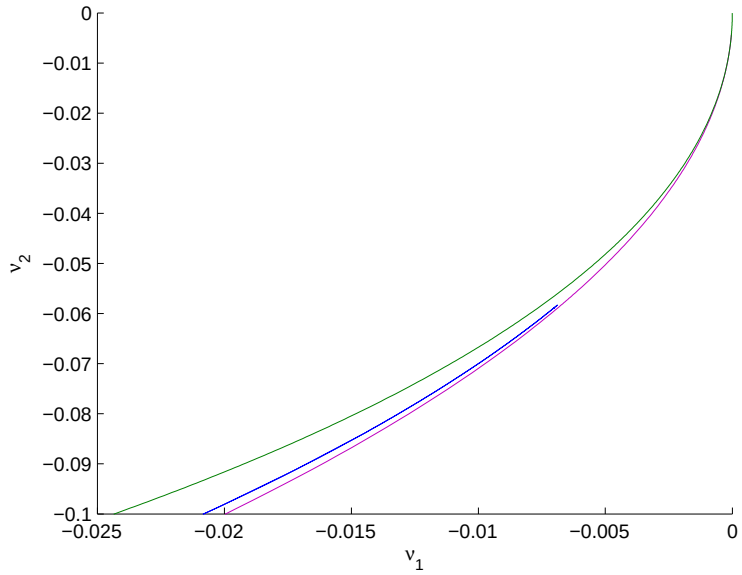


**Figure 2.24:** Close-up of figure 2.23 near the origin.

In order to get a discrete mapping along the homoclinic orbit from the expression (2.21), we replace the continuous time $t$ by the stepwise $t_0+k$, for some initial time choice $t_0$ and integers $k$. This leads to points $\xi_k(t_0,\varepsilon) := \xi_0(t_0+k,\varepsilon)$ along the homoclinic orbit for $k \in \mathbb{Z}$. At each of these points the normal vector $v_k$ is given by

$$v_k(t_0,\varepsilon) = \frac{\xi_k'(t_0,\varepsilon)}{\|\xi_0'(t_0,\varepsilon)\|}, \tag{2.24}$$

by taking the derivative of (2.21) with respect to $t$ at $t_0+k$ and normalize with respect to $v_0$.

### 2.3.4 Mel'nikov theory in the 1:1 resonance case

All the ingredients to compute the Mel'nikov function (1.32) for the normal form of 1:1 resonance are now in store. To summarize: as unperturbed map $F$ serves the third Picard iterate $\xi^{(3)}(1)$ given in (2.11). The perturbation part $\varepsilon G$ is given by equation (2.12). In the previous section we gave an approximation for the homoclinic orbit $\xi_0$ in (2.21), together with its unit normal vector $v$ in (2.24). Lastly, we have a prediction (2.22) at which values of the parameters $\nu_1, \nu_2$ this homoclinic orbit will occur.

We show here a few figures with computations of the Mel'nikov function for values of parameters at $\varepsilon = 0.1$ or $0.15$. The time $t$ runs between $\pm 20$ with steps of 0.1. Because our predicted homoclinic bifurcation curve does not lie inside the numerically obtained region of homoclinic structure (see figure 2.23), we vary the value of $\nu_2$ and fix $\nu_1$ in order to compute the Mel'nikov function for values inside the mentioned region.

Since we didn't work out the results of these computations, there has to be done some future work on this, i.e. to make the intersections of the normal form of 1:1 resonance visible at these small values of parameters and to verify that the predicted intersection points by the Mel'nikov function (at least one) is good enough. Moreover, we may ask the question what these graphs, the output of the Mel'nikov function, in this situation mean. What does a zero of this special function indicate?

Can we compare the situation of the McMillan map with the normal form of 1:1 resonance? In fact, these cases are different in the sense that in the case of the McMillan map we had a Hamiltonian system from which we derived (most of the) needed expressions; in this 1:1 resonance case, we didn't have a Hamiltonian in the original system, only via a transformation in the Bogdanov-Takens situation. Furthermore, we have to remark that the role of the parameter values, in particular of $\varepsilon$, is different in both maps. Besides that, we are able to compute the Mel'nikov function also outside the curve for which the ODE has a homoclinic orbit — in fact, we did it most of the time. Is our predictor (2.22) too far away from the real values? And how to interpret the result, in particular the 'intersection points', then?

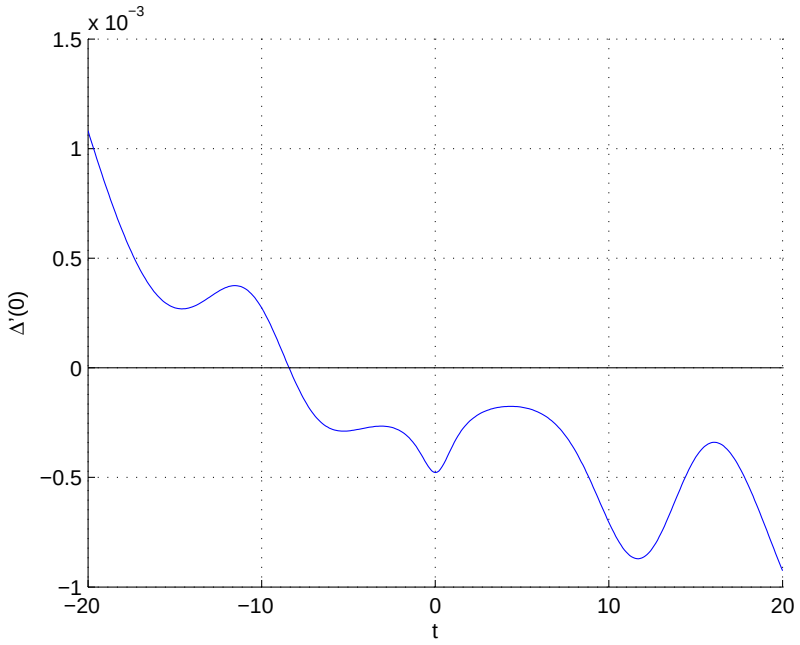


**Figure 2.25:** The Mel'nikov function for the case of the *normal form of 1:1 resonance*, computed with $\varepsilon = 0.15$, $\nu$ as in (2.22) and $k$ running from -10 to +10.

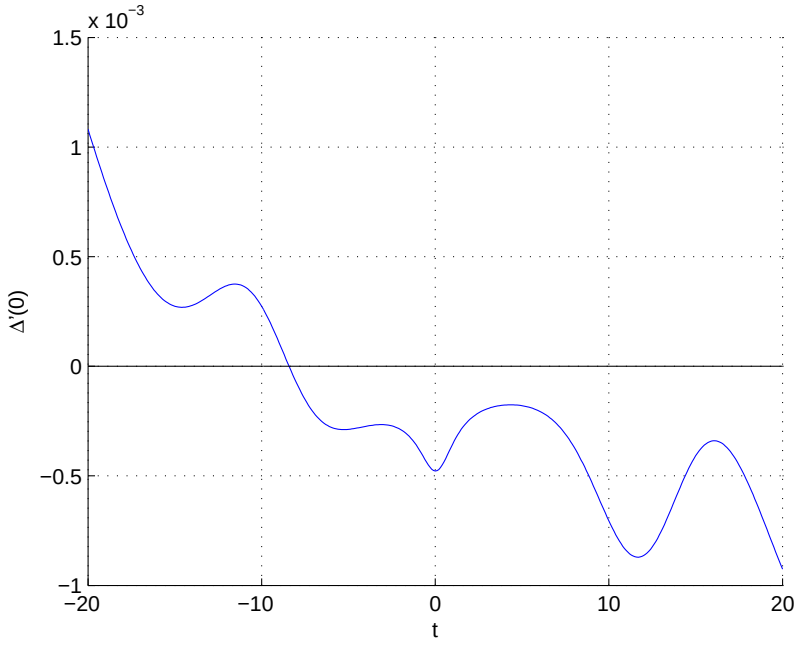


**Figure 2.26:** The Mel'nikov function for the case of the *normal form of 1:1 resonance*, computed with $\varepsilon = 0.15$, $\nu_2 = -0.03184$, $\nu_1$ as in (2.22) and $k$ running from -10 to +10.

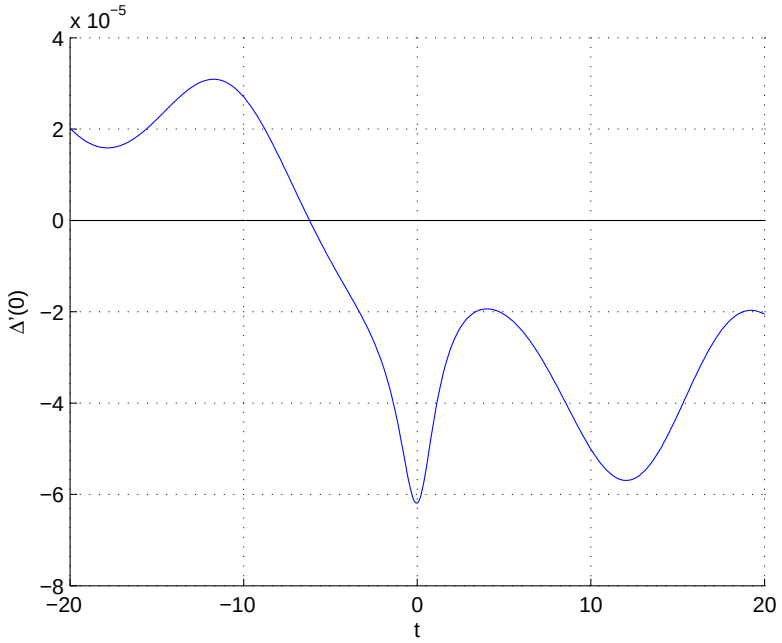


**Figure 2.27:** The Mel'nikov function for the case of the *normal form of 1:1 resonance*, computed with $\varepsilon = 0.1$, $\nu$ as in (2.22) and $k$ running from -10 to +10.

## 2.4 Normal form of 1:1 resonance (third order)

In this section we add some cubic terms to our 'standard' normal form of 1:1 resonance (2.8) to try to improve on the results for the first case. In third order the normal form is generally stated as

$$\begin{pmatrix} x \\ y \end{pmatrix} \mapsto \begin{pmatrix} x + y \\ y + \nu_1 + \nu_2 y + Ax^2 + Bxy + Kx^3 + Lx^2y + Mxy^2 + Ny^3 \end{pmatrix}, \quad (2.25)$$

with parameters $\alpha, \beta, A, B, K, L, M$ and $N$. Its fixed points are given by $(x_{0,1,2}, y_{0,1,2})$, where $y_{0,1,2} = 0$ and $x_{0,1,2}$ are solutions of the third-order polynomial $\alpha + Ax^2 + Kx^3$. From these three equilibrium points we select, for suitably chosen parameter values, the hyperbolic saddle $(x_0, 0)$ determined by the eigenvalues of the Jacobian at these points.

We compute the stable and unstable manifolds with the following parameters fixed to

$$(A, B, K, L, M, N) = (1.01, 1, 0.1, 0.1, 0.1, 0.2). \quad (2.26)$$

Choosing suitable $\nu_1$ and $\nu_2$ gives figures with transversal intersections like figure 2.28. The outcome doesn't differ much from the second order case, (Fig. 2.13): only the shape of the homoclinic connection is a bit changed and the oscillations became more wide. Variation of $\nu_1$ leads to the occurrence of homoclinic tangencies.

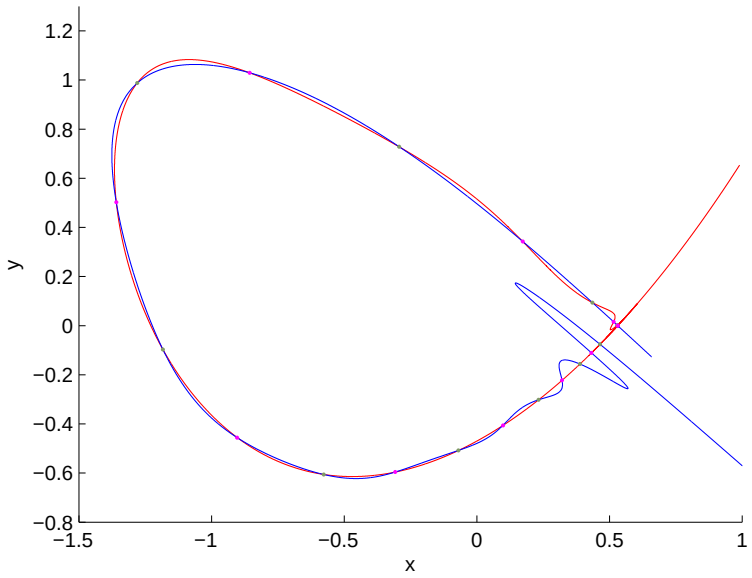


**Figure 2.28:** Transversal intersections of the stable (blue) and unstable (red) manifolds of the saddle point $(x_0, 0)$ of the third order *normal form of 1:1 resonance* (2.25) with parameter values $(\nu_1, \nu_2) = (-0.3, -0.375)$ and the others as in (2.26). Also shown, is the location of the intersection points between the two manifolds.

After doing the continuation of the homoclinic orbit with respect to $\nu_1$, we continue the curve of limit points in the two parameters $\nu_1$ and $\nu_2$. Adding some extra intersection points, as described in section 2.2.4, yields again a 'horn-like' shape for the region of homoclinic behaviour.

In figure 2.29 we show a bifurcation diagram near the *resonance 1:1* point, i.e. near the origin. The just computed 'horn' is shown in blue and labelled $T$. If we compare this figure to the one in case of the second order normal form, Fig. 2.18, we see that they are (insofar as we calculated it) locally topologically the same. As far as we can see, we may conclude that third order terms in the normal form do not change the bifurcation diagram near the point of 1:1 resonance dramatically.

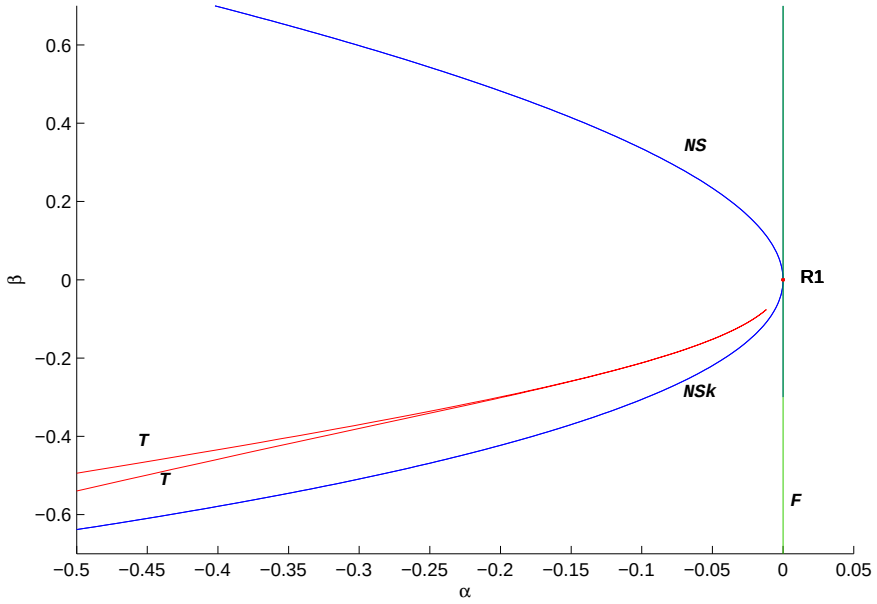


**Figure 2.29:** Bifurcation diagram of the third order *normal form of 1:1 resonance* (2.25) near the *resonance 1:1* point at the origin. The green line is the path of *Fold* points ($F$); the upper part ($NS$) of the red curve corresponds to the *Neutral Saddle* line, while the other one ($NSk$) is the *Neimark-Sacker* curve. The red curves, bounding the region of homoclinic structures, are labelled by $T$.

# A

# Deriving a homoclinic predictor

## A.1 The center manifold reduction

In this section we explain the method of center manifold reduction for a general $n$-dimensional system, as presented in [9]. With the help of this method we are able to find a homoclinic predictor near a Bogdanov-Takens bifurcation. We use this result to obtain the predictors (2.21) for the homoclinic orbit and (2.22) for the homoclinic bifurcation curve in the case of the normal form of 1:1 resonance.

First of all, we start with the ODE for which we want to compute the homoclinic orbit, here generally stated as a Taylor expansion at (0,0),

$$\begin{aligned}\dot{x} = f(x,\alpha) = Ax + \tfrac{1}{2}B(x,x) + A_1(x,\alpha) + J_1\alpha + \tfrac{1}{2}J_2(\alpha,\alpha) \\ + \mathcal{O}\left(\|x\|^3 + \|\alpha\|\|x\|^2 + \|\alpha\|^2\|x\| + \|\alpha\|^3\right),\end{aligned} \tag{A.1}$$

for $x \in \mathbb{R}^n, \alpha \in \mathbb{R}^m$, while $A = f_x(x_0,\alpha_0), J_1 = f_\alpha(x_0,\alpha_0)$ and $B, A_1$ and $J_2$ are the standard multilinear forms. Suppose, for $n \geq 2$ and $m = 2$, this system can have a (codim 2) bifurcation and let's assume the codimension 2 equilibrium for this bifurcation is $x = 0$ at $\alpha = 0$. We want to relate this system to the normal form corresponding to this bifurcation on its center manifold (i.e. the invariant manifolds on which the system exhibits this bifurcation), via,

$$\dot{w} = G(w,\beta), \quad G : \mathbb{R}^{n_c+2} \to \mathbb{R}^{n_c}. \tag{A.2}$$

Here, $n_c$ is the dimension of the center manifold, which itself is parametrised by $w \in \mathbb{R}^{n_c}$ with $\beta \in \mathbb{R}^2$ the unfolding parameters.

Suppose, a formula for the codim 1 bifurcation branch is available for (A.2). Then, in order to relate both systems to each other, we need a parametrisation $H$ of the center manifold in terms of the original variables

$x$ and a transformation $K$ of the bifurcation branch to the original parameters $\alpha$,

$$x = H(w, \beta), \quad H : \mathbb{R}^{n_c+2} \to \mathbb{R}^n,$$
$$\alpha = K(\beta), \quad K : \mathbb{R}^2 \to \mathbb{R}^2.$$

We thus obtained the center manifold $(x, \alpha) = (H, K)$ for this system. The fact that the center manifold should be invariant under system (A.1), yields the *homological equation*,

$$\dot{x} = H_w(w, \beta)G(w, \beta) = f(H(w, \beta), K(\beta)) = f(x, \alpha). \tag{A.3}$$

Solving this equation will eventually lead to an explicit expression for the mappings $H$ and $K$, and that allows us to transfer the known facts of the normal form (A.2) to our system of current study (A.1).

In the present case, we are dealing with a function $f$ which exhibits a Bogdanov-Takens bifurcation (see section 1.2.1), in which case the homoclinic orbit is well-known. A normal form on the center manifold (with $n_c = 2$) in this situation reads,

$$\dot{w} = G(w, \beta) = \begin{pmatrix} w_2 \\ \beta_1 + \beta_2 w_2 + a w_1^2 + b w_1 w_2 \end{pmatrix} + \mathcal{O}(\|w\|^3 + \|\beta\|\|w\|^2). \tag{A.4}$$

We can expand the mappings $H$ and $K$ as

$$\begin{aligned} H(w, \beta) = {} & q_1 w_1 + q_2 w_2 + H_{0010}\beta_1 + H_{0001}\beta_2 \\ & + \tfrac{1}{2}H_{2000}w_1^2 + H_{1100}w_1 w_2 + \tfrac{1}{2}H_{0200}w_2^2 \\ & + H_{1010}\beta_1 w_1 + H_{1001}\beta_2 w_1 + H_{0110}\beta_1 w_2 + H_{0101}\beta_2 w_2 \\ & + \tfrac{1}{2}H_{0020}\beta_1^2 + H_{0011}\beta_1\beta_2 + \tfrac{1}{2}H_{0002}\beta_2^2 + \mathcal{O}(|w\beta|^3), \end{aligned} \tag{A.5}$$

$$K(\beta) = K_{10}\beta_1 + K_{01}\beta_2 + \tfrac{1}{2}K_{20}\beta_1^2 + K_{11}\beta_1\beta_2 + \tfrac{1}{2}K_{02}\beta_2^2 + \mathcal{O}(|\beta|^3). \tag{A.6}$$

The solution of equation (A.3) provides us with the unknown coefficients of $H$ and $K$. The derivation of these coefficients is demonstrated in section A.4.1. We want to end up with results which are of order 4 in $\varepsilon$, so we truncate the previous expressions at second order in $w$ and $\beta$.

## A.2 An accurate homoclinic orbit for BT

In order to obtain accurate results for our system, we need to have an explicit expression for the homoclinic orbit of the Bogdanov-Takens normal form which is as close as possible to the real homoclinic orbit. We obtain

by applying an almost similar singular rescaling to the truncated normal form (A.4) as in Lemma 2 (choosing $\gamma_1 = -4$),

$$\begin{aligned} w_1 &= \tfrac{1}{a}\varepsilon^2 u; \\ w_2 &= \tfrac{1}{a}\varepsilon^3 v; \\ \beta_1 &= -\tfrac{4}{a}\varepsilon^4; \\ \beta_2 &= \tfrac{b}{a}\varepsilon^2 \tau, \end{aligned} \tag{A.7}$$

leading to the system

$$\begin{cases} \dot{u} = v, \\ \dot{v} = -4 + u^2 + \varepsilon\tfrac{b}{a} v(\tau + u). \end{cases} \tag{A.8}$$

As we pointed out in section 1.2.1, this system is Hamiltonian for $\varepsilon = 0$ and has the well-known solution

$$(u_0(t), v_0(t)) = \left(2 - 6\,\mathrm{sech}^2(t), 12\,\mathrm{sech}^2(t)\tanh(t)\right). \tag{A.9}$$

In order to obtain a proper homoclinic orbit for the system with $\varepsilon \neq 0$, we follow Beyn [2] in requiring the solutions $u$ and $v$ to satisfy

$$(u(t), v(t)) \in \mathcal{C}^1(\mathbb{R}, \mathbb{R}) \times \mathcal{C}^1(\mathbb{R}, \mathbb{R}),$$

for $\varepsilon, \tau \in \mathbb{R}$ and that the limits $\lim_{t\to\pm\infty}(u(t), v(t))$ and $\lim_{t\to\pm\infty}(\dot{u}(t), \dot{v}(t))$ exist. Moreover, we determine the phase of the homoclinic orbit by asking,

$$v(0) = 0, \tag{A.10}$$

which means that the homoclinic orbit passes the $u$-axis at $t = 0$. Note that the given solution $v_0$ has this property already. The homoclinic solutions to (A.8) can be parametrised by $\varepsilon$ up to any order, by $u(t) = u_0(t) + \varepsilon u_1(t) + \varepsilon^2 u_2(t) + \ldots$, $v(t) = v_0(t) + \varepsilon v_1(t) + \varepsilon^2 v_2(t) + \ldots$. The same can be done for $\tau = \tau_0 + \varepsilon\tau_1 + \varepsilon^2\tau_2 + \ldots$, which we will need in the next section to complete the description of the predicted homoclinic orbit and the homoclinic bifurcation curve up to order four in $\varepsilon$. Substituting these expressions up to order 2 into the system (A.8) gives four independent, linear, inhomogeneous systems, each of them corresponding to a different order of $\varepsilon$.

The case of $\varepsilon^0$ is already solved by (A.9). This solution is already homoclinic to the saddle fixed point of system (A.8), so we have to require all higher order corrections to the Hamiltonian homoclinic orbit should be zero in the limit. We therefore have to impose the conditions

$$\lim_{t\to\pm\infty}(u_k(t), v_k(t)) = (0, 0), \tag{A.11}$$

on our solutions $u_k(t)$ and its derivatives $v_k(t) = \frac{\mathrm{d}}{\mathrm{d}t}u_k(t)$, for all $k \geq 1$. What follows, is the derivation of these solution to the higher order systems. We don't give all explicit computations; in section A.4.2 we provide the MATHEMATICA-notebook with which these solutions are obtained.

After substituting the parametrisations in $\varepsilon$ of $u, v$ and $\tau$, we collect all $\varepsilon^1$-terms. These constitute the system,

$$\begin{cases} \dot{u}_1 = v_1, \\ \dot{v}_1 = 2u_0u_1 + \frac{b}{a}v_0(\tau_0 + u_0). \end{cases} \tag{A.12}$$

One can easily verify that $\varphi_1(t) = v_0(t) = \dot{u}_0$ forms a solution to the homogeneous part of this system,

$$\ddot{u}_1 = 2u_0u_1. \tag{A.13}$$

The other homoclinic solution $\varphi_2$ is derived from this one by setting $\varphi_2(t) = \chi(t)\varphi_1(t)$. Substituting this into (A.13) leads to

$$\ddot{\varphi}_2 = \ddot{\chi}v_0 + 2\dot{\chi}\dot{v}_0 + \chi\ddot{v}_0 = 2u_0\chi v_0,$$

and hence, since $v_0$ itself satisfies (A.13),

$$\ddot{\chi}v_0 + 2\dot{\chi}\dot{v}_0 = 0.$$

We can solve this for $\dot{\chi}(t)$ and recover $\chi$ itself by integrating the solution.[1] We thus get as second solution to the homogeneous problem,

$$\varphi_2 = 2\cosh^2(t) - 15\,\mathrm{sech}^2(t) + 15t\tanh(t)\,\mathrm{sech}^2(t) + 5.$$

The general solution $u_1$ to the inhomogeneous problem (A.12) can be found by variation of constants. First of all, the *Wronskian* $W$ of $\varphi_1$ and $\varphi_2$ is defined by,

$$W(\varphi_1, \varphi_2)(t) = \begin{vmatrix} \varphi_1(t) & \varphi_2(t) \\ \dot{\varphi}_1(t) & \dot{\varphi}_2(t) \end{vmatrix}.$$

Then the general solution $u_1$ is given by,

$$u_1(t) = \varphi_1(t)(c_1 - g_1(t)) + \varphi_2(t)(c_2 + f_1(t)),$$

where $f_1$ and $g_1$ are defined, using the Wronskian, by,

$$f_1(t) = \int \frac{\frac{b}{a}\varphi_1(t)v_0(\tau_0 + u_0)}{W(\varphi_1, \varphi_2)(t)}\mathrm{d}t,$$
$$g_1(t) = \int \frac{\frac{b}{a}\varphi_2(t)v_0(\tau_0 + u_0)}{W(\varphi_1, \varphi_2)(t)}\mathrm{d}t.$$

The condition (A.11) together with the phase condition sets the integration constants and defines

$$\tau_0 = \frac{10}{7},$$

[1] A suitable choice of the arbitrary integration constant in MATHEMATICA is $C = -\frac{2}{3}$.

in accordance with the result obtained by Beyn [2]. The desired functions $u_1$ and $v_1$ are thus derived and read as,

$$u_1(t) = -\frac{72b}{7a}\frac{\sinh t}{\cosh^3 t}\log(\cosh t),$$
$$v_1(t) = \frac{72b}{7a}\frac{\log(\cosh t)(1-2\sinh^2 t)+\sinh^2 t}{\cosh^4 t}.$$

Collecting all $\varepsilon^2$-terms together gives the following pair of inhomogeneous differential equations:

$$\begin{cases} \dot{u}_2 = v_2, \\ \dot{v}_2 = 2u_0u_2 + u_1^2 + \frac{b}{a}v_1(\tau_0+u_0) + \frac{b}{a}v_0(\tau_1+u_1). \end{cases} \tag{A.14}$$

Note that the homogeneous part is of the same form as in (A.12), which makes it easy for us, in that we can use the same homogeneous solutions $\varphi_1$ and $\varphi_2$. Again, we write the general solution as $u_2(t) = \varphi_1(t)(c_3 - g_2(t)) + \varphi_2(t)(c_4 + f_2(t))$, with $c_{3,4}$ some integration constants. With the conditions (A.10) and (A.11) taking into account, we derive the solution to (A.14),

$$\begin{aligned} u_2(t) = &-\frac{216b^2}{49a^2}\frac{\log^2(\cosh t)}{\cosh^4 t}(\cosh 2t - 2) - \frac{216b^2}{49a^2}\frac{\log(\cosh t)}{\cosh^4 t}(1-\cosh 2t) \\ &- \frac{18b^2}{49a^2}\frac{6t\sinh 2t - 7\cosh 2t + 8}{\cosh^4 t}, \\ v_2(t) = &\frac{288b^2}{49a^2}\frac{\sinh t}{\cosh^3 t}\left(3\log^2(\cosh t) - 6\log(\cosh t) - 1\right) \\ &- \frac{216b^2}{49a^2}\frac{\sinh t}{\cosh^5 t}\left(12\log^2(\cosh t) - 14\log(\cosh t) - 3\right) \\ &+ \frac{216b^2}{49a^2}\frac{t(2\cosh^2 t - 3)}{\cosh^4 t}, \end{aligned}$$

together with

$$\tau_1 = 0,$$

consistently with Beyn's statement that $\tau'(0) = 0$, see [2].

Lastly, collecting all $\varepsilon^3$-terms, we get the inhomogeneous system,

$$\begin{cases} \dot{u}_3 = v_3, \\ \dot{v}_3 = 2u_0u_3 + 2u_1u_2 + \frac{b}{a}v_2(\tau_0+u_0) + \frac{b}{a}v_1(\tau_1+u_1) + \frac{b}{a}v_0(\tau_2+u_2). \end{cases}$$

Again, the homogeneous part is the same, so the same procedure as for the first- and second-order case is applicable here. So, set the general solution

to $u_3(t) = \varphi_1(t)(c_5 - g_3(t)) + \varphi_2(t)(c_6 + f_3(t))$, with $c_{5,6}$ some integration constants, and require that (A.10) and (A.11) hold. This leads to the solutions

$$\begin{aligned}
u_3(t) = -\frac{27b^3}{2401a^3}\operatorname{sech}^5(t)\big(&-273\sinh t + 91\sinh 3t - 1232\sinh t\log^3(\cosh t)\\
&- 84t\cosh t(6\log(\cosh t) - 1) + 84t\cosh 3t(2\log(\cosh t) - 1)\\
&+ 112\sinh 3t\log^3(\cosh t) + 2016\sinh t\log^2(\cosh t)\\
&- 336\sinh 3t\log^2(\cosh t) + 904\sinh t\log(\cosh t)\\
&- 104\sinh 3t\log(\cosh t)\big),\\
v_3(t) = \frac{27b^3}{2401a^3}\operatorname{sech}^6(t)\big(&840t\sinh 2t - 168t\sinh 4t + 3696\log^3(\cosh t)\\
&- 7896\log^2(\cosh t) + \cosh 2t\big(-2912\log^3(\cosh t) + 7392\log^2(\cosh t)\\
&+ 40\log(\cosh t) - 1414\big) + \cosh 4t\big(112\log^3(\cosh t) - 504\log^2(\cosh t)\\
&+ 148\log(\cosh t) + 185\big) - 444\log(\cosh t)\\
&- 1680t\sinh 2t\log(\cosh t) + 168t\sinh 4t\log(\cosh t) + 1229\big),
\end{aligned}$$

and finally the value,

$$\tau_2 = \frac{288b^2}{2401a^2},$$

which completes the description of $\tau$ up to second order in $\varepsilon$.

## A.3 The homoclinic predictors

At this point we have determined an approximation of the emanating homoclinic orbit for the rescaled Bogdanov-Takens normal form (A.8). Using (A.7) we obtain the following expressions for the homoclinic orbit of (A.4) up to second order (i.e. up to fourth order in $\varepsilon$),

$$\begin{aligned}
w_1(t,\varepsilon) &= \frac{\varepsilon^2}{a}\big(u_0(\varepsilon t) + \varepsilon u_1(\varepsilon t) + \varepsilon^2 u_2(\varepsilon t)\big) + \mathcal{O}(\varepsilon^5);\\
w_2(t,\varepsilon) &= \frac{\varepsilon^3}{a}\big(v_0(\varepsilon t) + \varepsilon v_1(\varepsilon t) + \varepsilon^2 v_2(\varepsilon t)\big) + \mathcal{O}(\varepsilon^6),
\end{aligned}$$

where $u_0, v_0$ are given by (A.9), $u_1, v_1$ by (A.12) and $u_2, v_2$ by (A.14). Also, for the homoclinic bifurcation curve we find

$$\begin{aligned}
\beta_1(\varepsilon) &= -\frac{4}{a}\varepsilon^4 + \mathcal{O}(\varepsilon^5);\\
\beta_2(\varepsilon) &= \frac{b}{a}\tau_0\varepsilon^2 + \frac{b}{a}\tau_2\varepsilon^4 + \mathcal{O}(\varepsilon^5),
\end{aligned}$$

where

$$\tau_0 = \frac{10}{7}, \qquad \tau_2 = \frac{288b^2}{2401a^2}. \tag{A.15}$$

From the expression (A.5) of $H$ we are now able to derive an approximation for the homoclinic orbit in our original system (A.1) by collecting all terms that are quadratic, cubic or of order four in $\varepsilon$:

$$\begin{aligned} x_0(t) = H(w,\beta) = \varepsilon^2 &\left(\frac{b}{a}\tau_0 H_{0001} + \frac{1}{a}u_0(\varepsilon t)q_1\right) \\ &+ \varepsilon^3\left(\frac{1}{a}v_0(\varepsilon t)q_2 + \frac{1}{a}u_1(\varepsilon t)q_1\right) \\ &+ \varepsilon^4\left(-\frac{4}{a}H_{0010} + \frac{b}{a}H_{0001}\tau_2 + \frac{1}{a}u_2(\varepsilon t)q_1 + \frac{1}{a}v_1(\varepsilon t)q_2 + \right. \\ &\left. + \frac{1}{2a^2}H_{2000}u_0^2(\varepsilon t) + \frac{b}{a^2}\tau_0 H_{1001}u_0(\varepsilon t) + \frac{b^2}{2a^2}\tau_0^2 H_{0002}\right). \end{aligned} \tag{A.16}$$

The same goes for the parameters using the expansion of $K$, (A.6), also up to order four in $\varepsilon$:

$$\alpha = K(\beta) = \frac{b}{a}\tau_0 K_{01}\varepsilon^2 + \left(-\frac{4}{a}K_{10} + \frac{b}{a}\tau_2 K_{01} + \frac{b^2}{2a^2}\tau_0^2 K_{02}\right)\varepsilon^4. \tag{A.17}$$

Formulae (A.16) and (A.17) complete the derivation of the predictors of both the homoclinic orbit and the homoclinic bifurcation curve for a general ODE (A.1).

## A.4 Formulae for all elements of the predictor

### A.4.1 Derivation of ingredients of homological equation

The left-hand-side of equation (A.3) is obtained explicitly as follows. Using the normal form (A.4) and the expansions (A.5) and (A.6) of $H$ and $K$, respectively, we find — put in lexicographical order and the terms of order 3 and higher omitted —,

$$\begin{aligned} H_w(w,\beta)G(w,\beta) &= \frac{\partial H}{\partial w_1}\cdot w_2 + \frac{\partial H}{\partial w_2}\cdot(\beta_1 + \beta_2 w_2 + a w_1^2 + b w_1 w_2) \\ &= (q_1 + H_{2000}w_1 + H_{1100}w_2 + H_{1010}\beta_1 + H_{1001}\beta_2)w_2 \\ &\quad + (q_2 + H_{1100}w_1 + H_{0200}w_2 + H_{0110}\beta_1 + H_{0101}\beta_2)\cdot \\ &\quad\quad \cdot(\beta_1 + \beta_2 w_2 + a w_1^2 + b w_1 w_2) \\ &= q_1 w_2 + q_2\beta_1 \\ &\quad + a q_2 w_1^2 + (b q_2 + H_{2000})w_1 w_2 + H_{1100}w_2^2 \\ &\quad + H_{1100}\beta_1 w_1 + (H_{1010} + H_{0200})\beta_1 w_2 + (H_{1001} + q_2)\beta_2 w_2 \\ &\quad + H_{0110}\beta_1^2 + H_{0101}\beta_1\beta_2. \end{aligned} \tag{A.18}$$

Substituting $H$ and $K$ into $f(x,\alpha)$, the right-hand-side of (A.3) reads (again, we omit terms of order 3 and higher),

$$f(H(w,\beta),K(\beta)) = A\big(q_1 w_1 + q_2 w_2 + H_{0010}\beta_1 + H_{0001}\beta_2 +$$

$$
\begin{aligned}
&\quad + \tfrac{1}{2}H_{2000}w_1^2 + H_{1100}w_1w_2 + \tfrac{1}{2}H_{0200}w_2^2 \\
&\quad + H_{1010}\beta_1w_1 + H_{1001}\beta_2w_1 + H_{0110}\beta_1w_2 + H_{0101}\beta_2w_2 \\
&\quad + \tfrac{1}{2}H_{0020}\beta_1^2 + H_{0011}\beta_1\beta_2 + \tfrac{1}{2}H_{0002}\beta_2^2\big) \\
&+ \tfrac{1}{2}B(q_1w_1 + q_2w_2 + H_{0010}\beta_1 + H_{0001}\beta_2, q_1w_1 + q_2w_2 + H_{0010}\beta_1 + H_{0001}\beta_2) \\
&+ A_1(q_1w_1 + q_2w_2 + H_{0010}\beta_1 + H_{0001}\beta_2, K_{10}\beta_1 + K_{01}\beta_2) \\
&+ J_1\big(K_{10}\beta_1 + K_{01}\beta_2 + \tfrac{1}{2}K_{20}\beta_1^2 + K_{11}\beta_1\beta_2 + \tfrac{1}{2}K_{02}\beta_2^2\big) \\
&+ \tfrac{1}{2}J_2(K_{10}\beta_1 + K_{01}\beta_2, K_{10}\beta_1 + K_{01}\beta_2) \\
&= Aq_1w_1 + Aq_2w_2 + AH_{0010}\beta_1 + AH_{0001}\beta_2 \\
&\quad + \tfrac{1}{2}AH_{2000}w_1^2 + AH_{1100}w_1w_2 + \tfrac{1}{2}AH_{0200}w_2^2 \\
&\quad + AH_{1010}\beta_1w_1 + AH_{1001}\beta_2w_1 + AH_{0110}\beta_1w_2 + AH_{0101}\beta_2w_2 \\
&\quad + \tfrac{1}{2}AH_{0020}\beta_1^2 + AH_{0011}\beta_1\beta_2 + \tfrac{1}{2}AH_{0002}\beta_2^2 \\
&+ \tfrac{1}{2}\big(B(q_1,q_1)w_1^2 + B(q_1,q_2)w_1w_2 + B(q_1,H_{0010})\beta_1w_1 + B(q_1,H_{0001})\beta_2w_1 \\
&\quad + B(q_2,q_1)w_1w_2 + B(q_2,q_2)w_2^2 + B(q_2,H_{0010})\beta_1w_2 + B(q_2,H_{0001})\beta_2w_2 \\
&\quad + B(H_{0010},q_1)\beta_1w_1 + B(H_{0010},q_2)\beta_1w_2 + B(H_{0010},H_{0010})\beta_1^2 \\
&\quad + B(H_{0010},H_{0001})\beta_1\beta_2 + B(H_{0001},q_1)\beta_2w_1 + B(H_{0001},q_2)\beta_2w_2 \\
&\quad + B(H_{0001},H_{0010})\beta_1\beta_2 + B(H_{0001},H_{0001})\beta_2^2\big) \\
&+ A_1(q_1,K_{10})\beta_1w_1 + A_1(q_1,K_{01})\beta_2w_1 + A_1(q_2,K_{10})\beta_1w_2 \\
&\quad + A_1(q_2,K_{01})\beta_2w_2 + A_1(H_{0010},K_{10})\beta_1^2 + A_1(H_{0010},K_{01})\beta_1\beta_2 \\
&\quad + A_1(H_{0001},K_{10})\beta_1\beta_2 + A_1(H_{0001},K_{01})\beta_2^2 \\
&+ J_1K_{10}\beta_1 + J_1K_{01}\beta_2 + \tfrac{1}{2}J_1K_{20}\beta_1^2 + J_1K_{11}\beta_1\beta_2 + \tfrac{1}{2}J_1K_{02}\beta_2^2 \\
&+ \tfrac{1}{2}\big(J_2(K_{10},K_{10})\beta_1^2 + J_2(K_{10},K_{01})\beta_1\beta_2 \\
&\quad + J_2(K_{01},K_{10})\beta_1\beta_2 + J_2(K_{01},K_{01})\beta_2^2\big) \\
&= Aq_1w_1 + Aq_2w_2 \qquad\qquad (A.19) \\
&\quad + (AH_{0010} + J_1K_{10})\beta_1 + (AH_{0001} + J_1K_{01})\beta_2 \\
&\quad + \tfrac{1}{2}(AH_{2000} + B(q_1,q_1))w_1^2 \\
&\quad + (AH_{1100} + B(q_1,q_2))w_1w_2 \\
&\quad + \tfrac{1}{2}(AH_{0200} + B(q_2,q_2))w_2^2 \\
&\quad + \big(AH_{1010} + B(q_1,H_{0010}) + A_1(q_1,K_{10})\big)\beta_1w_1 \\
&\quad + \big(AH_{1001} + B(q_1,H_{0001}) + A_1(q_1,K_{01})\big)\beta_2w_1 \\
&\quad + \big(AH_{0110} + B(q_2,H_{0010}) + A_1(q_2,K_{10})\big)\beta_1w_2 \\
&\quad + \big(AH_{0101} + B(q_2,H_{0001}) + A_1(q_2,K_{01})\big)\beta_2w_2 \\
&\quad + \tfrac{1}{2}\big(AH_{0020} + B(H_{0010},H_{0010}) + 2A_1(H_{0010},K_{10}) \\
&\quad\quad + J_1K_{20} + J_2(K_{10},K_{10})\big)\beta_1^2 \\
&\quad + \big(AH_{0011} + B(H_{0010},H_{0001}) + A_1(H_{0010},K_{01}) \\
&\quad\quad + A_1(H_{0001},K_{10}) + J_1K_{11} + J_2(K_{10},K_{01})\big)\beta_1\beta_2 +
\end{aligned}
$$

$$+\tfrac{1}{2}\big(AH_{0002}+B(H_{0001},H_{0001})+2A_1(H_{0001},K_{01})$$
$$+J_1K_{02}+J_2(K_{01},K_{01})\big)\beta_2^2.$$

Note that we use in the last step the properties of multilinear forms that we can take out scalars and — for the symmetric form $B$ — that we can interchange both sides. The homological equation is now simply obtained by equating (A.18) and (A.19). We can solve the unknown coefficients of $H$ and $K$ by collecting the terms with equal components in $w$ and $\beta$. This leads to the following fourteen equations:

$$0 = Aq_1, \tag{A.20a}$$
$$q_1 = Aq_2, \tag{A.20b}$$
$$q_2 = AH_{0010}+J_1K_{10}, \tag{A.20c}$$
$$0 = AH_{0001}+J_1K_{01}, \tag{A.20d}$$
$$aq_2 = \tfrac{1}{2}(AH_{2000}+B(q_1,q_1)), \tag{A.20e}$$
$$bq_2+H_{2000} = AH_{1100}+B(q_1,q_2), \tag{A.20f}$$
$$H_{1100} = \tfrac{1}{2}(AH_{0200}+B(q_2,q_2)), \tag{A.20g}$$
$$H_{1100} = AH_{1010}+B(q_1,H_{0010})+A_1(q_1,K_{10}), \tag{A.20h}$$
$$0 = AH_{1001}+B(q_1,H_{0001})+A_1(q_1,K_{01}), \tag{A.20i}$$
$$H_{1010}+H_{0200} = AH_{0110}+B(q_2,H_{0010})+A_1(q_2,K_{10}), \tag{A.20j}$$
$$H_{1001}+q_2 = AH_{0101}+B(q_2,H_{0001})+A_1(q_2,K_{01}), \tag{A.20k}$$
$$H_{0110} = \tfrac{1}{2}\big(AH_{0020}+B(H_{0010},H_{0010})+2A_1(H_{0010},K_{10}) + J_1K_{20}+J_2(K_{10},K_{10})\big), \tag{A.20l}$$
$$H_{0101} = AH_{0011}+B(H_{0010},H_{0001})+A_1(H_{0010},K_{01}) + A_1(H_{0001},K_{10})+J_1K_{11}+J_2(K_{10},K_{01}), \tag{A.20m}$$
$$0 = \tfrac{1}{2}\big(AH_{0002}+B(H_{0001},H_{0001})+2A_1(H_{0001},K_{01}) + J_1K_{02}+J_2(K_{01},K_{01})\big), \tag{A.20n}$$

Obviously, the first two do not show anything, but just the definition of the generalized eigenvectors $q_{1,2}$. The next two, (A.20c) and (A.20d), will become useful later on to compute $\hat{H}_{01}$ and $\hat{K}_1$.

Before we proceed, we remark that, by the properties of the generalized eigenvectors, it holds that $p_2^TA=0$, $p_1^TA=p_2$, $p_1^Tq_2=0$ and $p_2^Tq_2=1$. These facts can be used to get orthogonal relations in the equations in (A.20), and thus simplify them.

First of all, we multiply (A.20e) with $p_2^T$ from the left and obtain,

$$a = ap_2^Tq_2 = \tfrac{1}{2}(p_2^TAH_{2000}+p_2^TB(q_1,q_1)) = \tfrac{1}{2}p_2^TB(q_1,q_1),$$

which is equation (2.17). Moreover, by multiplying the same equation with $p_1^T$ from the left, we gain,

$$\tfrac{1}{2}(p_1^TAH_{2000}+p_1^TB(q_1,q_1)) = \tfrac{1}{2}(p_2^TH_{2000}+p_1^TB(q_1,q_1)) = ap_1^Tq_2 = 0,$$

and hence,

$$p_2^T H_{2000} = -p_1^T B(q_1, q_1), \tag{A.21}$$

which is useful in the computation of $b$. To compute $b$, multiply (A.20f) with $p_2^T$ from the left and use (A.21) in the result to obtain equation (2.18):

$$\begin{aligned} b = bp_2^T q_2 &= p_2^T A H_{1100} + p_2^T B(q_1, q_2) - p_2^T H_{2000} \\ &= p_2^T B(q_1, q_2) + p_1^T B(q_1, q_1). \end{aligned}$$

The equations (A.20e) and (A.20f) also provide us with expressions for $H_{2000}$ and $H_{1100}$. But $A$ is not invertible, since it has $\lambda = 0$ as eigenvalues, so we have to use another operator $A^{INV}$ which is defined such that $x = A^{INV} y$ by solving the non-singular bordered system (see [8]),

$$\begin{pmatrix} A & p_2 \\ q_1^T & 0 \end{pmatrix} \begin{pmatrix} x \\ s \end{pmatrix} = \begin{pmatrix} y \\ 0 \end{pmatrix},$$

where $x, y \in \mathbb{R}^n$ and $s \in \mathbb{R}$. This operator then returns formulae (2.19):

$$\begin{aligned} H_{2000} &= A^{INV}(2aq_2 - B(q_1, q_1)), \\ H_{1100} &= A^{INV}(bq_2 + H_{20,0} - B(q_1, q_2)). \end{aligned}$$

From (A.20g) we obtain by multiplying with $p_2^T$ from the left, the useful relation,

$$p_2^T H_{1100} = \tfrac{1}{2}(p_2^T A H_{0200} + p_2^T B(q_2, q_2)) = \tfrac{1}{2} p_2^T B(q_2, q_2). \tag{A.22}$$

The same equation (A.20g) multiplied with $p_1^T$ yields

$$p_1^T H_{1100} = \tfrac{1}{2}(p_1^T A H_{0200} + p_1^T B(q_2, q_2)) = \tfrac{1}{2}(p_2^T H_{0200} + p_1^T B(q_2, q_2)),$$

and hence

$$p_2^T H_{0200} = 2p_1^T H_{1100} - p_1^T B(q_2, q_2). \tag{A.23}$$

Multiplying both (A.20h) and (A.20i) from the left with $p_2^T$ yields,

$$\begin{aligned} p_2^T H_{1100} &= p_2^T B(q_1, H_{0010}) + p_2^T A_1(q_1, K_{10}), \\ 0 &= p_2^T B(q_1, H_{0001}) + p_2^T A_1(q_1, K_{01}). \end{aligned}$$

In the first equation we can replace the term $p_2^T H_{1100}$ with (A.22). Reversing left and right sides, we then obtain,

$$p_2^T B(q_1, \hat{H}_{01}) + p_2^T A_1(q_1, K_1) = [\tfrac{1}{2} p_2^T B(q_2, q_2), 0], \tag{A.24}$$

where $\hat{H}_{01}$ is short-hand notation for $[H_{0010}, H_{0001}]$ and $\hat{K}_1$ for $[K_{10}, K_{01}]$.

Equations (A.20h) and (A.20i), being multiplied from the left with $p_1^T$, give

$$\begin{aligned} p_1^T H_{1100} &= p_1^T A H_{1010} + p_1^T B(q_1, H_{0010}) + p_1^T A_1(q_1, K_{10}) \\ &= p_2^T H_{1010} + p_1^T B(q_1, H_{0010}) + p_1^T A_1(q_1, K_{10}), \\ 0 &= p_1^T A H_{1001} + p_1^T B(q_1, H_{0001}) + p_1^T A_1(q_1, K_{01}) \\ &= p_2^T H_{1001} + p_1^T B(q_1, H_{0001}) + p_1^T A_1(q_1, K_{01}). \end{aligned}$$

These provide us, after rearranging, with the two following useful expressions,

$$\begin{aligned} p_2^T H_{1010} &= -p_1^T B(q_1, H_{0010}) - p_1^T A_1(q_1, K_{10}) + p_1^T H_{1100}, \\ p_2^T H_{1001} &= -p_1^T B(q_1, H_{0001}) - p_1^T A_1(q_1, K_{01}). \end{aligned} \tag{A.25}$$

The next two, (A.20j) and (A.20k), multiplied with $p_2^T$ from the left,

$$\begin{aligned} p_2^T H_{1010} + p_2^T H_{0200} &= p_2^T A H_{0110} + p_2^T B(q_2, H_{0010}) + p_2^T A_1(q_2, K_{10}), \\ p_2^T H_{1001} + p_2^T q_2 &= p_2^T A H_{0101} + p_2^T B(q_2, H_{0001}) + p_2^T A_1(q_2, K_{01}) \end{aligned}$$

and each first term on the left-hand-side replaced with (A.25),

$$\begin{aligned} -p_1^T B(q_1, H_{0010}) - p_1^T A_1(q_1, K_{10}) + p_1^T H_{1100} + p_2^T H_{0200} \\ = p_2^T B(q_2, H_{0010}) + p_2^T A_1(q_2, K_{10}), \\ -p_1^T B(q_1, H_{0001}) - p_1^T A_1(q_1, K_{01}) + 1 \\ = p_2^T B(q_2, H_{0001}) + p_2^T A_1(q_2, K_{01}), \end{aligned}$$

give the rearranged and combined equation

$$\begin{aligned} p_1^T B(q_1, \hat{H}_{01}) + p_1^T A_1(q_1, K_1) + p_2^T B(q_2, \hat{H}_{01}) + p_2^T A_1(q_2, K_1) \\ = [p_1^T H_{1100} + p_2^T H_{0200}, 1], \end{aligned}$$

where we use again the short-hand $\hat{H}_{01} = [H_{0010}, H_{0001}]$ and $\hat{K}_1 = [K_{10}, K_{01}]$. We can reduce the number of unknowns in this formula further by substituting $p_2^T H_{0200}$ with (A.23):

$$\begin{aligned} p_1^T B(q_1, \hat{H}_{01}) + p_1^T A_1(q_1, K_1) + p_2^T B(q_2, \hat{H}_{01}) + p_2^T A_1(q_2, K_1) \\ = [-p_1^T B(q_2, q_2) + 3p_1^T H_{1100}, 1]. \end{aligned} \tag{A.26}$$

Summarizing, when we collect (A.20c), (A.20d), (A.24) and (A.26), we gain the 4-dimensional system

$$\begin{aligned} &\begin{pmatrix} A & J_1 \\ p_2^T B q_1 & p_2^T A_1 q_1 \\ p_1^T B q_1 + p_2^T B q_2 & p_1^T A_1 q_1 + p_2^T A_1 q_2 \end{pmatrix} \begin{pmatrix} \hat{H}_{01} \\ \hat{K}_1 \end{pmatrix} \\ &= \begin{pmatrix} q_2 & 0 \\ \frac{1}{2} p_2^T B(q_2, q_2) & 0 \\ -p_1^T B(q_2, q_2) + 3p_1^T H_{1100} & 1 \end{pmatrix}, \end{aligned} \tag{A.27}$$

from which we can determine $\hat{H}_{01}$ and $\hat{K}_1$.

Next, we want to determine the remaining quadratic coefficients, to start with $K_{02}$ and $H_{0002}$. These two can be obtained from (A.20n). Multiply this equation from the left with $p_2^T$ to obtain

$$0 = p_2^T B(H_{0001}, H_{0001}) + 2p_2^T A_1(H_{0001}, K_{01}) + p_2^T J_1 K_{02} + p_2^T J_2(K_{01}, K_{01}). \tag{A.28}$$

Apply the vector $p_2^T$ also to (A.20c) to get

$$1 = p_2^T q_2 = p_2^T A H_{0010} + p_2^T J_1 K_{10} = p_2^T J_1 K_{10}.$$

This result removes the $J_1$ in front of $K_{02}$ at the cost of an extra (known) $K_{10}$. Furthermore, using the abbreviation

$$z = B(H_{0001}, H_{0001}) + 2A_1(H_{0001}, K_{01}) + J_2(K_{01}, K_{01}),$$

formula (A.28) provides a short equation for $K_{02}$:

$$K_{02} = -(p_2^T z)K_{10}.$$

Knowing $K_{02}$, we can get rid of the other unknown $H_{0002}$ in the same equation (A.20n) by applying the operator $A^{INV}$ as described above. This yields the other part of equation (2.20),

$$H_{0002} = -A^{INV}(z + J_1 K_{02}).$$

The operator $A^{INV}$ can serve to tackle the seven remaining unknowns in equations (A.20e)–(A.20m):

$$\begin{aligned}
H_{0200} &= A^{INV}(2H_{1100} - B(q_2, q_2)),\\
H_{1010} &= A^{INV}(H_{1100} - B(q_1, H_{0010}) - A_1(q_1, K_{10})),\\
H_{1001} &= -A^{INV}(B(q_1, H_{0001}) + A_1(q_1, K_{01})),\\
H_{0110} &= A^{INV}(H_{1010} + H_{0200} - B(q_2, H_{0010}) - A_1(q_2, K_{10})),\\
H_{0101} &= A^{INV}(H_{1001} + q_2 - B(q_2, H_{0001}) - A_1(q_2, K_{01})),\\
H_{0020} &= A^{INV}\big(2H_{0110} - B(H_{0010}, H_{0010}) - 2A_1(H_{0010}, K_{10})\\
&\qquad - J_1 K_{20} - J_2(K_{10}, K_{10})\big),\\
H_{0011} &= A^{INV}(H_{0101} - B(H_{0010}, H_{0001}) - A_1(H_{0010}, K_{01})\\
&\qquad - A_1(H_{0001}, K_{10}) - J_1 K_{11} - J_2(K_{10}, K_{01})).
\end{aligned}$$

In the last two expressions, we use the components $K_{20}$ and $K_{11}$, which still have to be determined . These can be computed from (A.20l) and (A.20m) in the same manner as we obtained $K_{02}$, giving,

$$\begin{aligned}
K_{20} &= p_2^T\big(2H_{0110} - AH_{0020} - B(H_{0010}, H_{0010})\\
&\qquad - 2A_1(H_{0010}, K_{10}) - J_2(K_{10}, K_{10})\big)K_{10},\\
K_{11} &= p_2^T\big(H_{0101} - AH_{0011} - B(H_{0010}, H_{0001}) - A_1(H_{0010}, K_{01})\\
&\qquad - A_1(H_{0001}, K_{10}) - J_2(K_{10}, K_{01})\big)K_{10}.
\end{aligned}$$

This completes the calculation of all unknown coefficients in the expansions (A.5) and (A.6) of $H$ and $K$, respectively.

### A.4.2 *Mathematica*-code to compute homoclinic orbit for rescaled BT

In this section we present the MATHEMATICA-code which is used to obtain the solutions $u_1, v_1, u_2, v_2, u_3, v_3$ and $\tau_0, \tau_1, \tau_2$ to (A.12), (A.14) and (A.15), presented in section A.2. The script is structured as follows: there are four sections according to each power of $\varepsilon$. Within each section there are first the known functions stated. The computation of the needed functions follows. After that we take the required limits from the results and equate them to 0. The last part gives the final answers of the section.

#### Solutions for $\varepsilon^0$-components

```
u0[t_]:=2(1-3*Sech[t]^2)
v0[t_]:=12*Sech[t]^2*Tanh[t]
```

#### Solutions for $\varepsilon^1$-components

```
phi1[t_]:=v0[t]
phi2[t_]:=2*Cosh[t]^2+5+15*t*Sinh[t]/Cosh[t]^3-15/Cosh[t]^2
W=Wronskian[{phi1[t],phi2[t]},t];

W1[t_]:=phi1[t]*b/a*v0[t]*(tau0+u0[t])
W2[t_]:=phi2[t]*b/a*v0[t]*(tau0+u0[t])
uf1[t_]:=Integrate[W1[t]/W,t]
ug1[t_]:=Integrate[W2[t]/W,t]
u1[t_]:=phi1[t]*(C2-ug1[t])+phi2[t]*(C1+uf1[t])
v1[t_]:=D[u1[s],s]/.{s->t}

Limit[phi1[t],t->Infinity]
Limit[phi2[t],t->Infinity]
coef1=Solve[{Limit[C1+uf1[t],t->Infinity],
             Limit[C1+uf1[t],t->-Infinity]}=={0,0},{tau0,C1}];
v1[0]/.%[[1]];
coefC2=Solve[%==0,C2];

repl1=Union[coef1[[1]],coefC2[[1]]]
u1[t]/.repl1//Simplify
v1[t]/.repl1//Simplify
```

#### Solutions for $\varepsilon^2$-components

```
f2[t_]:=u1[t]^2+b/a*tau1*v0[t]+b/a*u1[t]*v0[t]
        +b/a*tau0*v1[t]+b/a*u0[t]*v1[t]/.repl1
```

```
W3[t_]:=phi1[t]*f2[t]
W4[t_]:=phi2[t]*f2[t]
uf2[t_]:=Integrate[W3[t]/W,t]
ug2[t_]:=Integrate[W4[t]/W,t]
u2[t_]:=phi1[t]*(C4-ug2[t])+phi2[t]*(C3+uf2[t])
v2[t_]:=D[u2[s],s]/.{s->t}

coef2=Solve[{Limit[C3+uf2[t],t->Infinity],
             Limit[C3+uf2[t],t->-Infinity]}=={0,0},{C3,tau1}];
v2[0]/.%[[1]];
coefC4=Solve[%==0,C4];

repl2=Union[coef2[[1]],coefC4[[1]]]
u2final[t_]:=u2[t]/.repl2//Simplify
v2final[t_]:=v2[t]/.repl2//Simplify
u2final[t]
v2final[t]
```

### Solutions for $\varepsilon^3$-components

```
f3[t_]:=2*u1[t]*u2final[t]+b/a*tau2*v0[t]+b/a*u2final[t]*v0[t]
        +b/a*tau1*v1[t]+b/a*u1[t]*v1[t]+b/a*tau0*v2final[t]
        +b/a*u0[t]*v2final[t]/.repl1/.repl2

W5[t_]:=phi1[t]*f3[t]
W6[t_]:=phi2[t]*f3[t]
uf3[t_]:=Integrate[W5[t]/W,t]
ug3[t_]:=Integrate[W6[t]/W,t]
u3[t_]:=phi1[t]*(C6-ug3[t])+phi2[t]*(C5+uf3[t])
v3[t_]:=D[u3[s],s]/.{s->t}

coef3=Solve[{Limit[C5+uf3[t],t->Infinity],
             Limit[C5+uf3[t],t->-Infinity]}=={0,0},{C5,tau2}];
v3[0]/.%[[1]];
coefC6=Solve[%==0,C6];

repl3=Union[coef3[[1]],coefC6[[1]]]
u3final[t_]:=u3[t]/.repl3//Simplify
v3final[t_]:=D[u3final[t],t]//Simplify
u3final[t]
v3final[t]
```

# B

# Bibliography


[1] D.K. Arrowsmith, J.H.E. Cartwright, A.N. Lansbury, and C.M. Place. The Bogdanov Map: Bifurcations, Mode Locking, and Chaos in a Dissipative System. *International Journal of Bifurcation and Chaos*, 3(4):803–842, 1993.

[2] W.-J. Beyn. Numerical Analysis of Homoclinic Orbits emanating from a Takens-Bogdanov Point. *IMA Journal of Numerical Analysis*, 14:381–410, 1994.

[3] J.P. Chávez. Starting Homoclinic Tangencies near 1:1 Resonances. *International Journal of Bifurcation and Chaos*, 20(10):3157–3172, 2010.

[4] M.L. Glasser, V.G. Papageorgiou, and T.C. Bountis. Mel'nikov's Function for Two-Dimensional Mappings. *SIAM Journal of Applied Mathematics*, 49(3):692–703, June 1989.

[5] J. Guckenheimer and Ph. Holmes. *Nonlinear Oscillations, Dynamical Systems, and Bifurcation of Vector Fields.* New York: Springer-Verlag, 1983.

[6] R. Khoshiar Ghaziani, W. Govaerts, Yu.A. Kuznetsov, and H.G.E. Meijer. Numerical Continuation of Connecting Orbits of Maps in MATLAB. *Journal of Difference Equations and Applications*, 15(8–9):1–31, 2009.

[7] B. Krauskopf, H.M. Osinga, and J. Galán-Vioque (eds.). *Numerical Continuation Methods for Dynamical Systems.* Dordrecht: Springer, 2007.

[8] Yu.A. Kuznetsov. *Elements of Applied Bifurcation Theory.* New York: Springer-Verlag, 3rd edition, 2004.

[9] Yu.A. Kuznetsov, H.G.E. Meijer, B. Al Hdaibat, V. De Witte, and W. Govaerts. Improved Homoclinic Predictor for Bogdanov-Takens Bifurcation. *International Journal of Bifurcation and Chaos*, To be published.